PL-TR-92-2070

SPECIALIZED STUDIES IN YIELD ESTIMATION

L. J. Burdick
C. K. Saikia
J. P. McLaren
L. S. Zhao
D. V. Helmberger

Woodward-Clyde Consultants
566 El Dorado Street,
Suite 100
Pasadena, CA 91101

20 May 1992

Final Report
1 August 1990 - 28 February 1992

PHILLIPS LABORATORY
AIR FORCE SYSTEMS COMMAND
HANSCOM AIR FORCE BASE, MASSACHUSETTS 01731-5000

SPONSORED BY
Defense Advanced Research Projects Agency
Nuclear Monitoring Research Office
ARPA ORDER NO. 5307

MONITORED BY
Phillips Laboratory
Contract F19628-89-C-0216

The views and conclusions contained in this document are those of the authors and should not be interpreted as representing the official policies, either expressed or implied, of the Defense Advanced Research Projects Agency or the U.S. Government.

This technical report has been reviewed and is approved for publication.

JAMES F. LEWKOWICZ
Contract Manager
Solid Earth Geophysics Branch
Earth Sciences Division

JAMES F. LEWKOWICZ
Branch Chief
Solid Earth Geophysics Branch
Earth Sciences Division

DONALD H. ECKHARDT, Director
Earth Sciences Division

This report has been reviewed by the ESD Public Affairs Office (PA) and is releasable to the National Technical Information Service (NTIS).

Qualified requestors may obtain additional copies from the Defense Technical Information Center. All others should apply to the National Technical Information Service.

If your address has changed, or if you wish to be removed from the mailing list, or if the addressee is no longer employed by your organization, please notify PL/IMA, Hanscom AFB, MA 01731-5000. This will assist us in maintaining a current mailing list.

Do not return copies of this report unless contractual obligations or notices on a specific document requires that it be returned.

REPORT DOCUMENTATION PAGE

Form Approved
OMB No 0704-0188

1. AGENCY USE ONLY (Leave blank)	2. REPORT DATE	3. REPORT TYPE AND DATES COVERED
	20 May 1992	Final Report 8/1/90 - 2/28/92

4. TITLE AND SUBTITLE

Specialized Studies in Yield Estimation.

5. FUNDING NUMBERS

PE 62714E
PR 9A10 TA DA WUBJ
Contract #
F19628-89-C-0216

6. AUTHOR(S)

L. J. Burdick, C. K. Saikia, J. P. McLaren,
L. S. Zhao, & D. V. Helmberger.

7. PERFORMING ORGANIZATION NAME(S) AND ADDRESS(ES)

Woodward-Clyde Consultants
566 El Dorado Street, Suite 100
Pasadena, CA 91101

8. PERFORMING ORGANIZATION REPORT NUMBER

9. SPONSORING/MONITORING AGENCY NAME(S) AND ADDRESS(ES)

Phillips Laboratory
Hanscom AFB, Bedford, MA 01731-5000

Contact Manager: James Lewkowics/GPEH

10. SPONSORING/MONITORING AGENCY REPORT NUMBER

PL-TR-92-2070

11. SUPPLEMENTARY NOTES

12a. DISTRIBUTION/AVAILABILITY STATEMENT

Approved for Public Release; Distribution Unlimited.

12b. DISTRIBUTION CODE

13. ABSTRACT *(Maximum 200 words)*

Although the main problems with test ban treaty monitoring involve improving methods for discrimination of source types, there are certain problems of continuing interest in the field of yield estimation. In terms of short period body waves and the dependence of m_b on yield, these involve the effects of anelastic attenuation, pP, nonlinear phenomena such as spall and the influence of 3D structure on amplitudes. A related problem involves the transportability of yield scaling relationships between sites in different tectonic settings. We have carried out a number of studies directed at solving these problems. Much of the work has been presented in previous reports, but common themes among the studies are the use of a waveform analysis technique called intercorrelation and a focus on the use of the newly released data from internal Soviet stations. The first study reported here concerns the use of the intercorrelation approach on the onset of regional P_n waves to estimate yield. The yield dependence of the source time functions can be clearly observed and measured in the data. The importance of the method is that it provides a yield estimate based on an entirely new type of information (the waveform of the onset of P_n), and it is the type of information available from very small events at short distances. These are the types of data most crucial in the current treaty monitoring environment. The second study is an examination of broad-band yield scaling laws from all U.S. test sites and a correlation with them of results from Soviet sites. The important off-test-site events, GASBUGGY, RULISON and FAULTLESS are considered. The third section considers trade-offs between yield estimation and Q for regional and far-regional data from the newly opened stations at GARM, ARU, OBN and KIV.

14. SUBJECT TERMS

Yield estimation, Intercorrelation, Regional data, Attenuation.

15. NUMBER OF PAGES

126

16. PRICE CODE

17. SECURITY CLASSIFICATION OF REPORT	18. SECURITY CLASSIFICATION OF THIS PAGE	19. SECURITY CLASSIFICATION OF ABSTRACT	20. LIMITATION OF ABSTRACT
UNCLASSIFIED	UNCLASSIFIED	UNCLASSIFIED	SAR

TABLE OF CONTENTS

INTRODUCTION

The scope of the project includes a number of separate specialized investigations directed at solving problems associated with yield estimation utilizing short and long period body waves. We here present the results of our research on three of them. In terms of short period body waves, these problems involve the effects of anelastic attenuation, pP and nonlinear effects such as spall on seismic amplitude and on m_b. In a portion of the work, we have developed an entirely new approach to yield estimation. In another we have investigated the transportability of yield scaling laws from site to site, considering both U.S. and Soviet testing areas. We also have performed studies on the effects of regional and teleseismic Q on attempts at estimating explosion source strength.

The first study which is reported on is an attempt to generalize the relative waveform analysis procedure called intercorrelation, to regional teleseismic P_n waves. This approach has been used almost exclusively to analyze teleseismic data in the past. There is a current need to characterize the behavior and uncertainty in magnitude-yield relations down to body wave magnitudes which are as small as possible. Of course, the seismic data with good signal to noise ratios for such small events will be restricted to regional distances. It has recently come to light that the P_n waveform in the western U.S. is highly stable and that it shows a strong variation with event size. Intercorrelation has been used to measure source function scaling for well coupled events below the water table down to magnitude 3.9. It has been established in a number of separate studies by many investigators that the behavior of pP from nuclear tests is not consistent with elastic reflection from a simple point compressional source. Direct observation of isolated pP_n appears to confirm this. Because of the relatively low attenuation of P_n with respect to teleseismic P, it is possible to isolate the direct P_n arrival from pP_n. The parameters of the source time function can be studied independently from this data using the intercorrelation approach. It was found that the relative yield of events could be reliably determined from the direct P_n wave shapes alone using the method.

The second investigation we have undertaken is a study of the broad-band nature of seismic signals from explosions. We examine both long period and short period types of information in an attempt to develop yield scaling laws which are highly transportable. Along with the usual short period body waves on which standard m_b-yield curves are based, we consider such information as long period P, long period pS and near field signals. We consider all the U.S. test sites including those of GASBUGGY, RULISON and FAULTLESS, which are essentially single event sites and the NTS and Amchitka testing areas. We correlate our results with those from the Soviet test site at Shagan River.

Though the new internal seismic data from the Soviet Union is exciting and very significant to the yield estimation process, it is still relatively sparse and the familiar problems of trade-offs between Q and explosion source strength emerge. We have undertaken two unusual studies of Q, one involving regional data and the other far regional to teleseismic data. In the former, we examine Pnl data from the Soviet station at GARM and compare it to similar data from the U.S. station at Harvard. In the latter, we consider broad-band data from Soviet stations KIV, OBN and ARU.

INTERCORRELATION OF REGIONAL P_n

The first study we will discuss is an attempt to take advantage of some recent observations made by Burdick et al. (1991c) regarding the waveform of the onset of regional P_n. It appears clear that these waveforms are very directly comparable to those of teleseismic P. Rather than being true head waves, these arrivals seem to be turning rays in the uppermost mantle above the low velocity zone. At short times, they can be represented as a simple convolution of a source, Q and instrument operator just as teleseismic short period P can. However, because they never penetrate the low velocity zone, the effect of attenuation is tremendously reduced. Instead of t^* having a value of approximately 1.0 s, as it does for teleseismic P from NTS, it has a a value close to 0.1s; an order of magnitude change in the exponential. This allows the direct P to be separated from the pP through simple time domain windowing.

Before discussing the regional P_n yield scaling behavior, we will review the procedure known as waveform intercorrelation. It is a method which allows the reduction of the observations of many events at a common test site to source models for the events. The source models are parameterized mathematical functions which describe the reduced displacement potential and, for teleseismic data, a representation for the free surface interaction and perhaps even spall. The RDP representation is typically an explicit function of yield with the free parameters defined in terms of yield scaling laws. The changes in the shape of the RDP for events at a common site are thus related to changes in yield. The key advancement in this study is that the free surface parameters can be neglected. The most important goal is to attempt to estimate yield directly from the evolution of the **shape** of the P_n onset.

The classic intercorrelation procedure is illustrated in Figure 1. Each seismogram from a given event is convolved with the source function and a spike train representing P and pP from another event. The seismograms from the other event are convolved with the P+pP spike train and parameterized RDP from the first event. The two intercorrelation waveforms at each station are then analytically compared to each other and the source functions that produce the best waveform

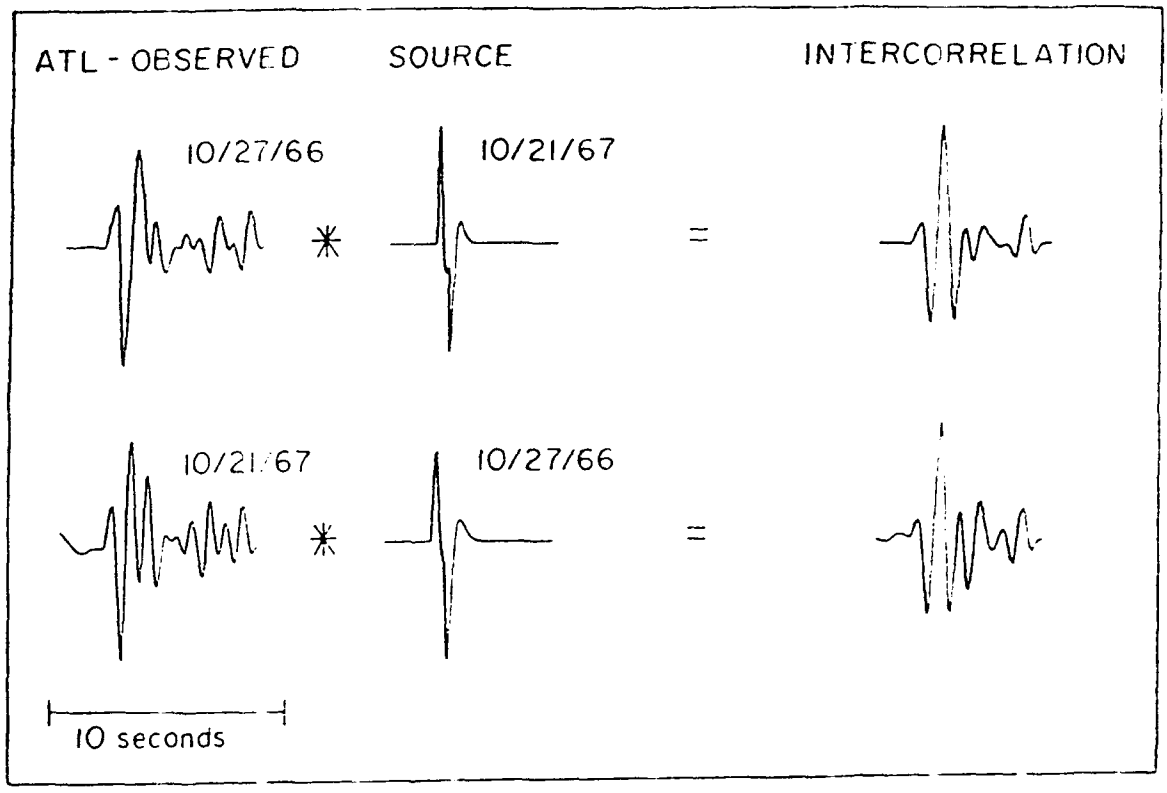

Figure 1. An Illustration of the standard intercorrelation procedure. The left column shows two teleseismic short period P waveforms from a common test site at a common station. The center column shows source estimates for each event paired with the signals from the opposite event. The source estimates are described in terms of both a source time function and pP reflection. The cross-paired sources and records are convolved and the resultants equlaized in a grid search operation using an analytic norm. The results for this case are shown on the right. In the new procedure used here, the pP phase is windowed out and only the source parameters are searched for.

match are found. The procedure is applied to all possible matching stations simultaneously. In th s instance, these are two Novaya Zemlya events as observed at station ATL. The equalization of the two dissimilar waveforms on the left after the intercorrelation procedure is very good as shown on the right.

To incorporate differences in event yields, it is necessary to adopt a parameterized description of the explosion source. Such parameterizations are abundant in the literature (Murphy, 1977; von Seggern and Blandford, 1972; Helmberger and Hadley, 1981). Here we adopt the Murphy (1977) source representation and yield scaling though we emphasize that the other two are equally valid and would perform as well if need be. The intercorrelation waveforms for each station pair are typically compared using one or two norms. The waveform norm is given by

$$N_w = \frac{1}{n}\Sigma(1 - CCC)$$

CCC is the normalized cross correlation coefficient and n is the number of stations. This norm is most sensitive to differences in zero crossing times and is often used in waveform inversion studies. Absolute amplitude information is typically retained using a standard least squares norm if need be, but in this investigation we have utilized only the waveform norm.

Over the past few decades the state of digital-broad-band seismic recording has gone through a major revolution. Fortunately for the endeavor of test ban treaty monitoring, many of the highest quality stations were located in the western U.S. where they recorded many NTS nuclear events. Figure 2 is a map of the stations from which we have assembled the data base we have used in this work. The stations shown were installed over a substantial period of time and illustrate the development of digital seismic recording. The ones which were installed first were DWWSSN stations ALQ and JAS. Recording was and is made in several pass-bands and is available on the standard Network Day Tapes. The four LLNL stations, MNV, ELK, KNB and LAC represent a major upgrade in recording capability because they are broad-band with a wide dynamic range. (We note that there were important analog stations at these same sites decades in the past.) The

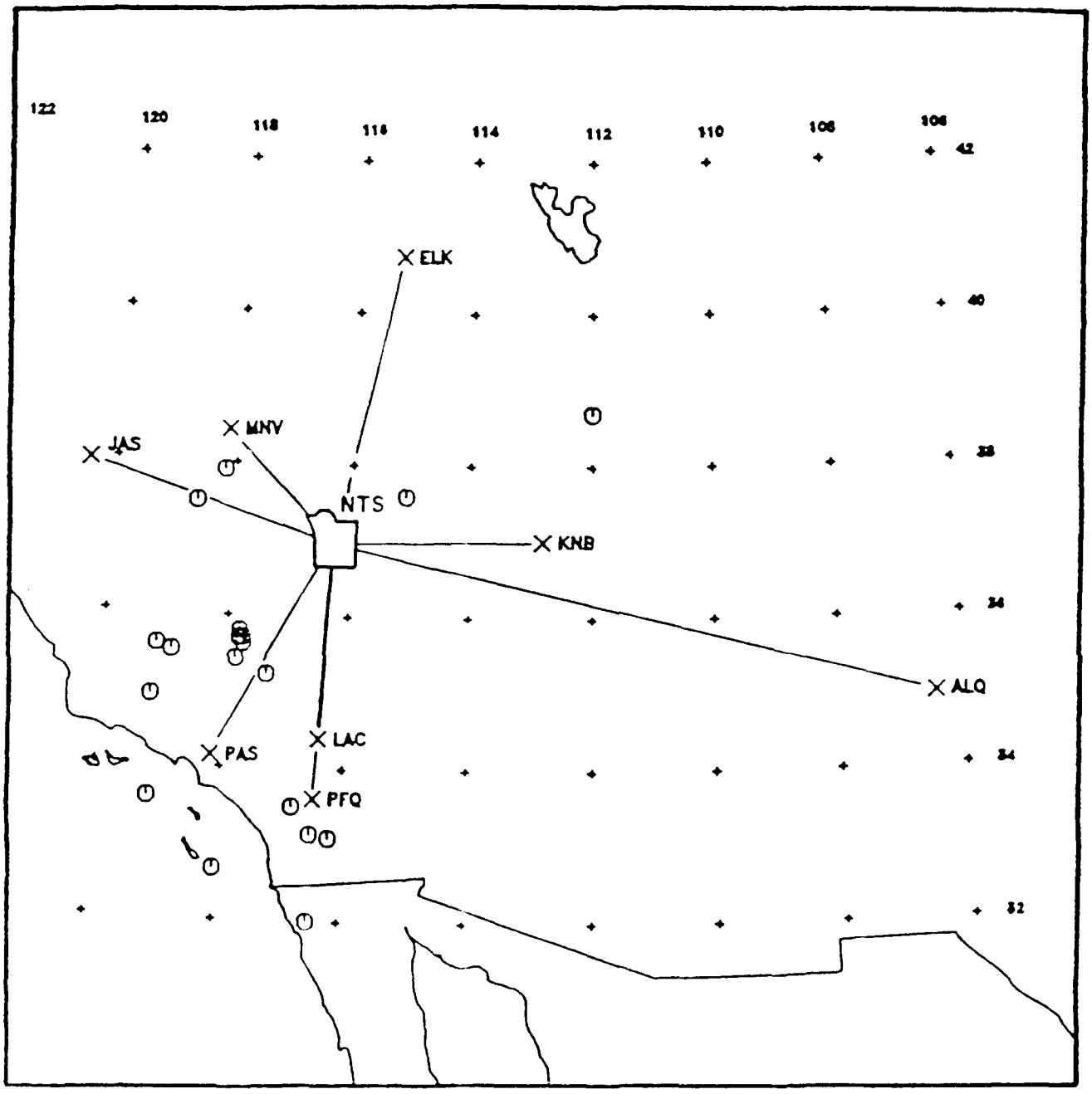

Figure 2. The western U.S. digital array as defined for the purpose of this study. MNV, KNB, LAC and ELK are LLNL stations. ALQ amd JAS are DWWSSN stations, and PAS and PFO are university run stations. The open circles are the location of earthquakes in the discrimination data base.

two stations PAS and PFO have state-of-the-art Streckeisen instruments which are the same as those used in the IRIS net. The important point in terms of his study is that they all record regional P_n and have provided an ample data base for this investigation.

The concept of using the intercorrelation methodology to measure yield from the onset of regional P_n is not without foundation. In a recent work, Burdick et al. (1991c) showed that this onset was simple, stable and easy to interpret in terms of the standard concepts used to analyze teleseismic short period P waves. Figure 3 shows some of the typical data from the Burdick et al. (1991c) study. Observed deconvolved velocity waveforms from 4 Yucca Flat events as recorded at digital station MNV are shown in solid line. Almost 1.5 orders of magnitude are represented between the largest and smallest events. The frequency difference between them is clear even in the time domain. Synthetics computed using the Murphy (1977) source and an assumption of elastic pP behavior are shown as dashed lines. The observed and predicted pP arrivals are indicated by arrows. The observed pP_n arrivals are late and close to the elastic predictions in size, but in any case, in this representation it is simple to window out the distinct direct Pn arrival. In passing, we note that these observations lend additional credence to the intercorrelation results as opposed to spectral averaging results. We also note that the Murphy (1977) predictions of change in frequency content between the largest and smallest event are not satisfactory. The predicted changes in time function are less extreme than the observed. The data available from LLNL is limited, but in reviewing it we did find signals from eleven Yucca Flat events below the water table. Figure 4 compares the waveforms at common LLNL stations for the smallest and the largest, BORREGO (m_b = 3.9) and JORNADA (m_b = 5.9). The change in frequency content at all stations is dramatic. Under each complete P_n trace is a windowed trace where the window is a trapezoid with an 0.5 s lead a 1.0 s level beginning at estimated onset time and an 0.5 second fall. There are clearly waveform differences between the stations, particularly at ELK, but the principle of intercorrelation is to characterize the changes in waveshape at fixed stations allowing for the possibility of complex path effects. The window should allow good spectral measurements up to frequencies of 1 hz.

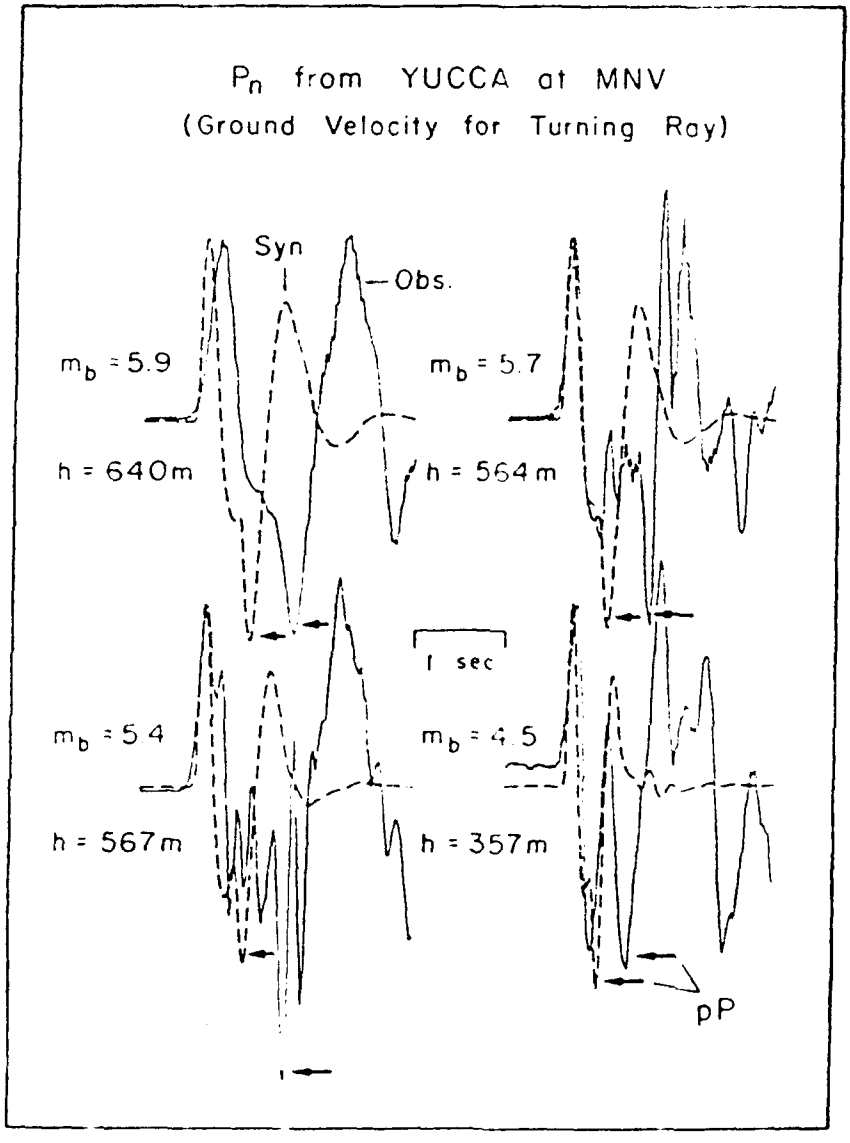

Figure 3. An illustration of the Pn waveform observations which motivate this study. Observed waveforms are shown as solid lines and synthetics as dashed. The pPn is a downward pulse as indicated by an arrow in both the data and the synthetics. The pPn is delayed in the observations and can be windowed out. This permits intercorrelation analysis of the isolated direct arrival.

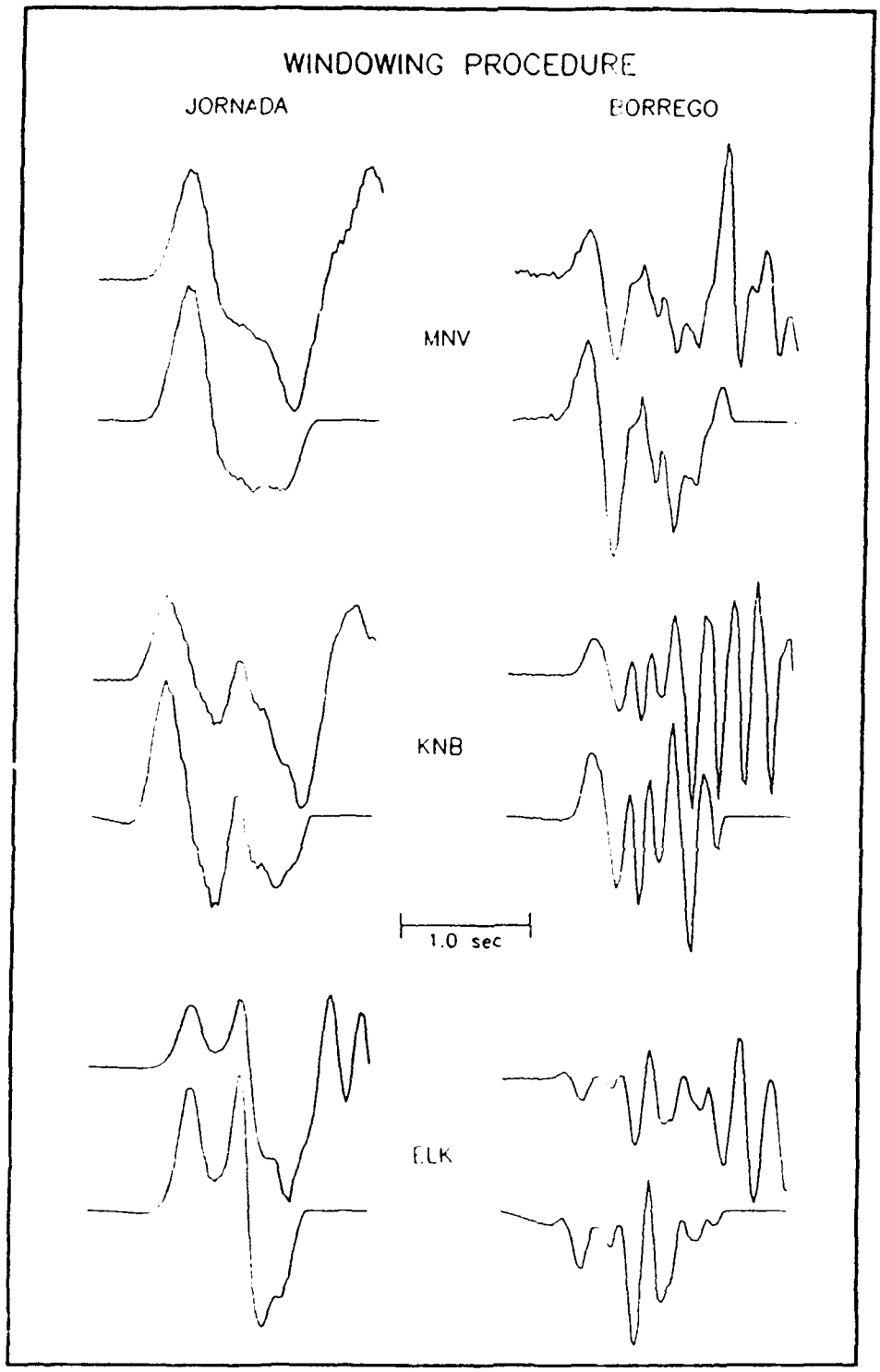

Figure 4. An illustration of the windowing procedure. The top trace shows the initial pulse. It is windowed with a trapazoid with an 0.5 s rise, an 0.75 s level time commencing at estimated arrival time and an 0.5 s fall. The removal or at least strong reduction of the pPn is apparent.

The procedure for intercorrelation has been presented in many previous reports (Burger et al., 1986, Lay et al., 1984a, Lay, 1985, 1991). As discussed above, the basic idea is to choose a reference event and an estimated source function for that event. If the signal includes pP, then pP parameters must also be included, but in this case, only direct P_n is present. We selected BORREGO and used the Murphy (1977) source. The procedure is then to find a source function for each other event which minimizes the differences between waveforms when a cross-convolution is performed. Since the depth of these events is known, the only free parameter is yield, and we simply stepped through yield values to find those for the non-reference events which optimized the waveform norm. The yield of BORREGO was estimated to be 0.7 kt from the scaling relation of Yacoub (1984) based on WWSSN records (Network AA) of Pahute and Yucca events below the water table. Figure 5 shows an additional unprocessed example for BORREGO and BOUSCHET which are also Yucca Flat events below the water table. This pairing of events is quite remarkable since they had identical depths. The shift in frequency content is quite clear, and because the depths are identical, it is almost certainly due to yield scaling. Figure 6 shows the results of the intercorrelation of those two events. The fits are quite remarkable in this example. It should also be noted that we are cross correlating waveforms from events differing by two orders of magnitude in size. The match of the complexity at ELKO is worth special recognition, and it would seem to indicate that the intercorrelation approach accounts for complex site effects as it was designed to do.

Figures 7 and 8 show similar initial and intercorrelated results for Yucca events above the water table. The reference event was selected as CORREO and the test event was TENAJA. In general, it seems best to select the smallest events for reference, perhaps because they have the richest frequency content. That is to say that the for the largest events, the high frequency information is washed out. The complexity of the ELKO station is still apparent and the equalized records for that station are comparable for events above and below the water table. The assembly of a data base for Pahute Mesa events below the water table is problematical since only a few have

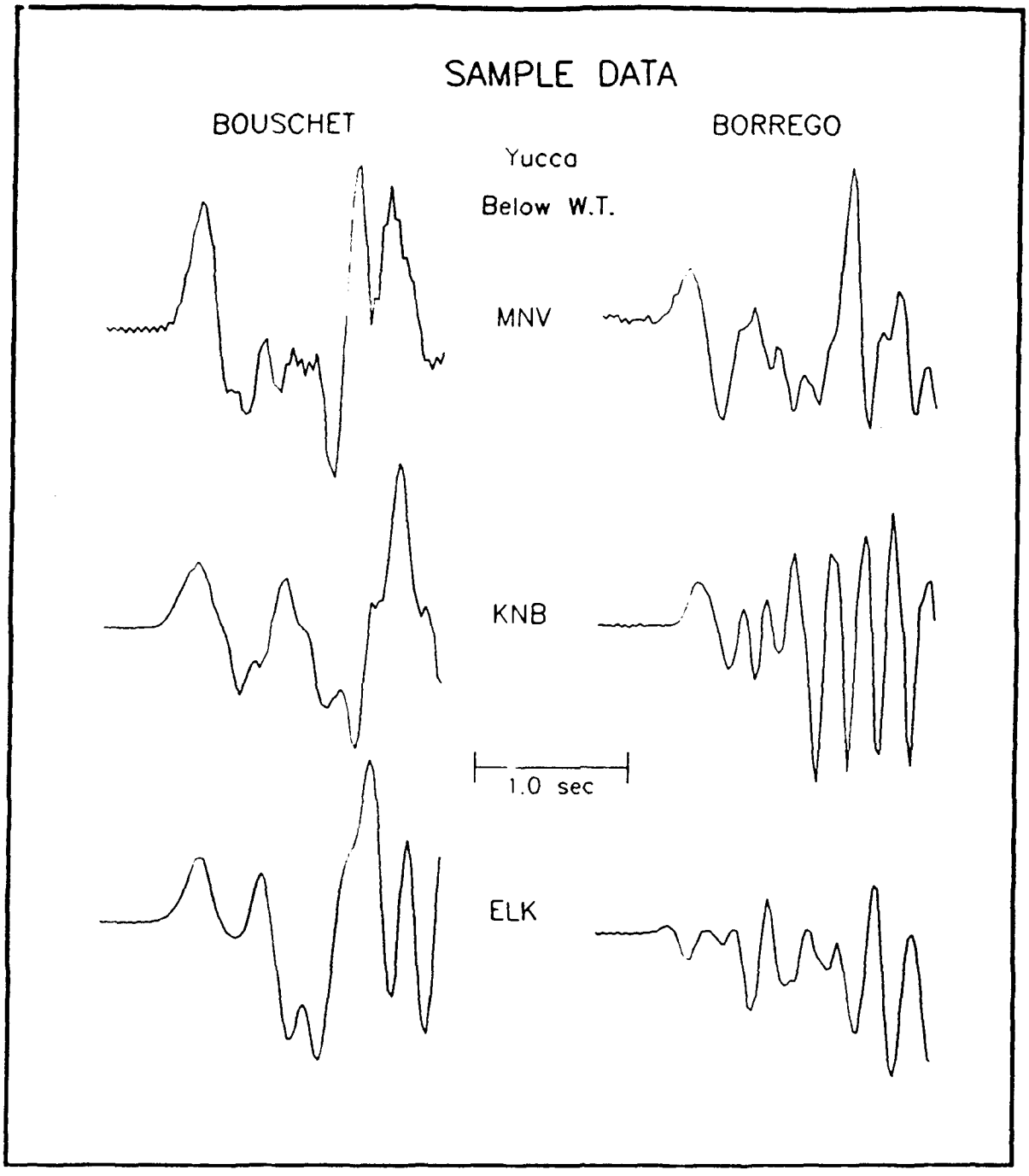

Figure 5. These are sample observations from one of the events in the data base of Yucca Flat events below the water table. The reference event on the right (BORREGO) had a depth of 564 m but a magnitude of only 3.9. BOUDCHET had a magnitude of 5.7 at the same depth. The shift in frequency content due to yield dependent variation in the source function is clear. Since it can be readily observed it can be quantified through intercorrelation analysis.

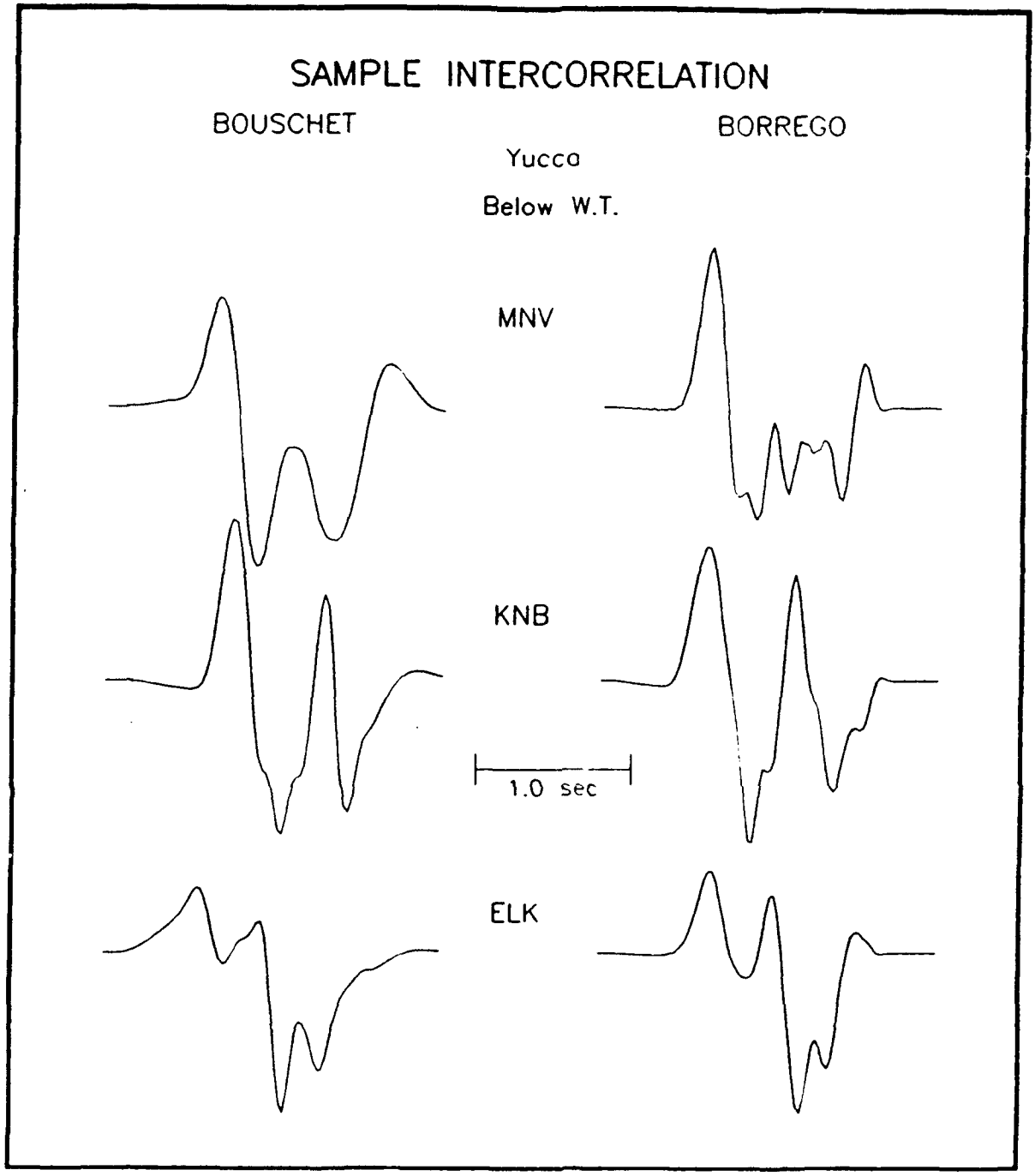

Figure 6. These are the intercorrelated signals shown in unprocessed form in Figure 5. The waveforms have been clearly equalized. The yield of the reference event was estimated at 0.7 kt from a standard NTS mb - yield relationship. The yield of BOUSCHET was estimated at 80 kt.

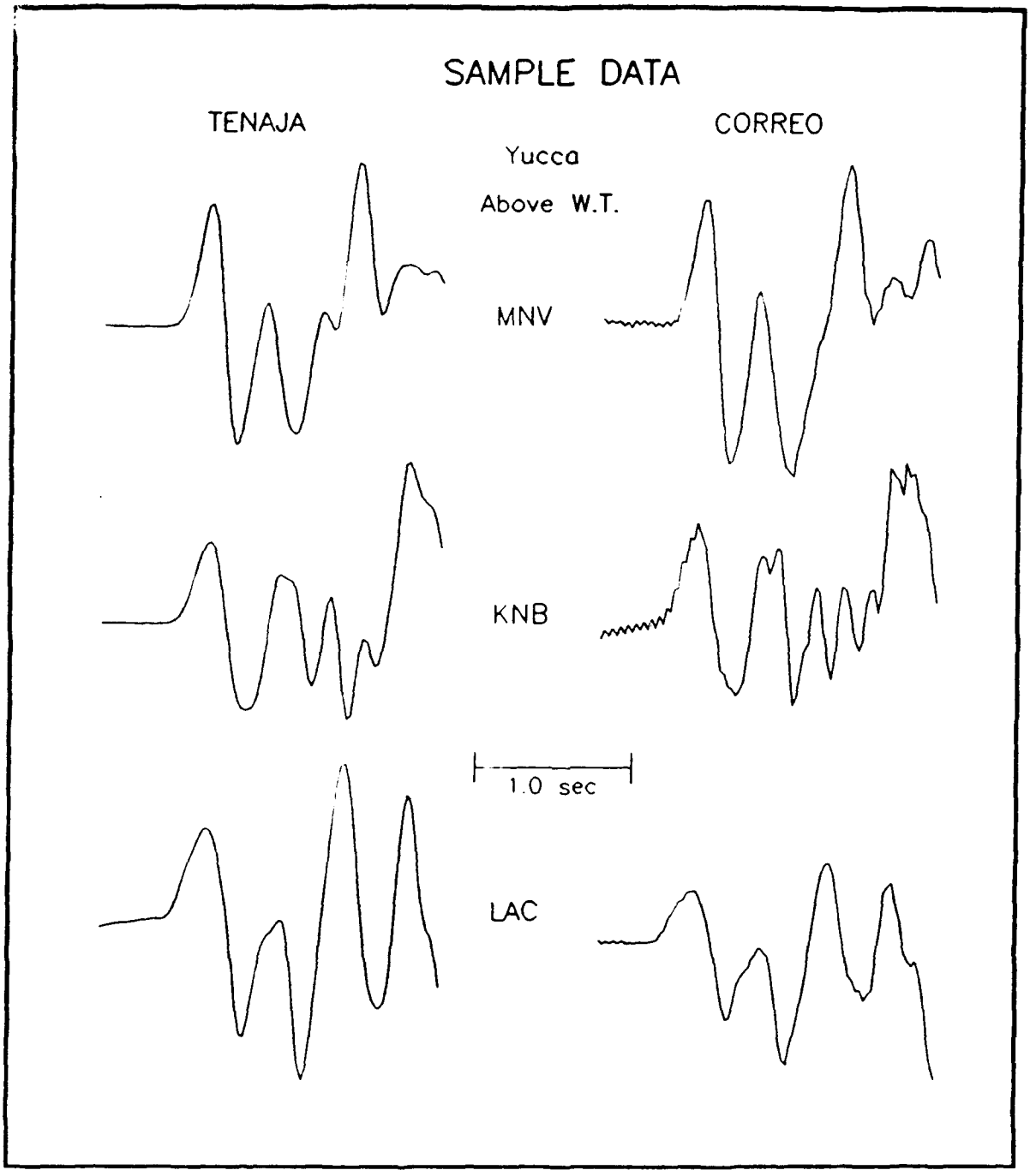

Figure 7. These are illustrative waveforms from the data base of Yucca Flat events above the water table. The events are shallower than those in the previous example, so windowing out of pP is less effective. The reference event selected for the analysis of this data base was CORREO with a depth of 335 m and a magnitude of 4.8. In this example TENAJA has a depth of 357 m and a magnitude of 4.5.

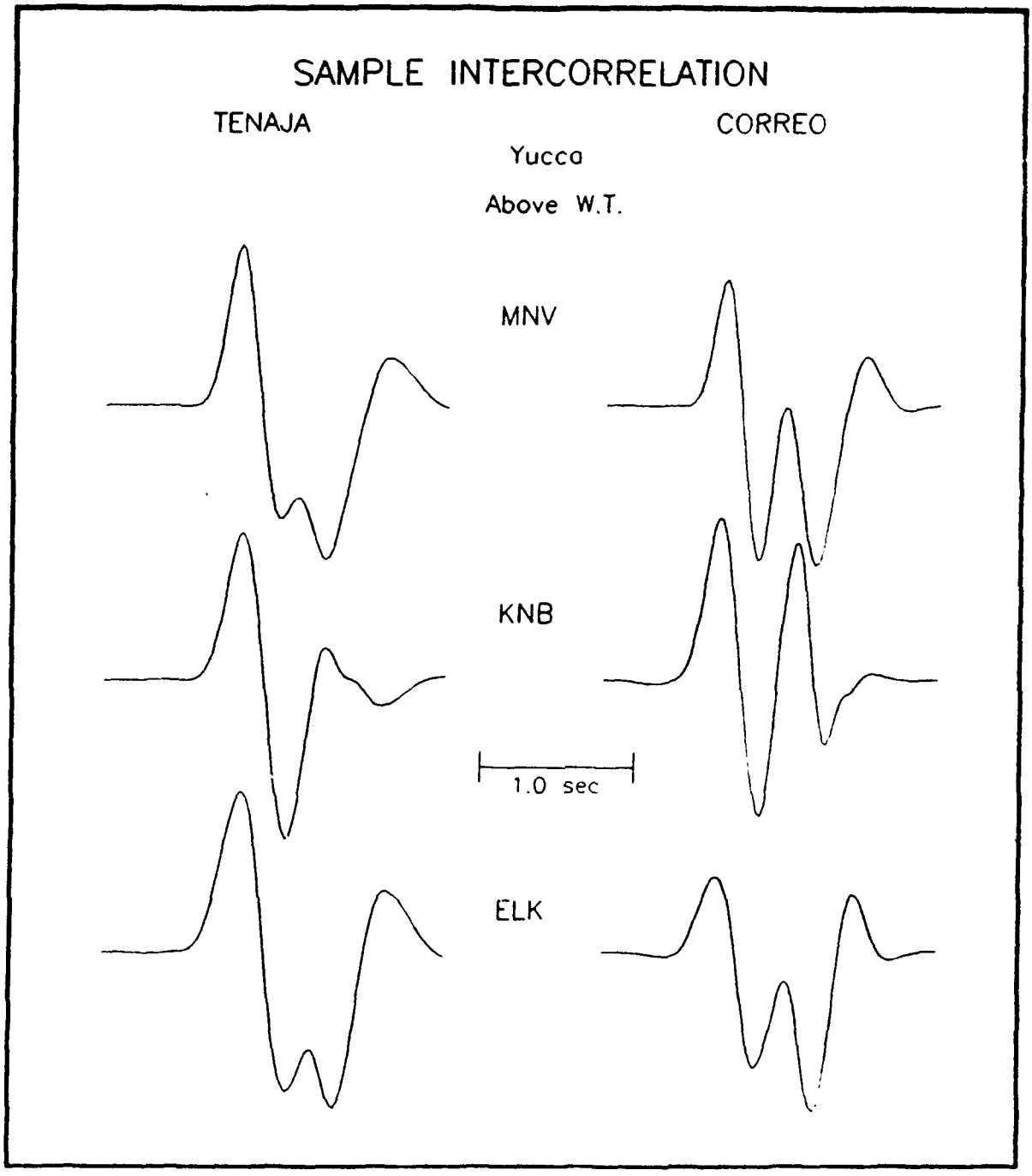

Figure 8. These are the intercorrelated signals shown in unprocessed form in Figure 7. The waveforms have again been effectively equalized using only the source function in the intercorrelation. The yiels of the reference event was estimated at 9.4 kt. The yield of TENAJA was estimated at 10 kt.

been detonated since the threshold test ban agreement of 150 kt. In the data base available from the LLNL digital stations, only two such events were recorded. To perform a partially legitimate test of our approach, we again selected BORREGO (Yucca Flat below the water table) as a reference event. Figure 9 shows the raw signals and Figure 10 shows the intercorrelation for event TOWANDA. The equalization of the waveforms is remarkable and the unusual complexity of the ELKO record persists. Finally, Figures 11 and 12 show samples of the raw data and intercorelations for Pahute events above the water table. The reference is KAPPELI and the test event is HOSTA. The procedure again appears successful.

As discussed above, we applied intercorrelation analysis to all the events available in our data base to predict the yield scaling behavior and to compare it to expected results. We review here exactly how the analysis proceeds once the relative yield has been determined. There are two basic goals in the structure of the analysis. The first is simply to estimate a yield for the master event. The second and much more important goal is to loosely relate our results to the widely accepted rules for yield scaling. There is little debate regarding the m_b-yield scaling relationships for events larger than 100 kt at NTS. From several possible choices, we selected the scaling law of Yacoub (1984). We then accept either the ISC or LLNL body wave magnitude (ISC preferred) for the master event. We then derive a yield for the master event from the Yacoub (1984) law. From this point forward, the procedure is completely automated and depends only on the intercorrelation analysis. Figure 13 shows the results for Yucca flat events below the water table. The selected master event was BORREGO. The solid line in the graph is the Yacoub (1984) curve and thus the master event falls directly on it. The other events scatter evenly about the predicted curve. One of the events is JORNADA which is compared with BORREGO in Figure 4. The implication is clear. The strong change in frequency content of direct P_n in that figure is directly related to yield. Furthermore, the large event scaling law appears to hold down to events as small as BORREGO.

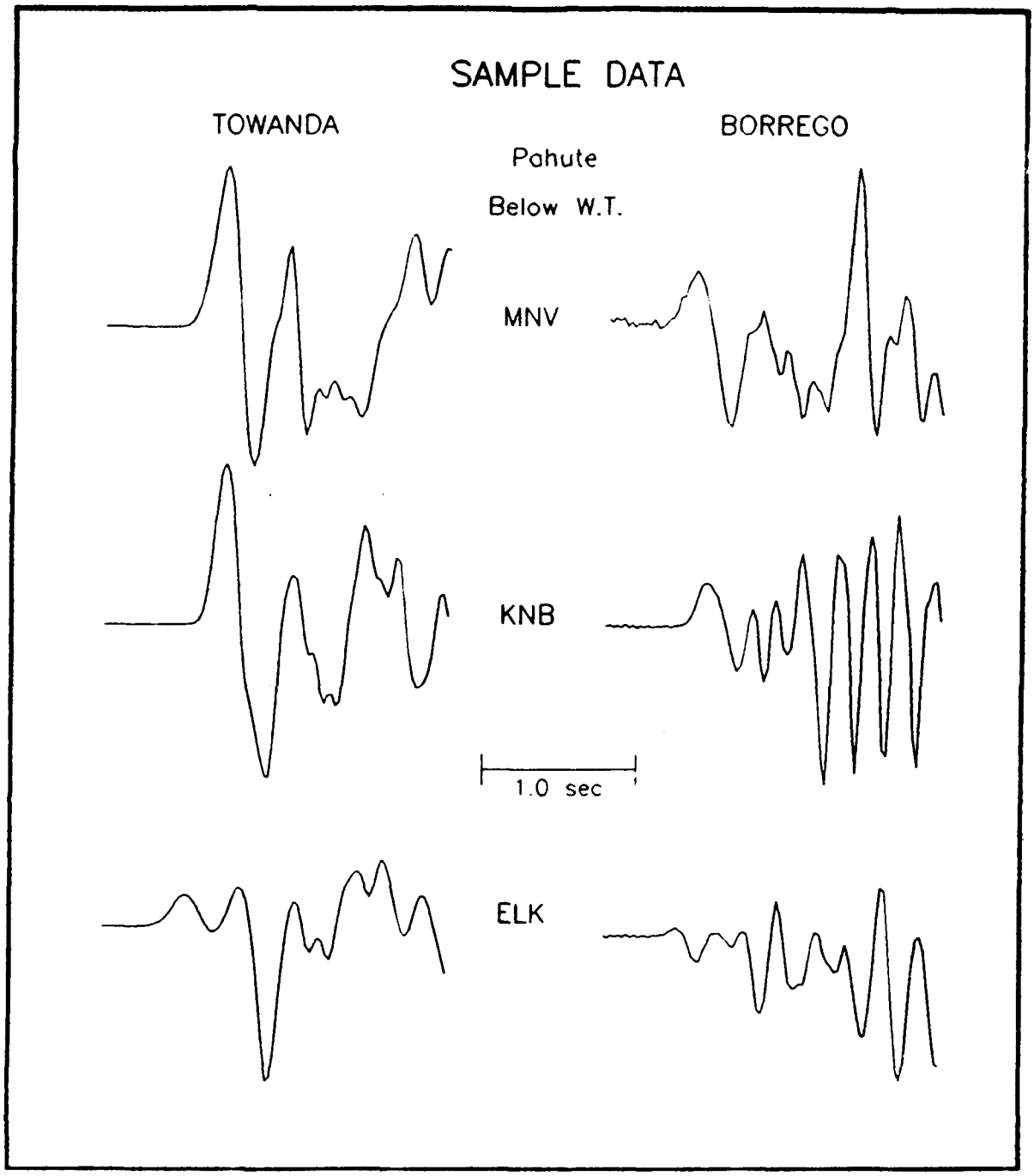

Figure 9. The waveforms on the left come form an event below the water table at Pahute Mesa. Only two events of almost identical size were available in the data base so BORREGO (Yucca below water table) was used as a reference as in Figure 5.

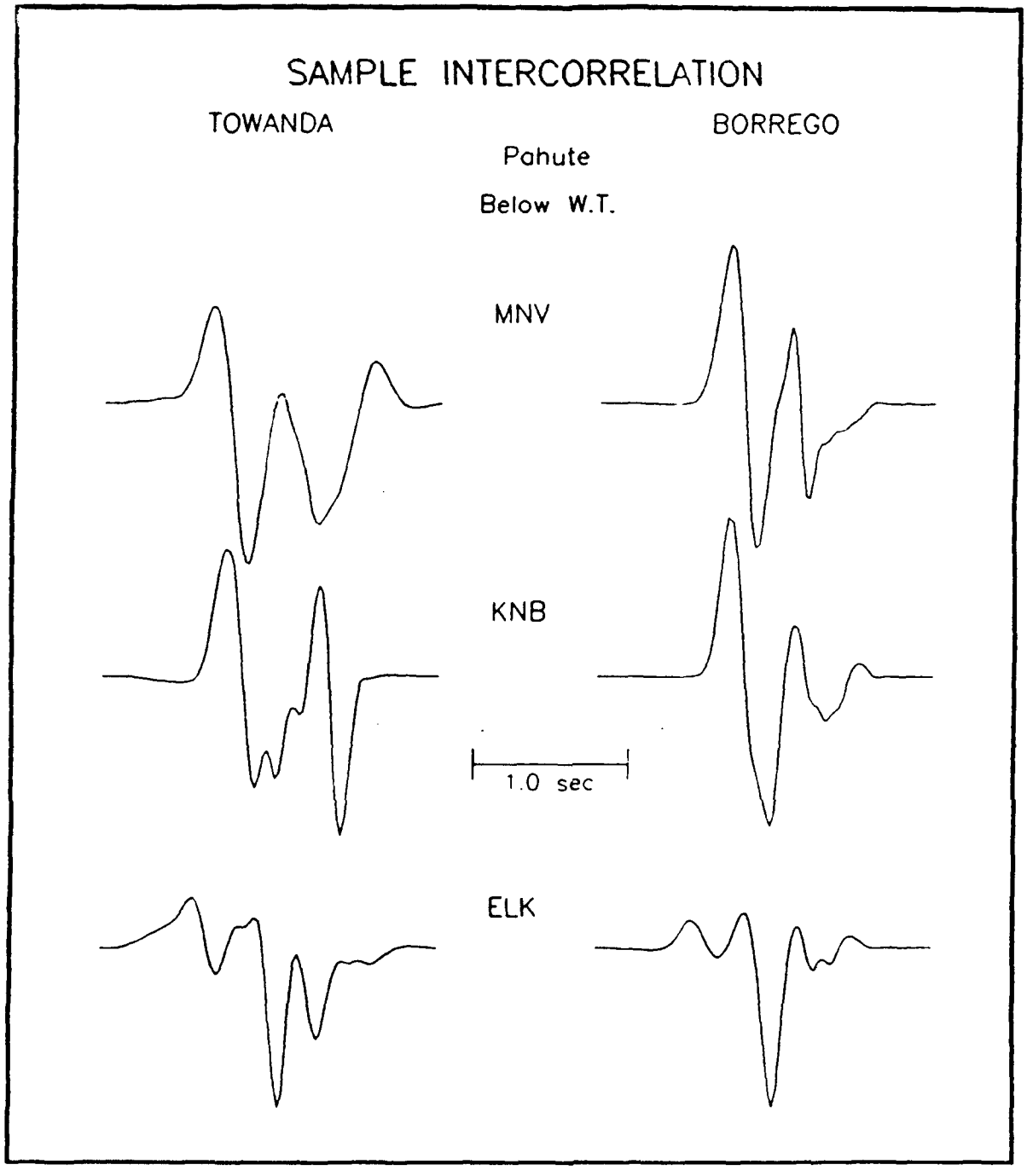

Figure 10. These are the intercorrelated signals shown in unprocessed form in Figure 9. The waveforms have again been effectively equalized using only the source function in the intercorrelation. The yield of the reference event was estimated at 0.7 kt and of TOWANDA at 24 kt.

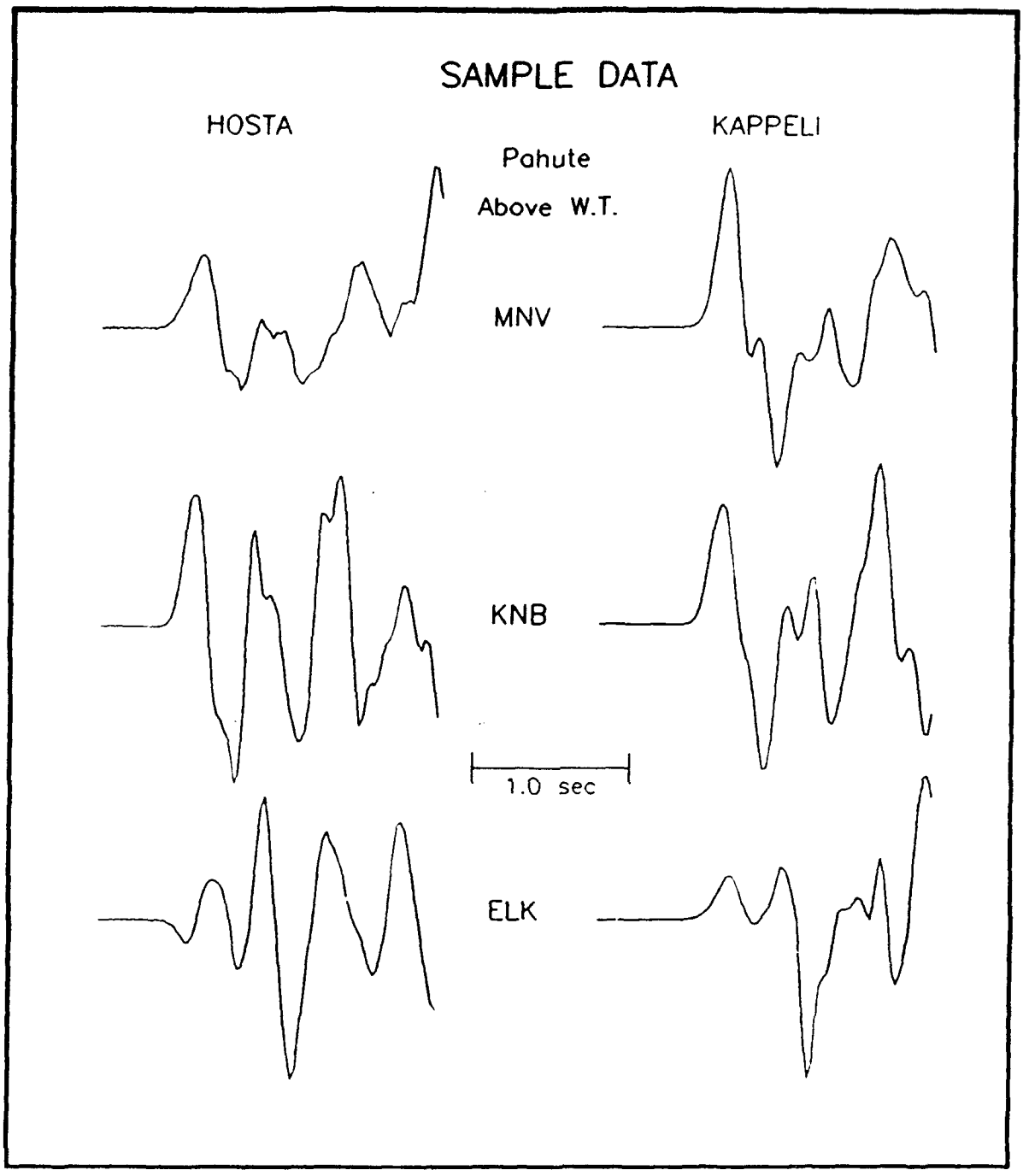

Figure 11. These waveforms are from Pahute events above the water table. The magnitude of reference event KAPPELI is 5.2 and of test event HOSTA is 5.6.

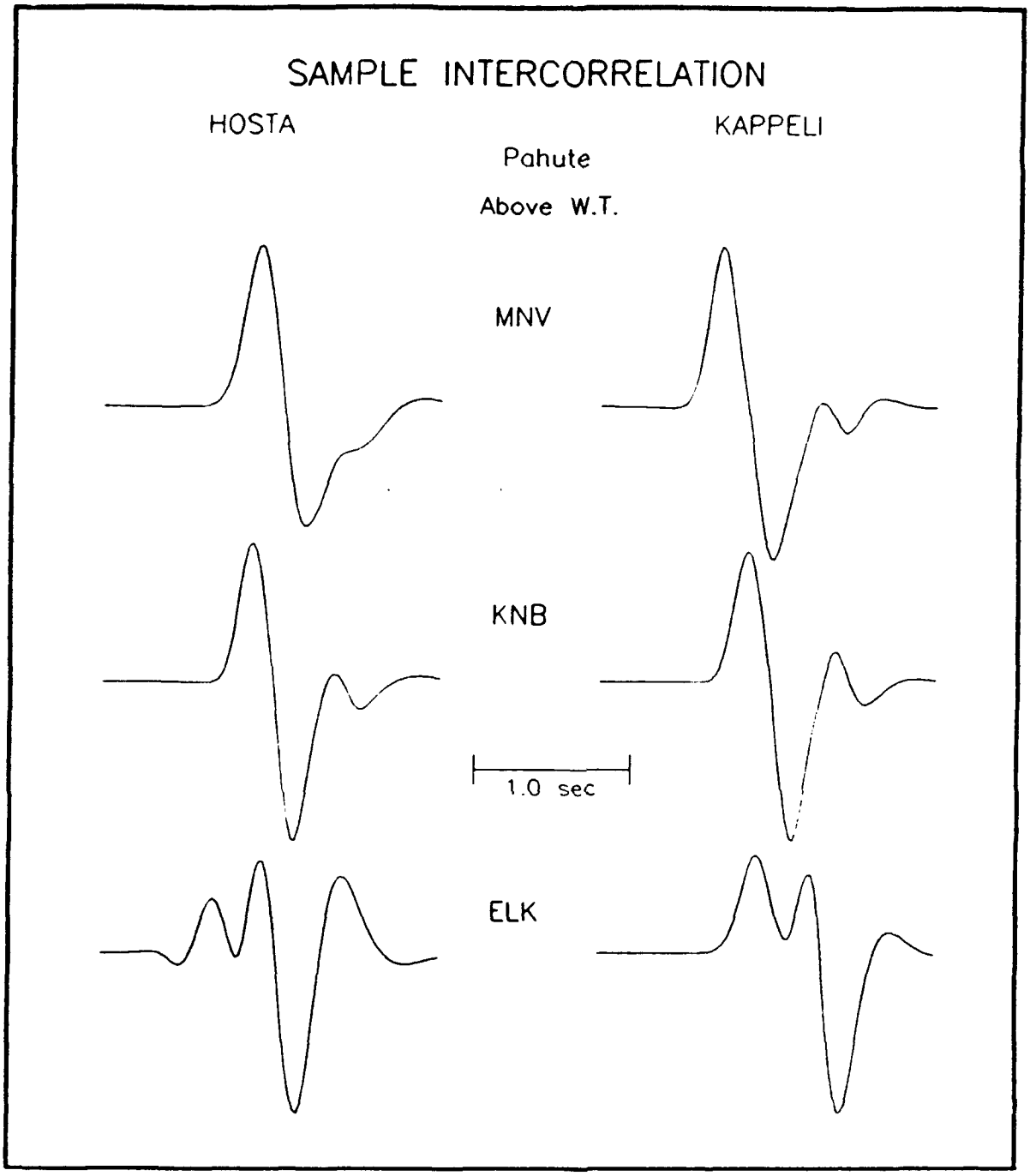

Figure 12. These are the intercorrelated signals shown in unprocessed form in Figure 10. The waveforms have again been effectively eqqualized using only the source function in the intercorrelation. The yields of the reference event was estimated at 35 kt and of HOSTA at 24 kt.

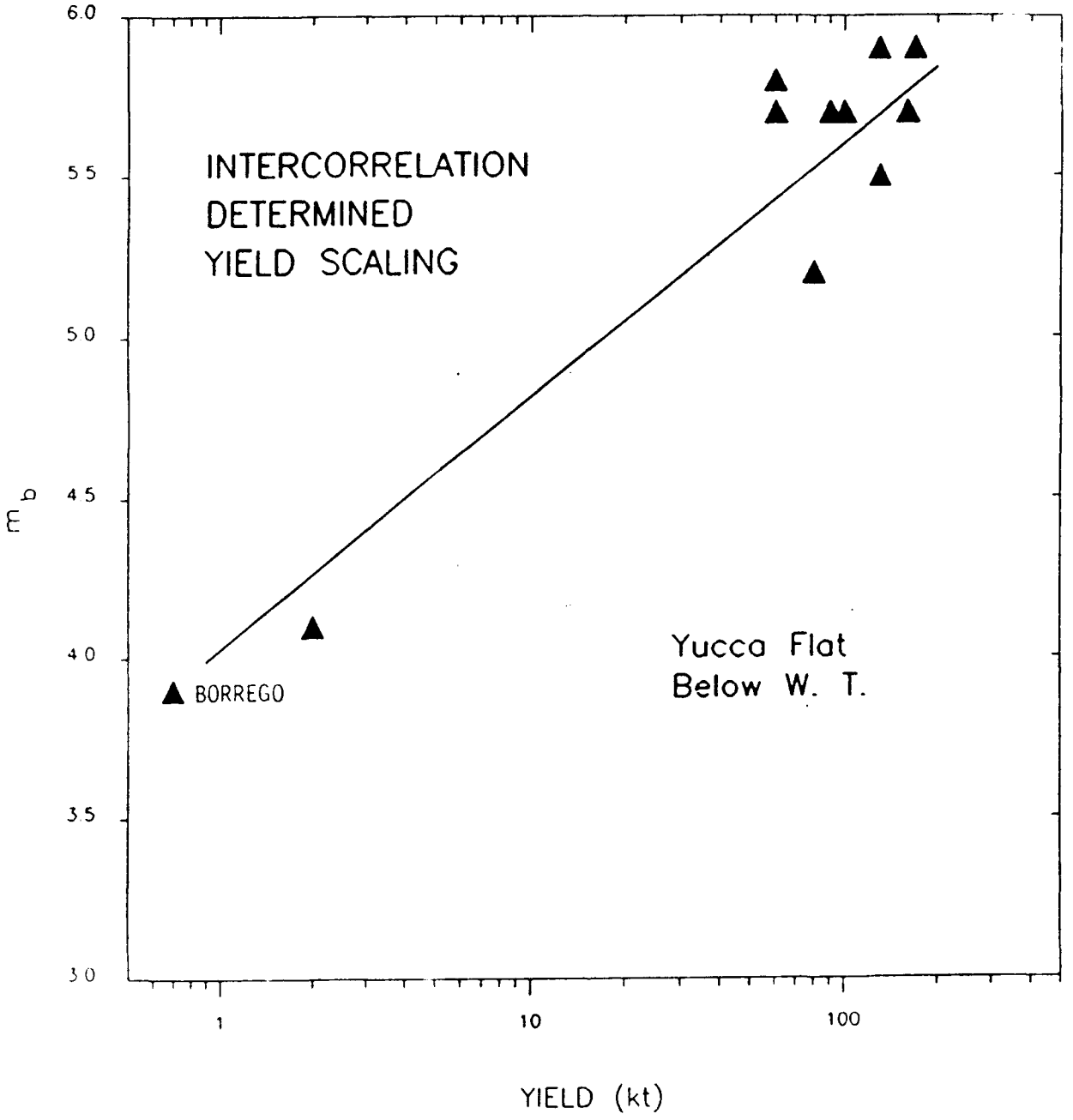

Figure 13. A comparison of yield scaling predictions based on only intercorrelation analysis of Pn compared to a standard scaling law for NTS. In this case, the data base included Yucca events below the water table. The reference event was BORREGO.

Figure 14 shows the results for Yucca Flat events above the water table. In this case, the reference event was chosen as CORREO which is approximately in the middle of the m_b distribution. The reason for this choice is that CORREO has the most complete recorded data base, though it is true that the smallest master events tend to give the best intercorrelation results. CORREO is near the top of the population as it distributes about the standard yield-scaling line. The remarkable fact is that the slope of the population follows very closely the prediction of the Yacoub (1984) line. There is an open question as to whether there are changes in slope of this line as events become very small. The evidence here is that the slope does not change for events with yields as low as about 2 kt. Also note that the distribution of events is much more even than in Figure 13. There seems to be little difference in behavior for events above and below the water table.

Figure 15 shows the results for Pahute events below the water table. As noted previously, there have been few such tests in recent history. BORREGO from beneath the water table was arbitrarily selected as the master. The Yacoub (1984) prediction holds reasonably well although a small increase in slope may be indicated by the data points. Figure 16 shows the results for Pahute Mesa events above the water table. The master event was chosen as KAPPELI. In this instance, there appears to be an indication of a decrease in slope in the data points. However, the distribution in magnitudes is quite limited. Clearly, the analysis of more data with a greater range of magnitudes would be desirable in the future.

Discussion: The importance of these discoveries in terms of modern treaty monitoring is very substantial. Though there is clearly the need for much more investigation, the P_n onset method of estimating yields represents a fourth new seismic approach for doing so, and one that can be used for very small events. The three classic methods are to examine m_b-yield scaling, M_S-yield scaling or M_0-yield scaling. The difference with the P_n onset approach is that it relies on wave shape changes as a function of yield as opposed to amplitude information, though the latter could certainly be incorporated into the procedure in the future. M_S scaling is generally simply a measure of the dependence of 20 second spectral amplitude on yield. Complete waveform information is

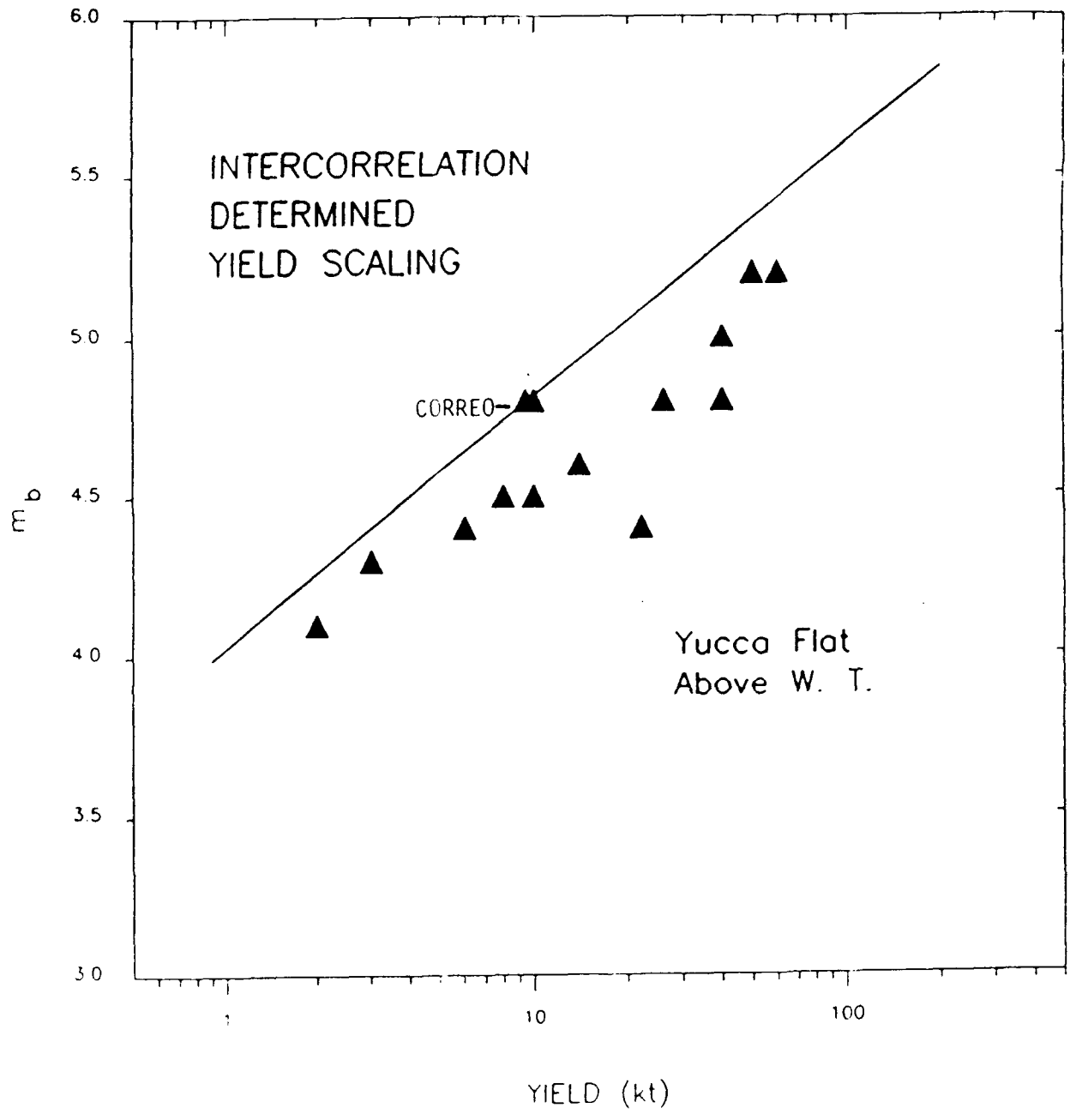

Figure 14. A comparison of yield scaling predictions based on only intercorrelation analysis of Pn compared to a standard scaling law for NTS. In this case, the data base included Yucca events above the water table. The reference event was CORREO.

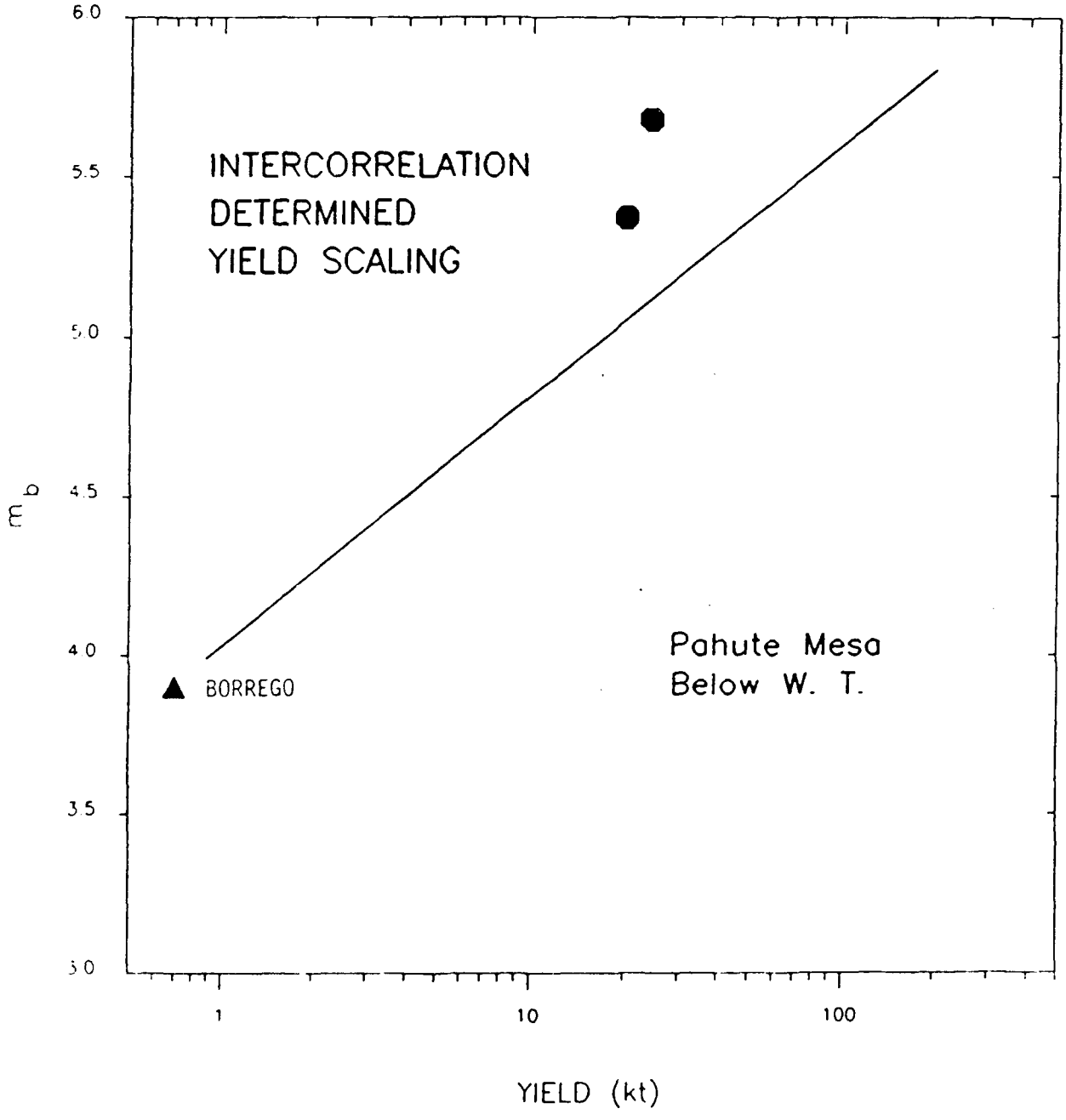

Figure 15. A comparison of yield scaling predictions based on only intercorrelation analysis of Pn compared to a standard scaling law for NTS. There were only two events available from Pahute below the water table. The reference event used was BORREGO (Yucca below the water table).

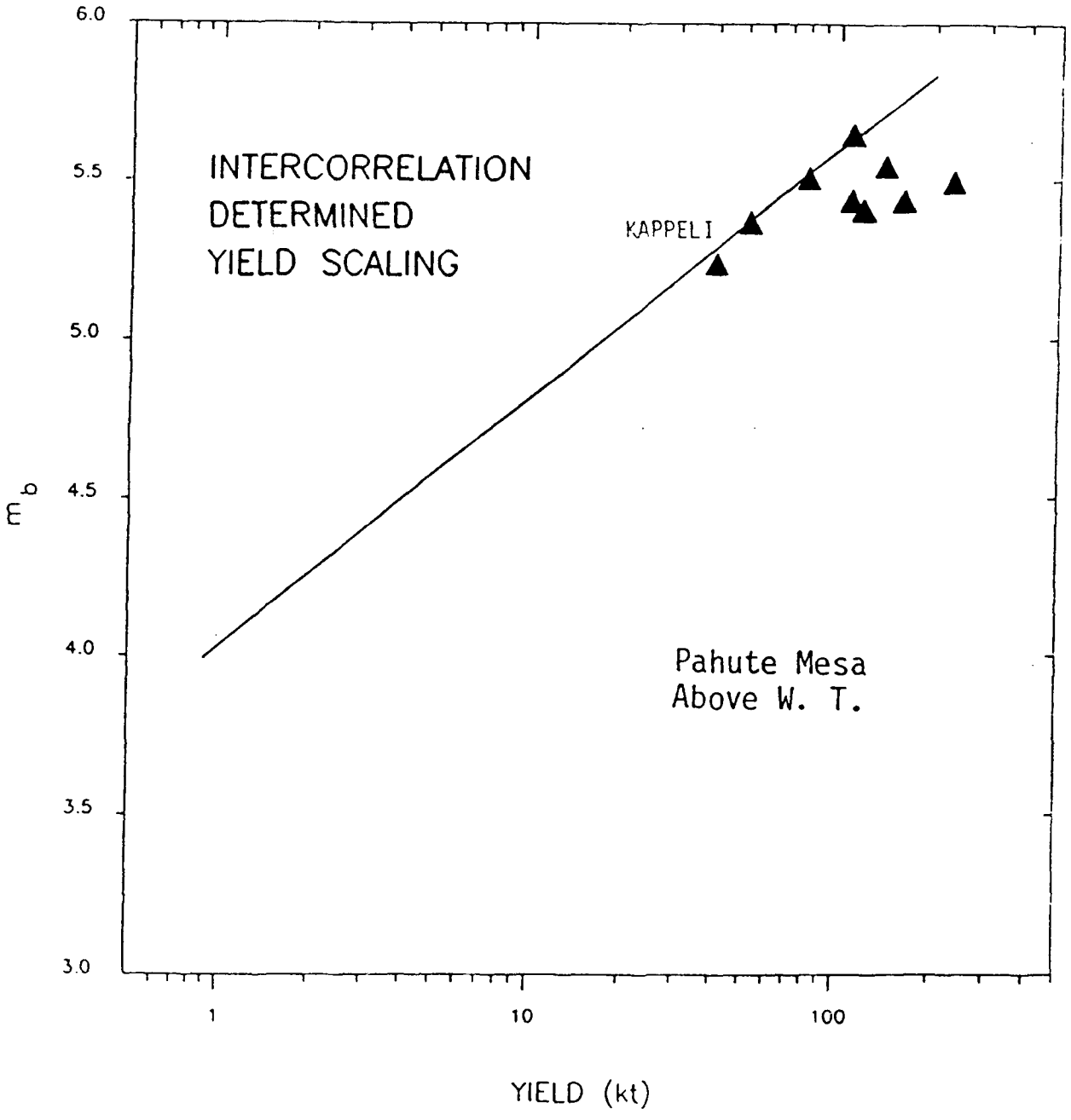

Figure 16. A comparison of yield scaling predictions based on only intercorrelation analysis of Pn compared to a standard scaling law for NTS. In this case, the data base included Yucca events above the water table. The reference event was KAPPELI. In this instance there appears to be some difference in slope between the intercorrelation measurements and the standard law.

not utilized. M_0 or moment scaling does utilize much more of the long period information, but both of these techniques suffer from serious difficulties at magnitudes less than 4.0. Body wave magnitude does depend on a single period measurement in that it scales as Log(A/T), but it hardly utilizes complete waveform information. Furthermore, m_b-yield scaling is the most widely accepted approach to yield estimation, and in those magnitude ranges where both m_b values and P_n waveforms are available both methods give the same results.

There are many directions which need to pursued in the future regarding yield estimation from P_n onset waveforms. The generality of the approach at alternate test sites remains a significant issue, though the physics of the approach are very simple and there is every reason to believe it will be transportable. The variability of the results with respect to events above and below the water table at Pahute Mesa is an important issue, but it can be investigated further by considering additional NTS events.

BROADBAND SOURCE MODELS FOR U.S. UNDERGROUND NUCLEAR EXPLOSIONS

Introduction: Recent broadband studies of earthquakes indicate considerable complexity and non-uniformity in source characteristics. Modern source descriptions are expressed in terms of seismic moment and asperity distribution on the fault surface. The latter is best established by studies of local strong-motion observations while the former can be obtained from teleseismic modeling of long-period body waves and surface waves. The recent deployment of the new IRIS systems consisting of the Weilandt-Strekeisen sensors and 24 bit Quanterra loggers allows the entire frequency band to be recorded and modeled locally (*e.g.*, Dreger and Helmberger, 1990). Since smaller events can not be seen teleseismically, the new data systems become essential in studying both earthquake and explosion sources and in establishing techniques for discrimination. The broadband nature of underground nuclear sources is the key question in discrimination. Furthermore, the detailed variations in these source descriptions for various test sites in the U.S. and in foreign environments are also important. We will address these issues with respect to U.S. explosions and attempt to establish some useful kinemetric source descriptions.

Source models and scaling relationships for underground explosions have been studied for several decades, but generally with an emphasis on comparing teleseismic data sets consisting of short-period m_b's and long-period surface wave M_S's. Classical amplitude measures on the *P*-wave such as m_b can only take account of complicating factors such as attenuation, *pP*, and initial source histories in a crude fashion. Similar measures on surface waves (M_S) suffer from their own complicating factors such as effective attenuation, tectonic contamination and source coupling. It has been apparent for many years that these two yield estimators show distinct regional behavior, presumably caused by differences in the above factors. Figure 17a displays measurements taken from a sample of NTS and SRS events. The regression lines for these two regions indicate distinctly different trends. The separation of these populations is well established at the larger yields, as demonstrated in many studies (Sykes and Cifuentes, 1984; Given and Mellman, 1986).

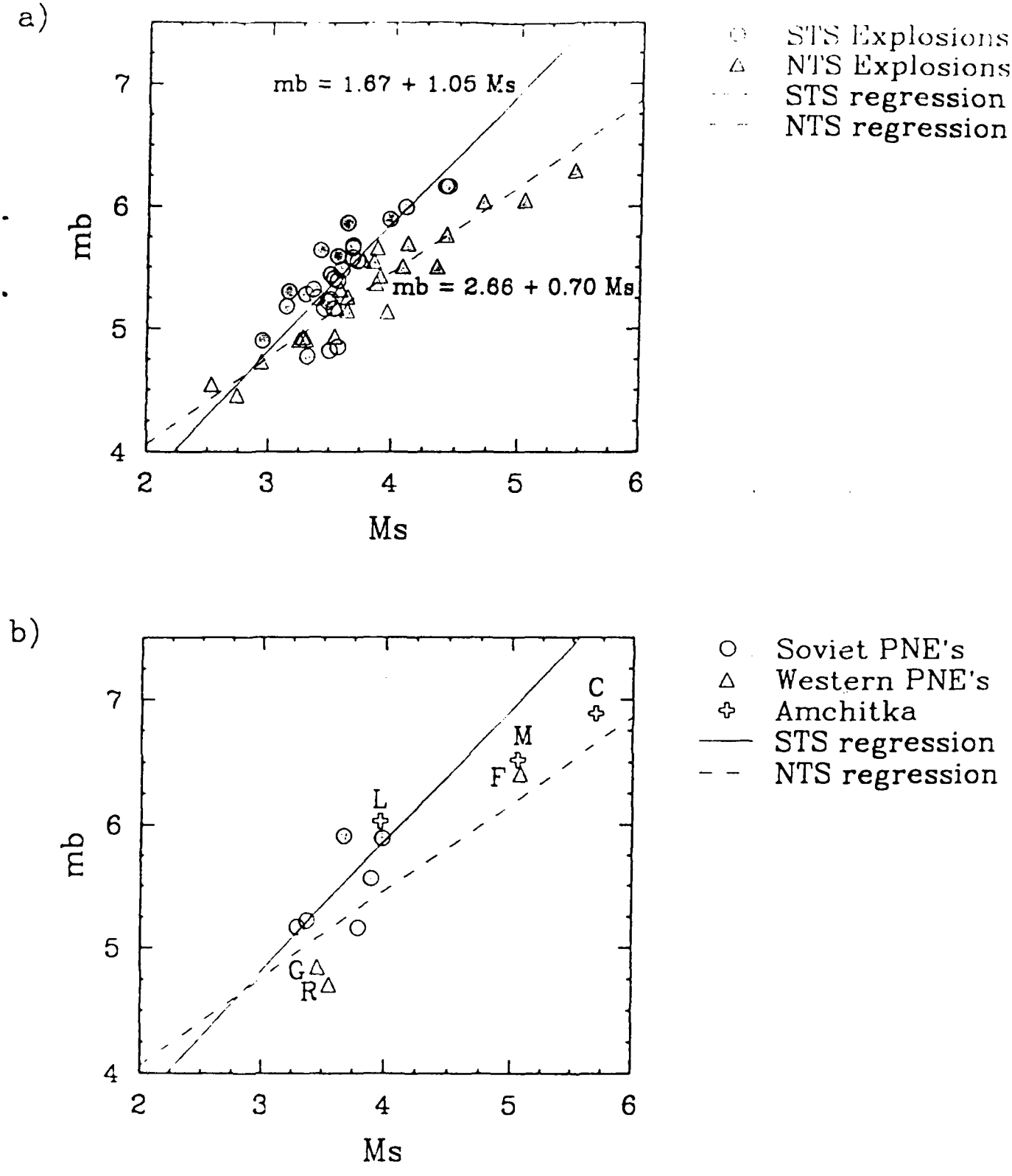

Figure 17. (a) Plots of m_b vs. M_S regression curves for Shagan River, USSR, and NTS explosions (after Marshall *et al.*, 1979). (b) Same regression curves as in (a) shown with Soviet PNE's and off-NTS explosions CANNIKIN, FAULTLESS, GASBUGGY, LONGSHOT, MILROW, and RULISON (indicated by the first letters of their names.)

Part of the scatter displayed in Figure 17a is caused by random effects and part is caused by deterministic factors which can be modeled and are correctable. Separating these two effects is fundamental to higher resolution attempts. Figure 17b shows the results of m_b *vs.* M_S comparisons for a sample of peaceful nuclear explosions. They show a great deal of variation which we can address to help isolate the deterministic elements of the source process and establish source properties.

Numerous papers have been written on why m_b and M_S values from Amchitka shots are different from those at Pahute. One of the earliest reports was given by Von Seggern (1972) who investigated the differences between BOXCAR (Pahute) and MILROW (Amchitka), two events of nearly the same yield. The m_b for BOXCAR is nearly 0.3 units less than that of MILROW while the M_S for BOXCAR is approximately 0.5 units larger than that of MILROW. He concluded that, since teleseismic *P*-waves from NTS are lower frequency than those from Amchitka, greater attenuation under NTS was the reason for the differences in m_b. He gave no explanation for the differences in M_S between the two events. Similarly, the recent Joint Verification Experiment, involving shots of the same yield in the U.S. and USSR, showed a similar m_b offset. This is generally believed to be caused by a difference in the attenuation beneath the two test sites. However, the M_S's from Shagan River events which are the least contaminated by tectonic release (as indicated by the absence of Love waves) are roughly 0.3 to 0.5 units less than NTS events for events near the 150kt testing limit (Stevens, 1986). Sykes and Cifuentes (1984) used these same events to argue for Soviet compliance. These discrepancies suggest that the long-period source levels sampled by M_S relative to the short-period levels sampled by m_b are site-dependent and, thus, these differences can be used to establish some working broadband source models.

The approach followed here is similar to that of Lay *et al.* (1984b). We assume a convenient modified Haskell source representation given by

$$\Psi(t) = \Psi_\infty \left(1 - e^{-Kt} \left\{ 1 + Kt + \frac{Kt^2}{2} - B(Kt)^3 \right\} \right)$$

where the RDP is defined by $\Psi(\tau)/R$. The reduced time τ is $\tau = t - (R/\alpha)$ where R is the distance between the source and receiver and α is the velocity. The study by Mueller and Murphy (1971) established the basic scaling laws relating the constants K and Ψ_∞ to yield. Their formalism is easily adapted to the above RDP. The parameter K is directly related to the corner frequency. The parameter B controls the overshoot which provides the means to uncouple the short-period signals, used for the m_b measurements, from the static level, which controls the M_S measurement (Figure 18). Thus, allowing B to vary provides the extra freedom in modeling extended data sets.

This study will address the determinations of the three constants, K, B and Ψ_∞ as a function of energy (yield) for the various U.S. test sites including the PNE's. We will begin with the simplest data set, Amchitka, followed by the most complex, NTS.

Scaling Relationships at Amchitka: The data set for Amchitka consists of near-in strong motion seismograms, and teleseismic seismograms containing body waves and surface waves (see Figure 19). In earlier efforts Burdick *et al.* (1984) and Lay *et al.* (1984a) established the linkage between these types of near-in data, Figure 19a, and the teleseismic short-period amplitudes. Their source models, while fitting the short-period data very well, do not fit the relative amplitudes of the Rayleigh waves given in Figure 19b. They predict CANNIKIN/MILROW long-period amplitude ratios of about 3 assuming B=1. The observed ratio is near 6. Note that the Amchitka events have negligible Love waves, so we would not expect to see any tectonic effects on the Rayleigh waves. The amplitude ratio of the observed long-period P-waves between these two events is about 2.8 which is not consistent with the short-period. The M_S's from the Amchitka shots are 3.9 (LONGSHOT), 4.9 (MILROW), and 5.7 (CANNIKIN) (Liebermann and Basham, 1971; Willis *et al.*, 1972) and fit the well known equation

$$M_S = \text{Log}\, Y + 2$$

which is an often quoted result.

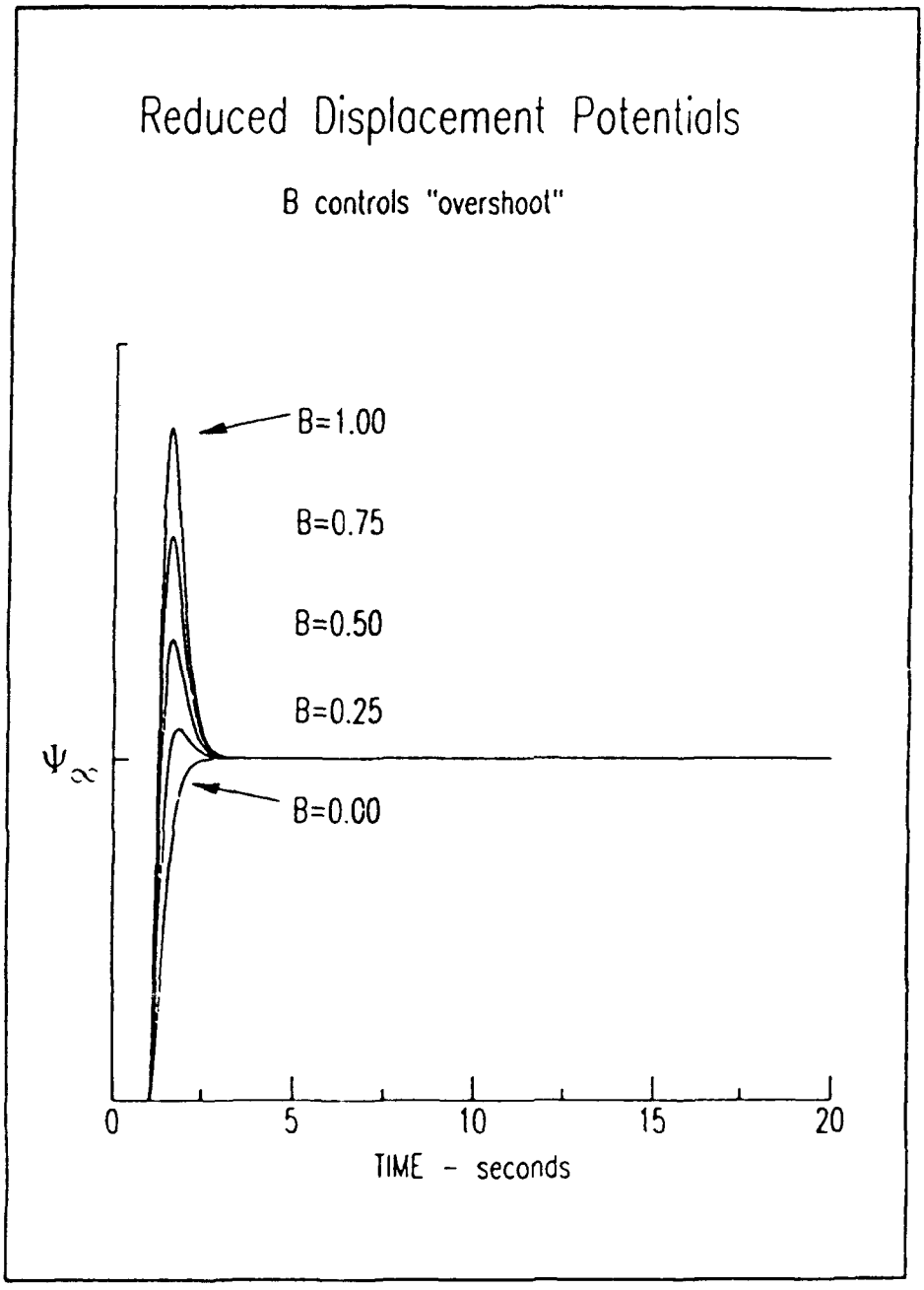

Figure 18. Reduced displacement potentials (RDP) for a fixed K (=6) and Ψ_∞ and various values of B (1.00, 0.75, 0.50, 0.25, 0.00). This figure demonstrates how B controls the degree of overshoot in RDP's.

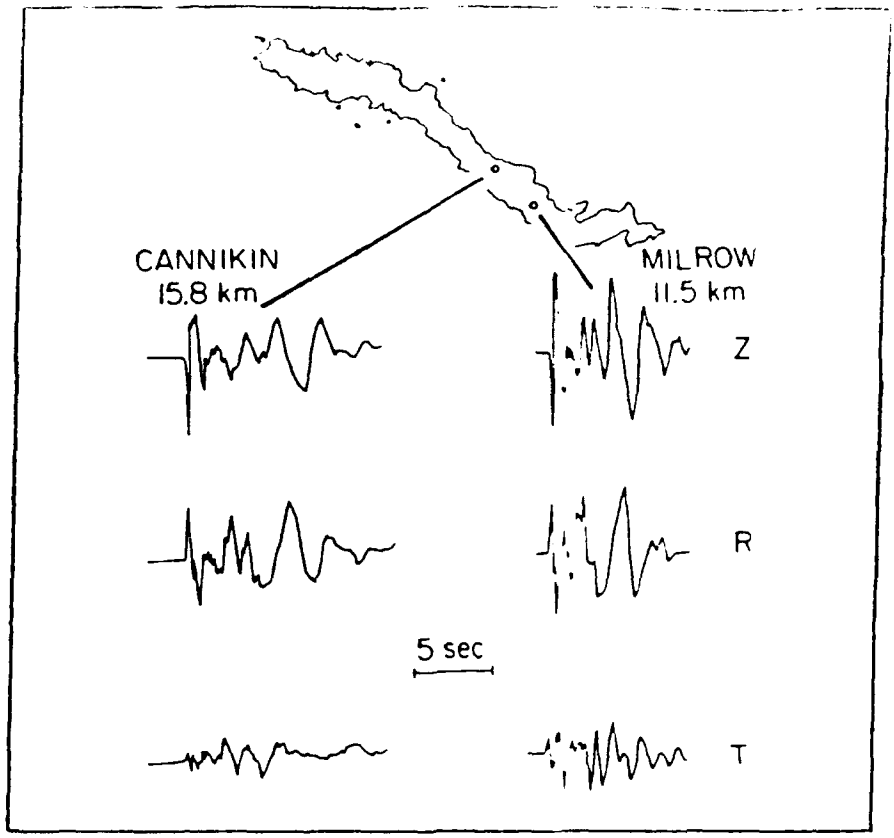

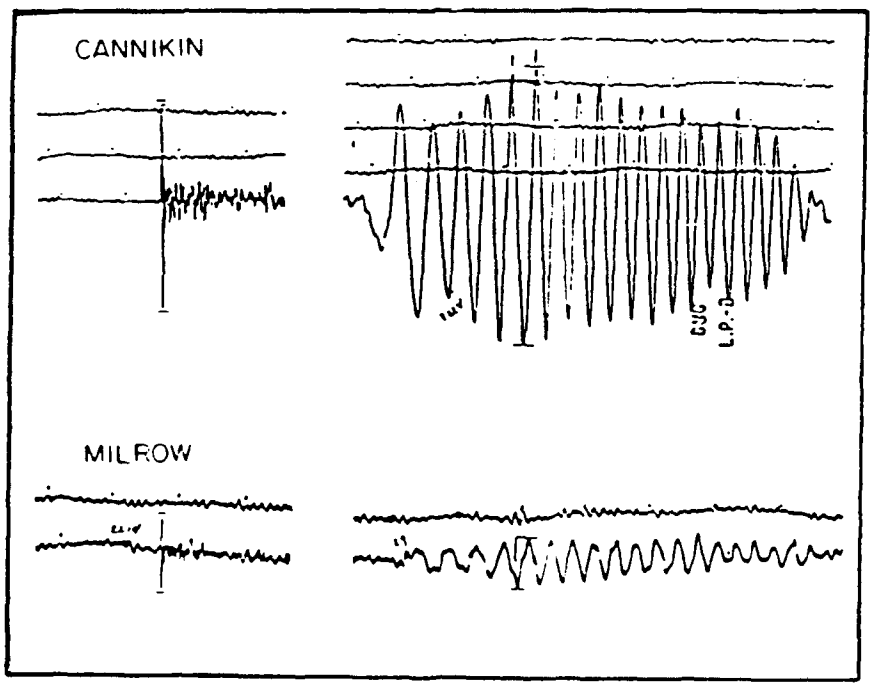

Figure 19. Shown in the top panel is Amchitka Island and records from events CANNIKIN and MILROW. Three component velocity seismograms are presented along with the slant distances from event to station. Bottom panel shows long-period vertical *P* and Rayleigh waves for CANNIKIN and MILROW at station DUG (Dugway, Utah). For MILROW the body wave is larger but for CANNIKIN the surface wave is larger.

Lay *et al.* (1984b) allowed B to vary and resolved this discrepancy. We will review some of these efforts and modify the final scaling laws to better match absolute amplitude levels.

Modeling Near-in Data: About six good sets of strong motion records of the type displayed in Figure 19a are available for both MILROW and CANNIKIN. A crustal model was derived to fit the travel times of these records and many others. These crustal structures were further refined by matching the entire recorded waveform with the synthetic waveform (Burdick *et al.*, 1984). The most stable portion of these observed-synthetic matches is the initial few seconds of motion as displayed in Figure 20a. The synthetic consists of the diving P followed by the opposite in polarity pulse, pP (see Vidale and Helmberger, 1987, for details and the effects of 2D structures). However, since pP cancels P it becomes difficult to resolve all three parameters B, K, and Ψ_- because of the Ψ_- *vs.* B trade-off, as displayed in Figure 20b. For instance, using $K = 6$, a source function with $\Psi_- = 7.3$ and $B = 0.5$ fits the data just as well as a source function with $\Psi_- = 4.3$ and $B = 1$. Holding B=1 allows an estimate of Ψ_- for the study events. These Ψ_-'s can be compared with large teleseismic short-period data sets to establish a realistic estimate of t^*_α and in this case, $t^*_\alpha = 0.9$ (as reported by Burdick *et al.* 1984). Adding the intercorrelation procedure (Lay *et al.*, 1984b) allows source strengths of other events such as LONGSHOT to be estimated and a scaling law developed based on short-period signals (see Figure 21a.) Lay *et al.* (1984a) fixed B at 1 for MILROW and adjusted the B's of LONGSHOT and CANNIKIN to match the Rayleigh wave differentials (Figure 21b). A further modification is possible if we can establish the absolute long-period level.

Three types of data are available for this purpose, namely long-period P-waves, the phase pS and the direct modeling of the Rayleigh waves. The long-period P-waves prove disappointing because the interactions of pP with t^* reduces the sensitivity to B. Thus ratios (SPZ/LPZ) of short-period vertical P-wave amplitudes to long-period vertical Rayleigh wave amplitudes depend mostly on the values of t^* (see Figure 22). The average observed ratio SPZ/LPZ using 28 long-period records is 0.65, and we again obtain a t^* near 1.0. The phase pS appears the most promising, since

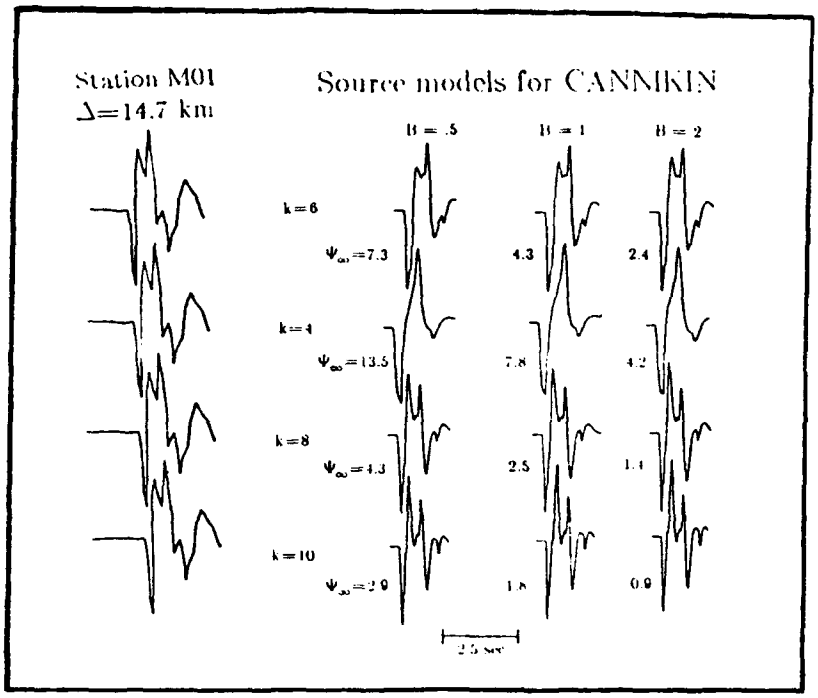

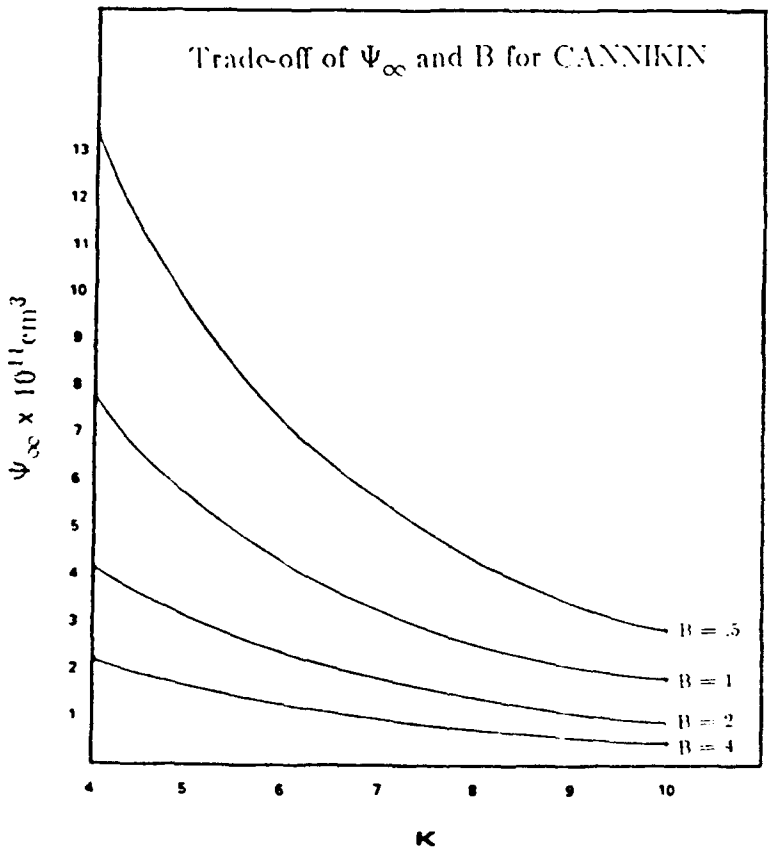

Figure 20. A suite of source models for event CANNIKIN (top panel). The Ψ_∞ determined from the first swing in the waveform is printed to the left of each synthetic. Bottom panel shows the trade-off of Ψ_∞ and B for CANNIKIN for a specific K.

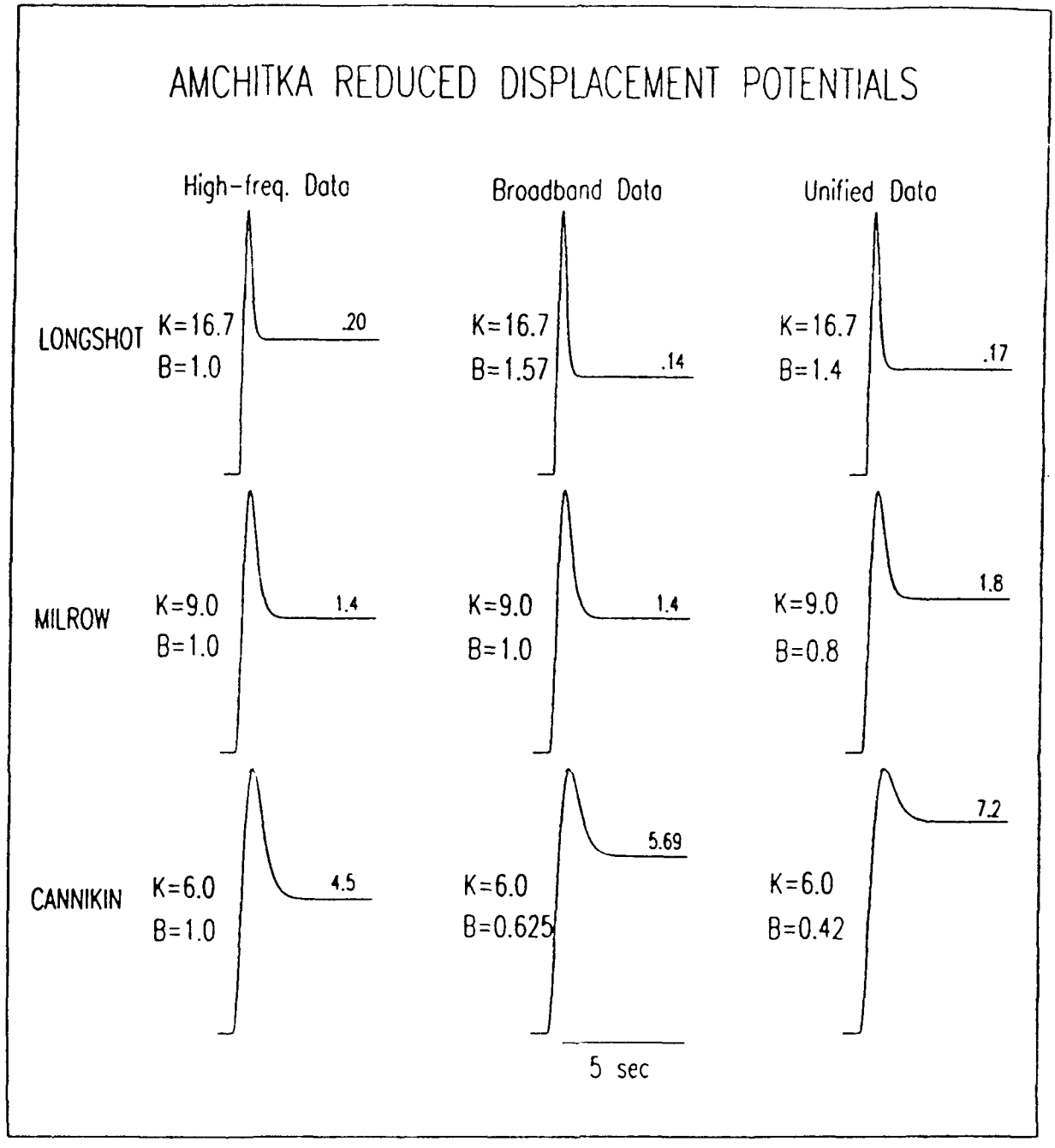

Figure 21. Reduced displacement potentials. (a) based on short period signals. (b) from broadband data: fixing B=1 for MILROW, and adjusting the B's of LONGSHOT and CANNIKIN to match Rayleigh wave differentials. (c) from broadband data: utilizing long-period P-waves, the phase pS, and Rayleigh waves. [Figure modified from Lay *et al.*, 1984.]

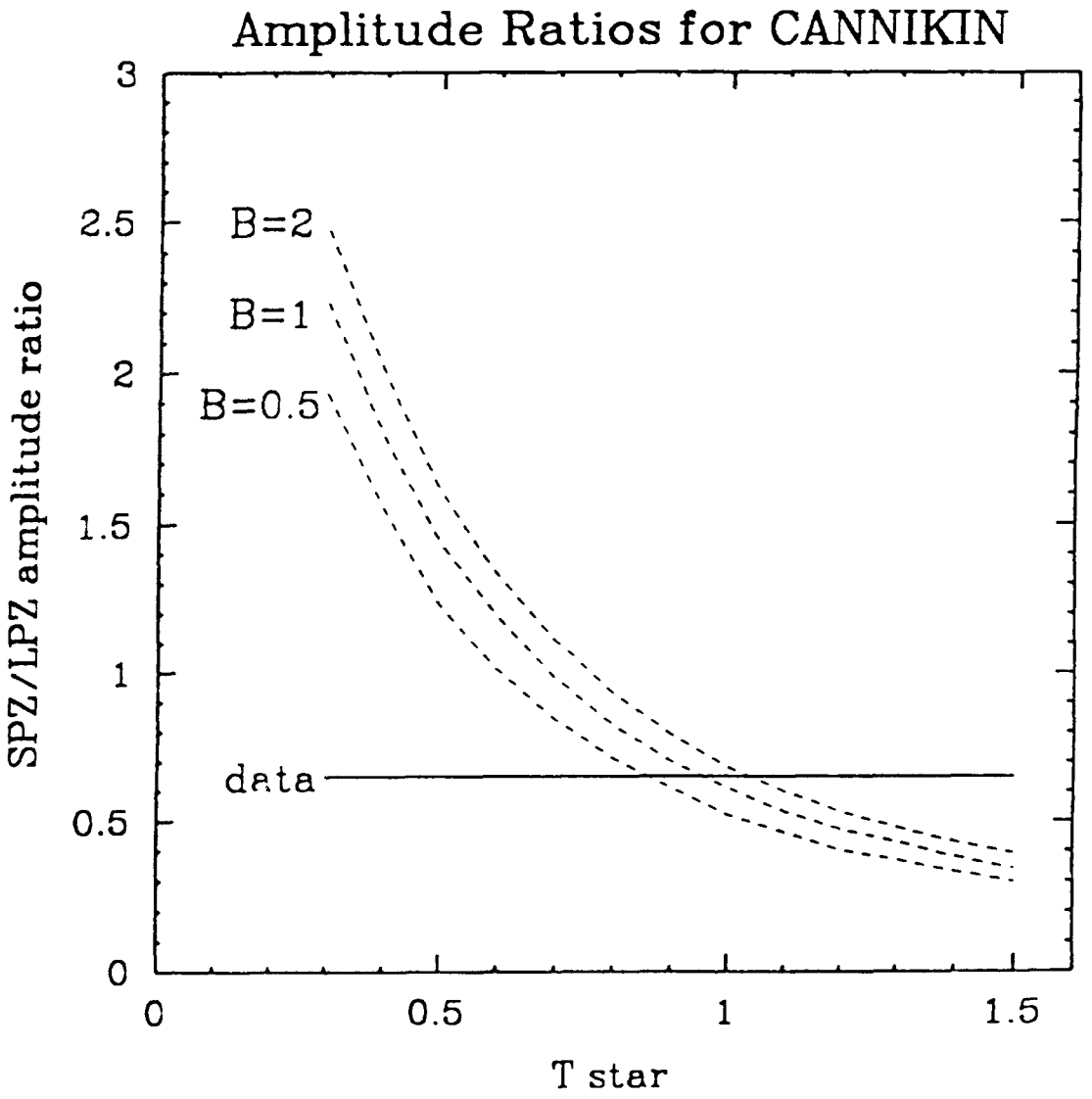

Figure 22. Amplitude ratios of short period vertical (SPZ) to long period vertical (LPZ) for event CANNIKIN. The average observed ratio using 28 LPZ records is 0.65, indicated by the solid line.

these waveforms are not subjected to any strong interference such as the *P-pP* waveforms. Some examples of the 21 observations available are given in Figure 23 However, one complication with this phase is the *S-P* conversion at the Moho beneath the receiver. Note the small positive pulse preceding the negative direct *pS* arrival. There can also be problems associated with later arrivals, the so-called *SV*-coupled *PL* waves. Other complications can occur at the source region caused by tectonic release and possible spall interaction. These problems are discussed at length by Cohee and Lay (1988) in their study of *pS* from some Novaya Zemlya events.

The synthetics displayed in Figure 23 were calculated assuming that the elastic conversion *P* to *S* is -0.456 for a ray parameter of 0.12 sec/km. This is consistent with the value used in modeling the phase *pS* in earthquake studies (Langston and Helmberger, 1975). Note that the actual reflection point occurs outside the region of strongest spall (a distance of roughly 1.5 km for CANNIKIN) because of the change in ray parameters (0.07 for *pP* and 0.12 for *sP*). The remaining difficulty is in estimating t_β^* (see Figure 24). If we assume that $t_\beta^* = 4t_\alpha^*$, we obtain the expected value of $t_\beta^* = 3.6$ Under this assumption, which is supported by many earthquake studies, it becomes possible to determine the appropriate combination of *B* and Ψ_∞ to satisfy the *pS* waveforms and absolute amplitude levels. The average amplitude of the *CANNIKIN pS* phase from 21 observations is 2083 $m\mu$ which implies that B=0.4 and $\Psi_\infty = 7.3x10^{11}cm^3$. This value of Ψ_∞ agrees remarkably well with that determined by Rayleigh wave modeling, as reported by Toksöz and Kehrer (1972) who obtained $\Psi_\infty = 7.2x10^{11}cm^3$. Thus, we set the absolute level of CANNIKIN to be 7.3 x 10^{11}cm^3 and adjust the other two events accordingly to obtain the RDP's given in Figure 21c. If we follow the basic scaling arguments of Mueller and Murphy (1971), namely that yield (Y) is proportional to effective cavity volume, we expect

$$\Psi_\infty = c_1 Y / h^{0.27} \qquad (1)$$

and

$$K = c_2 h^{0.42} / Y^{0.33} \qquad (2)$$

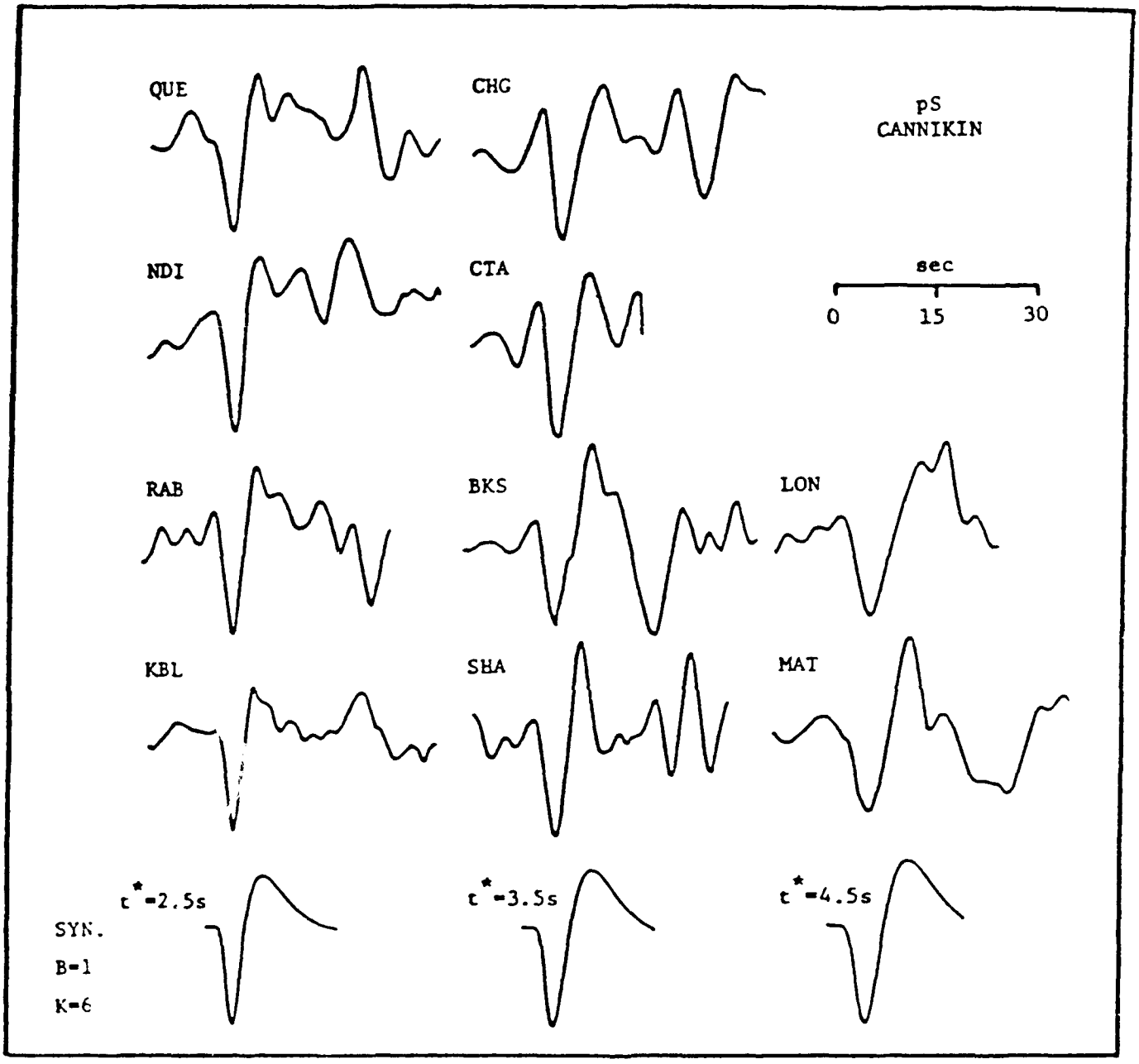

Figure 23. Comparison of observed long period *pS* waveforms and synthetics using different values of t_s^* for event CANNIKIN. The source model and velocity structure are obtained from near field modeling.

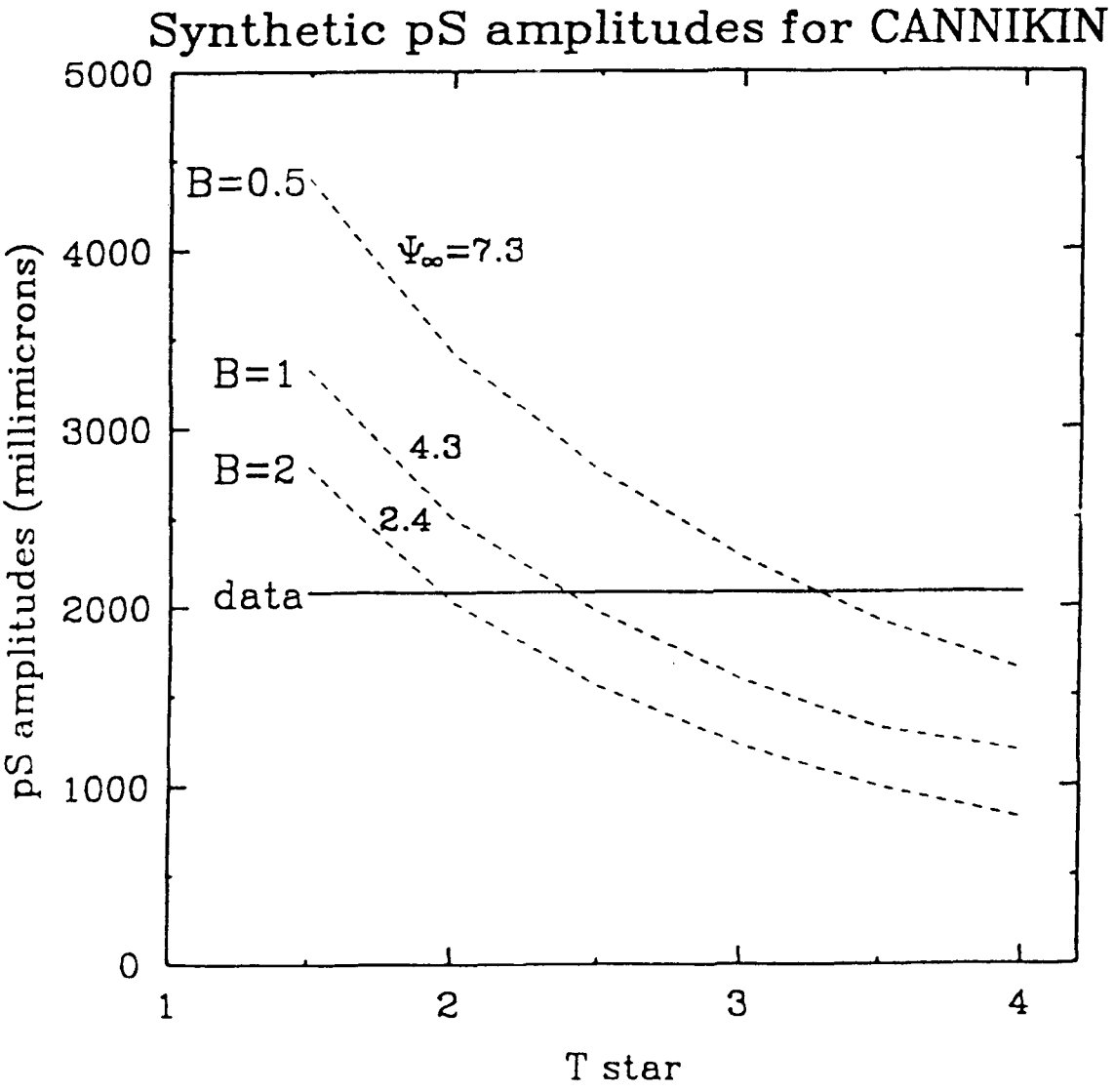

Figure 24. Synthetic *pS* amplitudes for event CANNIKIN, where the first peak amplitude is plotted against t^* for different values of B and Ψ_∞.

The two scaling constants, c_1 and c_2, can then be estimated by regression assuming the yields of LONGSHOT, MILROW and CANNIKIN. The results are

$$c_1=12.3 \times 10^8$$

$$c_2=4.7$$

The parameter B now depends on depth and is given by

$$\text{Log } B = -0.05 \times 1.3 \text{ Log } h$$

These formulas prove quite effective in explaining the GASBUGGY-RULISON tests as discussed later.

Scaling Relationships at NTS: The data set at NTS is much larger than that at Amchitka but again consists mostly of a collection of strong motion and teleseismic seismograms. There also exists an abundance of free-field data at distances of less than a few kilometers. Most of this type of data is for small events whose yield is less than 15 kilotons. The few measurements that do exist for larger events are inconsistent in most situations (Murphy, 1991).

The strong motion records at distances beyond a few kilometers are much more complicated at NTS than at Amchitka, presumably because of the complex local geology (Barker *et al.*, 1991). However, the initial motions of the type discussed earlier for CANNIKIN (Figure 20) can still be modeled using the structure derived in Barker *et al.* Figure 25a through 25e display complete seismograms for the best recorded events. The columns on the left are appropriate for the B=1 assumption used earlier in the extensive intercorrelation exercise (Lay *et al.*, 1984). The columns on the right correspond to using a slightly different scaling law than Barker *et al.* and allowing for an adjustment in B to fit the estimated long-period source strengths. The synthetics generated in Figure 25 were produced by Filon-AS, a frequency-wavenumber code. The crustal model is given in Table 1.

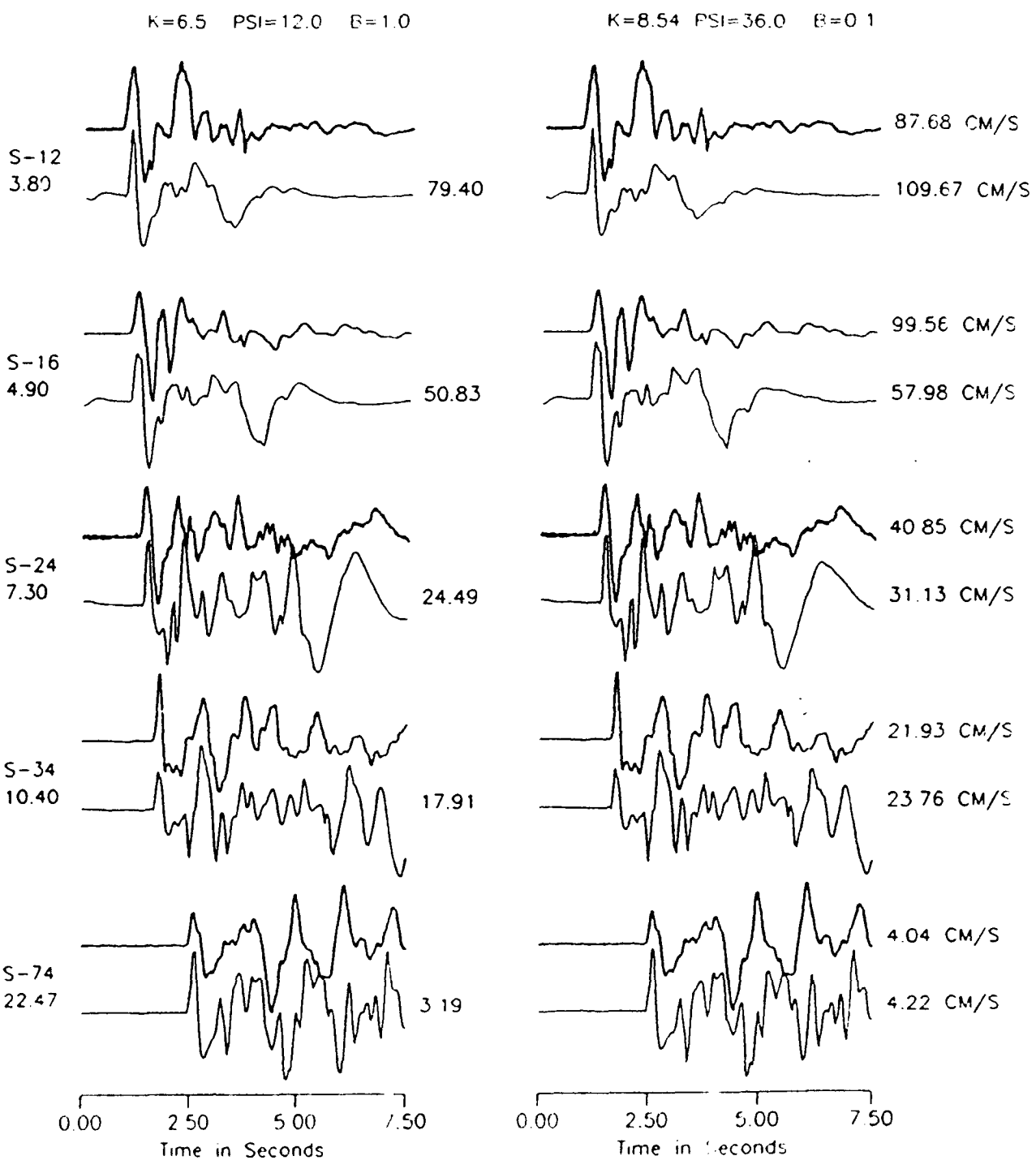

Figure 25 (a). Near-in observations (top bold traces) and predictions (bottom traces) for event BOXCAR. The station names and distances are printed on the left; amplitudes are printed on the right, and values of K, Ψ_- (PSI), and B are printed above each column.

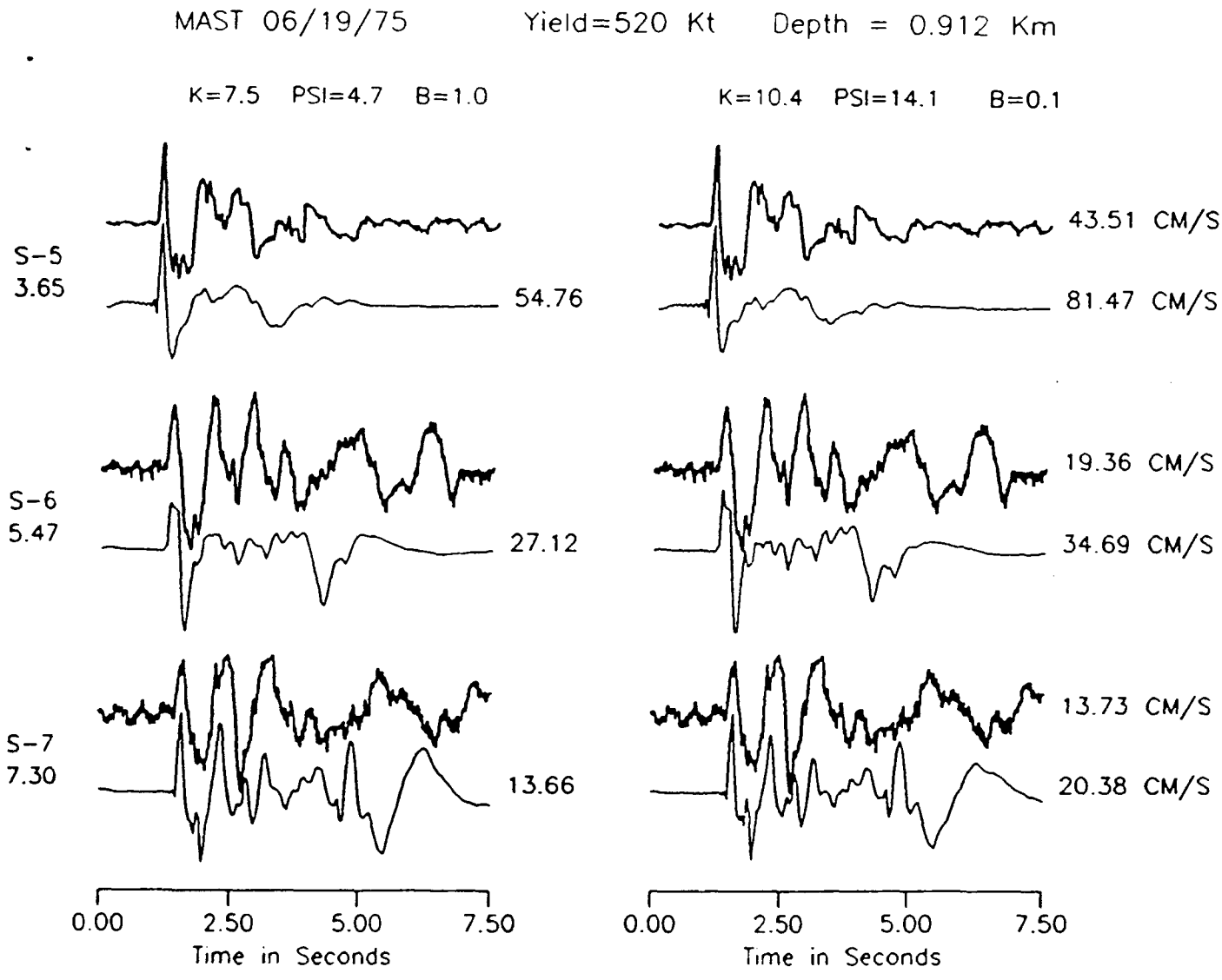

Figure 25 (b). Near-in observations (top bold traces) and predictions (bottom traces) for event MAST. The station names and distances are printed on the left; amplitudes are printed on the right, and values of K, $\Psi_{\cdot}$ (PSI), and B are printed above each column.

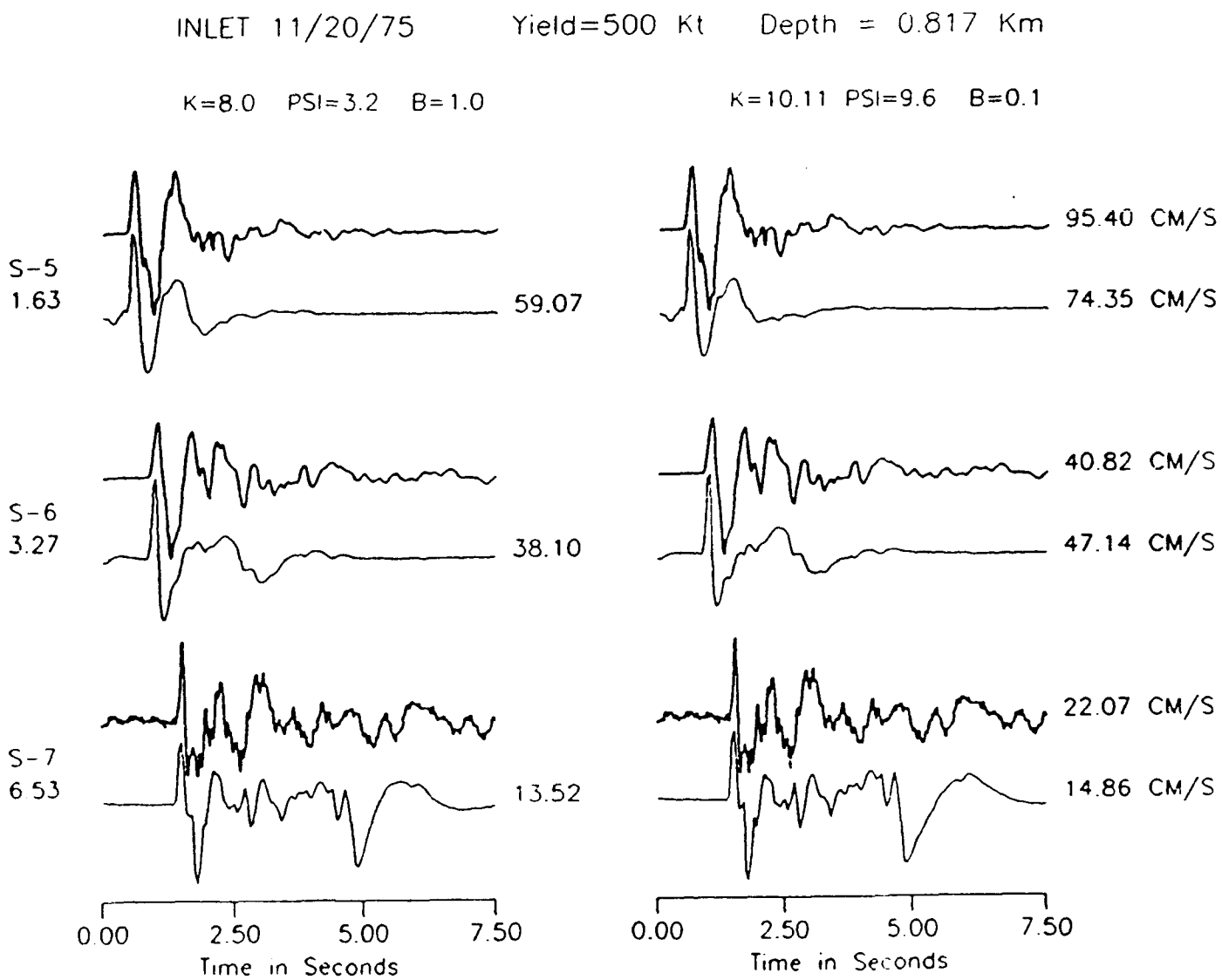

Figure 25 (c). Near-in observations (top bold traces) and predictions (bottom traces) for event INLET. The station names and distances are printed on the left; amplitudes are printed on the right, and values of K, Ψ_- (PSI), and B are printed above each column.

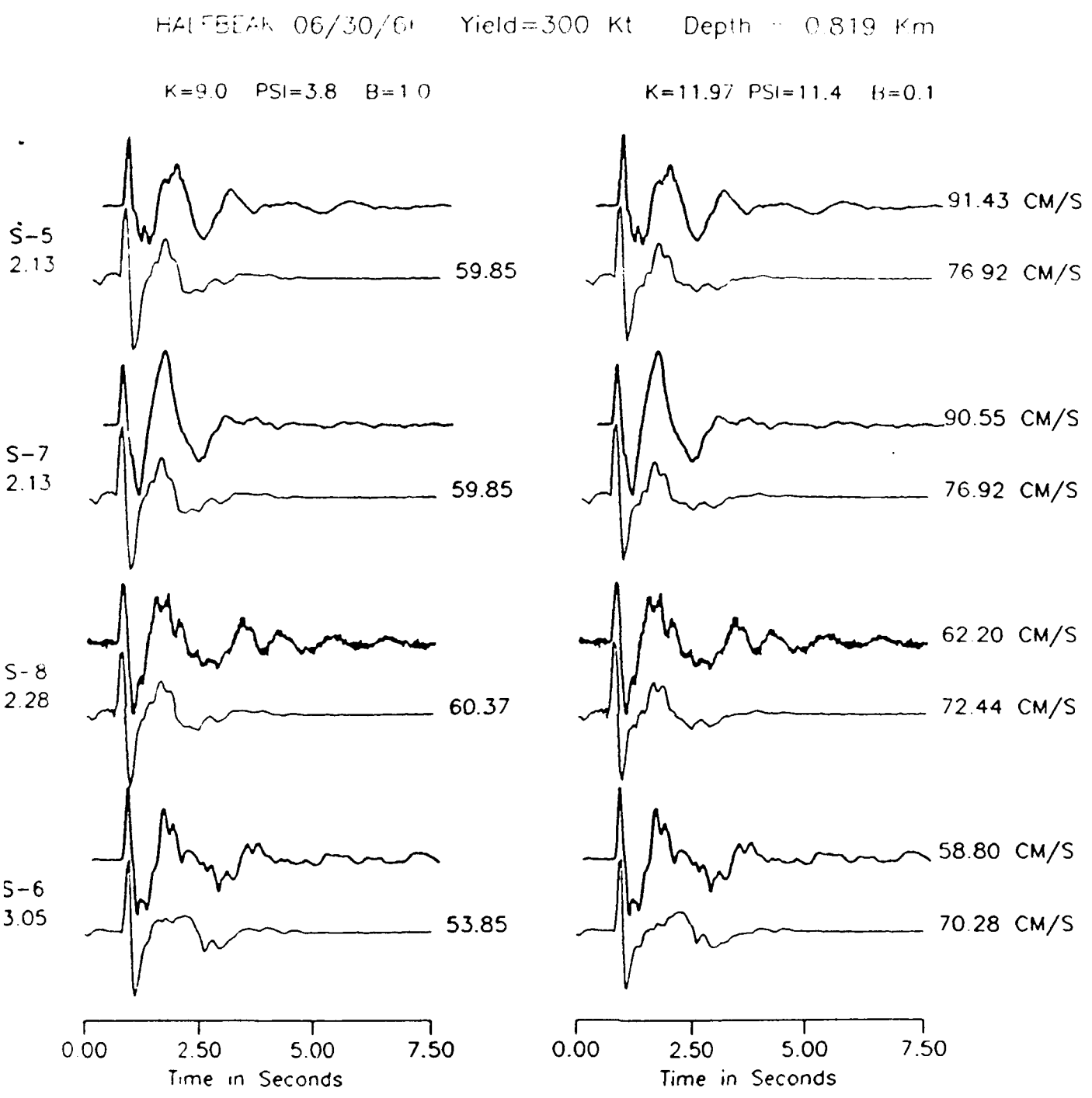

Figure 25 (d). Near-in observations (top bold traces) and predictions (bottom traces) for event HALFBEAK. The station names and distances are printed on the left; amplitudes are printed on the right, and values of K, Ψ_- (PSI), and B are printed above each column.

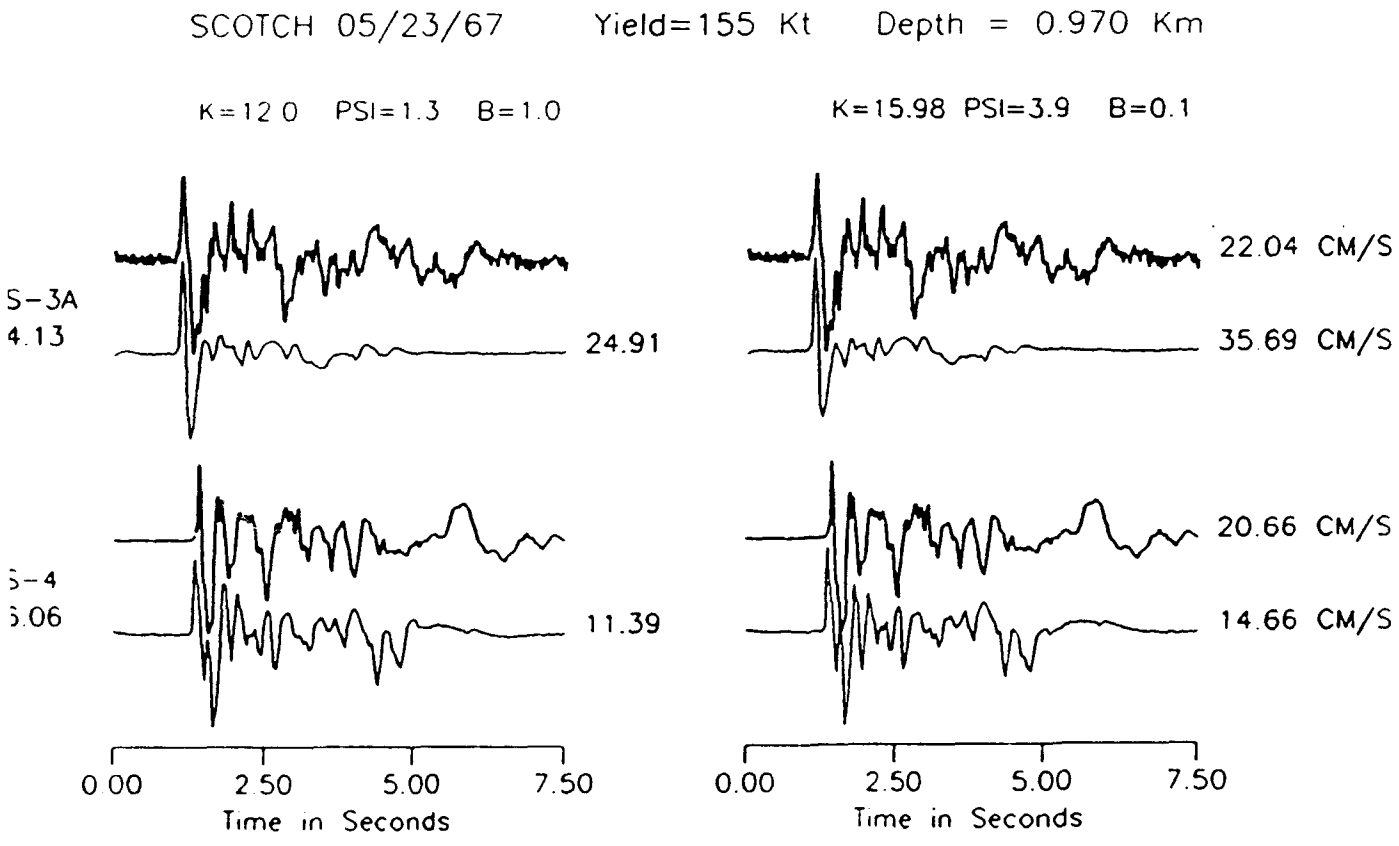

Figure 25 (e). Near-in observations (top bold traces) and predictions (bottom traces) for event SCOTCH. The station names and distances are printed on the left; amplitudes are printed on the right, and values of K, Ψ_{-} (PSI), and B are printed above each column.

TABLE 1. Velocity Structure Model

Layer	α, km/s	β, km/s	ρ, g/cm^3	Thickness, km
1	2.30	1.35	1.90	0.36
2	2.80	1.50	2.00	0.40
3	3.30	1.50	2.25	0.70
4	4.00	1.90	2.30	0.70
5	4.60	2.00	2.40	0.75
6	5.30	2.50	2.50	0.80
7	5.50	2.95	2.70	2.25
8	6.10	3.50	3.00	10.00
9	7.00	4.00	3.00	10.00

Model from Hartzell *et al.* (1983)

The long-period Ψ_- estimates are less certain for NTS events for several reasons. First, the F factor or tectonic release is much higher than at Amchitka, making it more difficult to correct the surface waves as well as the long-period SV-waves for contamination. Secondly, the geologic structure is more complex in the source region, so that individual shots sample different source parameters (Murphy, 1989). Results from Rayleigh wave modeling by Stevens (1986) is given in Table 2 along with Ψ_- estimates from the intercorrelation technique (Lay *et al.*, 1984a). Note that Ψ_- estimated from m_b is consistently smaller than Ψ_- estimated from M_S. The ratio is about three to one but with considerable scatter. The depth effect on B is not particularly obvious in this data set. Note that the event CHESHIRE is deeper than ESTUARY although its LP/SP ratio is smaller. This does not support the B *vs.* depth dependence discussed earlier in connection with Amchitka data. The Rayleigh wave strength given by Stevens (1986) is in general agreement with those given by Given and Mellman (1986) such that a factor of about three appears appropriate in the Ψ_- off-sets.

TABLE 2. Strength Estimates from Surface Waves and Body Waves

Events	Date	$\Psi_{\perp}(M_S)$	$\Psi_{\perp}(m_b)$	Depth (km)	Ratio
Scotch	05/23/67	0.91	0.19	0.98	4.8
Stinger	03/22/68	0.48	0.15	0.67	3.2
Sled	08/29/68	0.53	0.30	0.73	1.8
Almendro	06/06/73	1.9	0.68	1.06	2.8
Tybo	05/14/75	1.0	0.46	0.77	2.2
Stilton	06/03/75	0.48	0.24	0.73	2.0
Mast	06/19/75	1.2	0.49	0.91	2.4
Cheshire	02/14/76	2.0	0.35	1.17	5.7
Estuary	03/09/76	2.0	0.35	0.87	5.7
Pool	03/17/76	0.43	0.44	0.88	1.0

Following the results of strong-motion modeling assuming B=1 (Hartzell *et al.*, 1983) we used the parameterizations given earlier in equations (1) and (2) obtaining

$$c_1 = 20.1 \times 10^8$$

$$c_2 = 4$$

where c_1 has been increased by a factor of 3. These formulas apply when using B=1. If we used the corner frequency scaling relative to Amchitka we obtain the synthetic comparisons given in Figure 26. These begin to produce too much short-period energy at the nearest stations and do not fit the acceleration data (Helmberger *et al.*, 1991a). Thus, the corner frequency difference between the two sites appears real. We now have MILROW and BOXCAR with K's of 9 and 7 and $\Psi_{\perp}$'s of 1.8×10^{11}cm^3 and 3.6×10^{11}cm^3. The difference in $\Psi_{\perp}$ accounts for a δM_S=0.48 which we essentially constructed.

Off-Test Site Events: The local and teleseismic data from various off-test site events have been extensively studied in attempts to explain the scatter from standard m_b:M_S:Y curves. For example, LRSM stations were established at FAULTLESS, RULISON, and GASBUGGY epicenters to measure relative attenuation to explain δm_b's with respect to δ° differences. These results generally do not

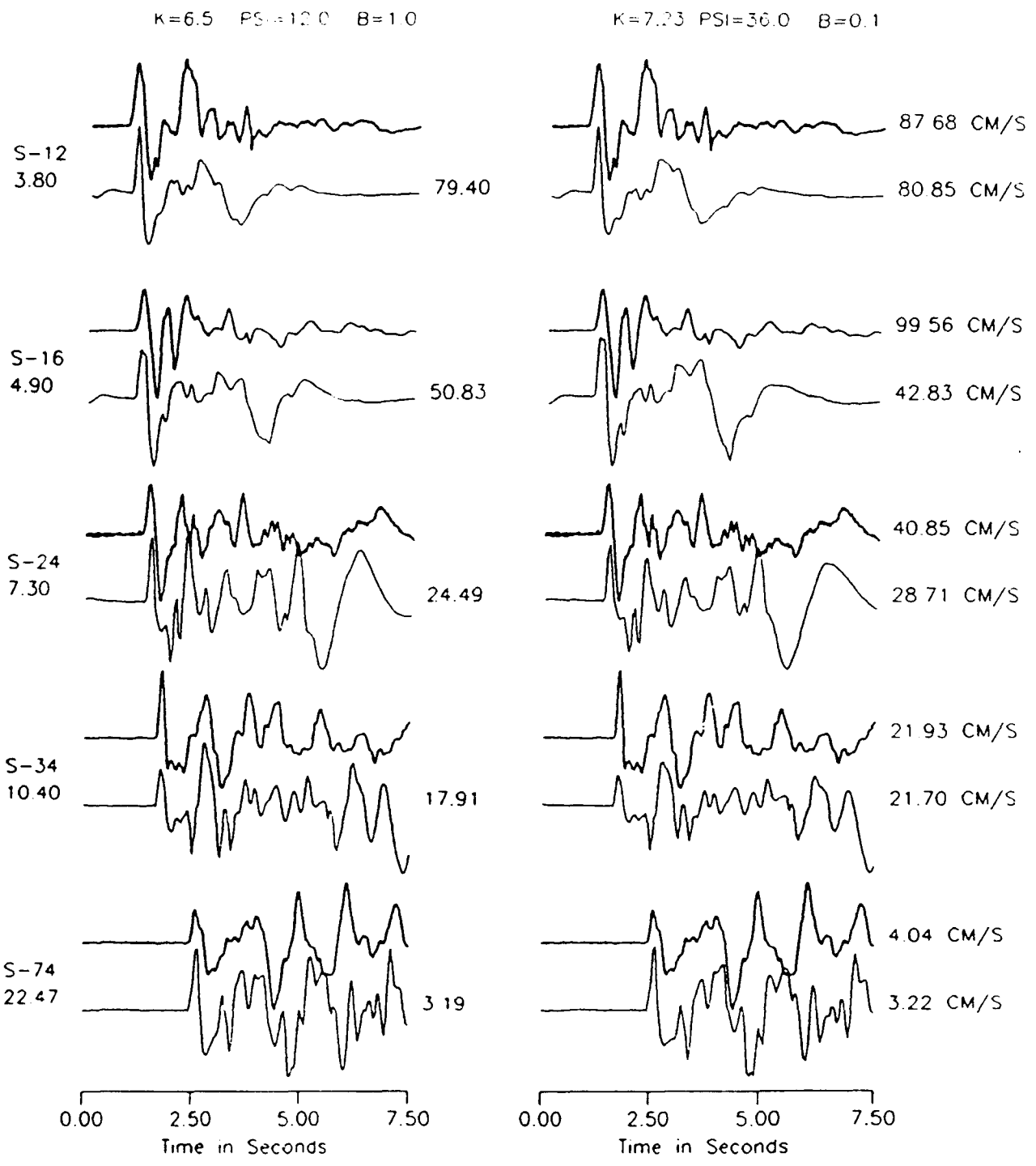

Figure 26 (a). Near-in observations (top bold traces) and predictions (bottom traces) for event BOXCAR using Amchitka scaling. The station names and distances are printed on the left; amplitudes are printed on the right, and values of K, Ψ_- (PSI), and B are printed above each column.

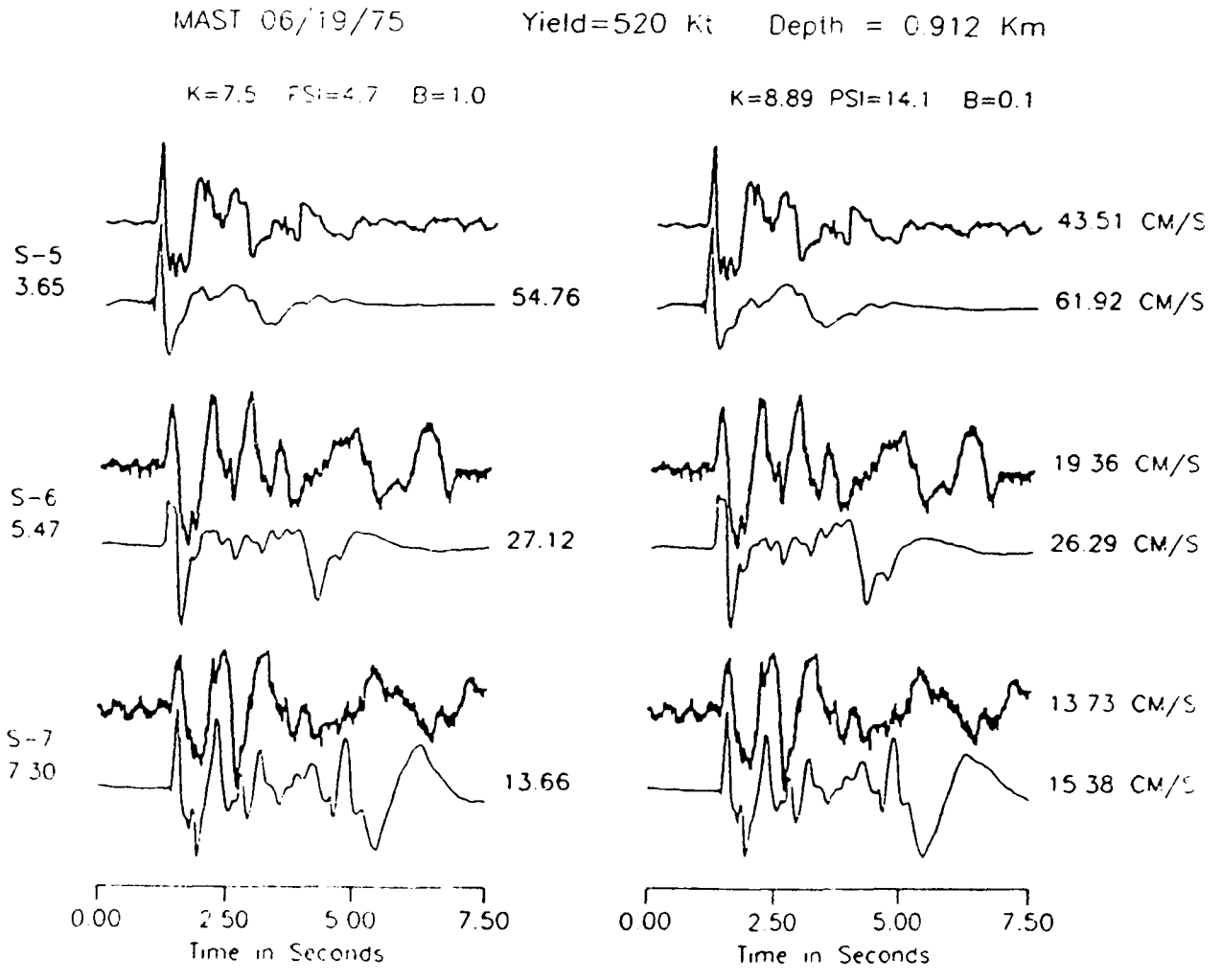

Figure 26 (b). Near-in observations (top bold traces) and predictions (bottom traces) for event MAST using Amchitka scaling. The station names and distances are printed on the left; amplitudes are printed on the right, and values of K, $\Psi_{\_}$ (PSI), and B are printed above each column.

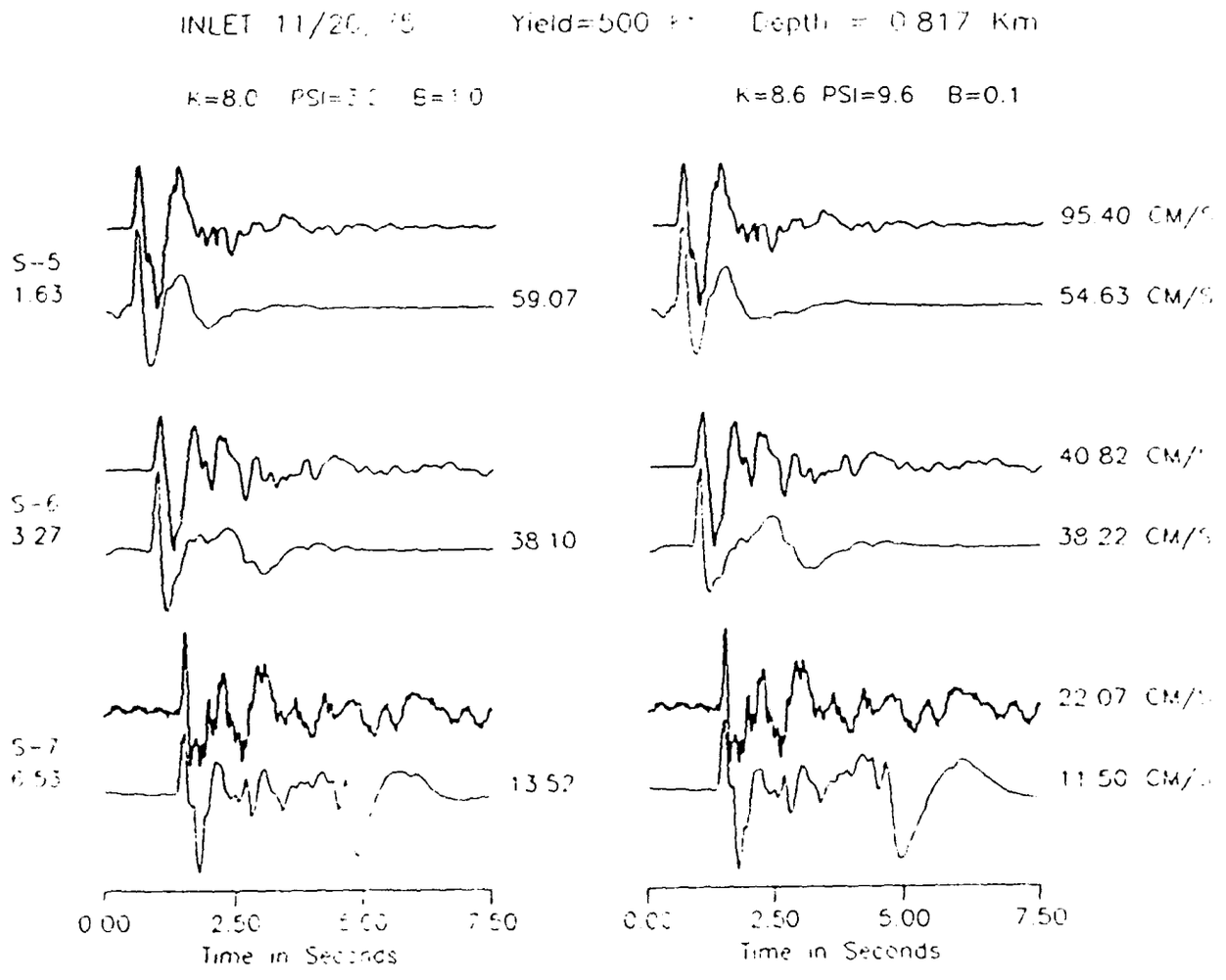

Figure 26 (c). Near-in observations (top bold traces) and predictions (bottom traces) for event INLET using Amchitka scaling. The station names and distances are printed on the left; amplitudes are printed on the right, and values of K, Ψ_a (PSI), and B are printed above each column.

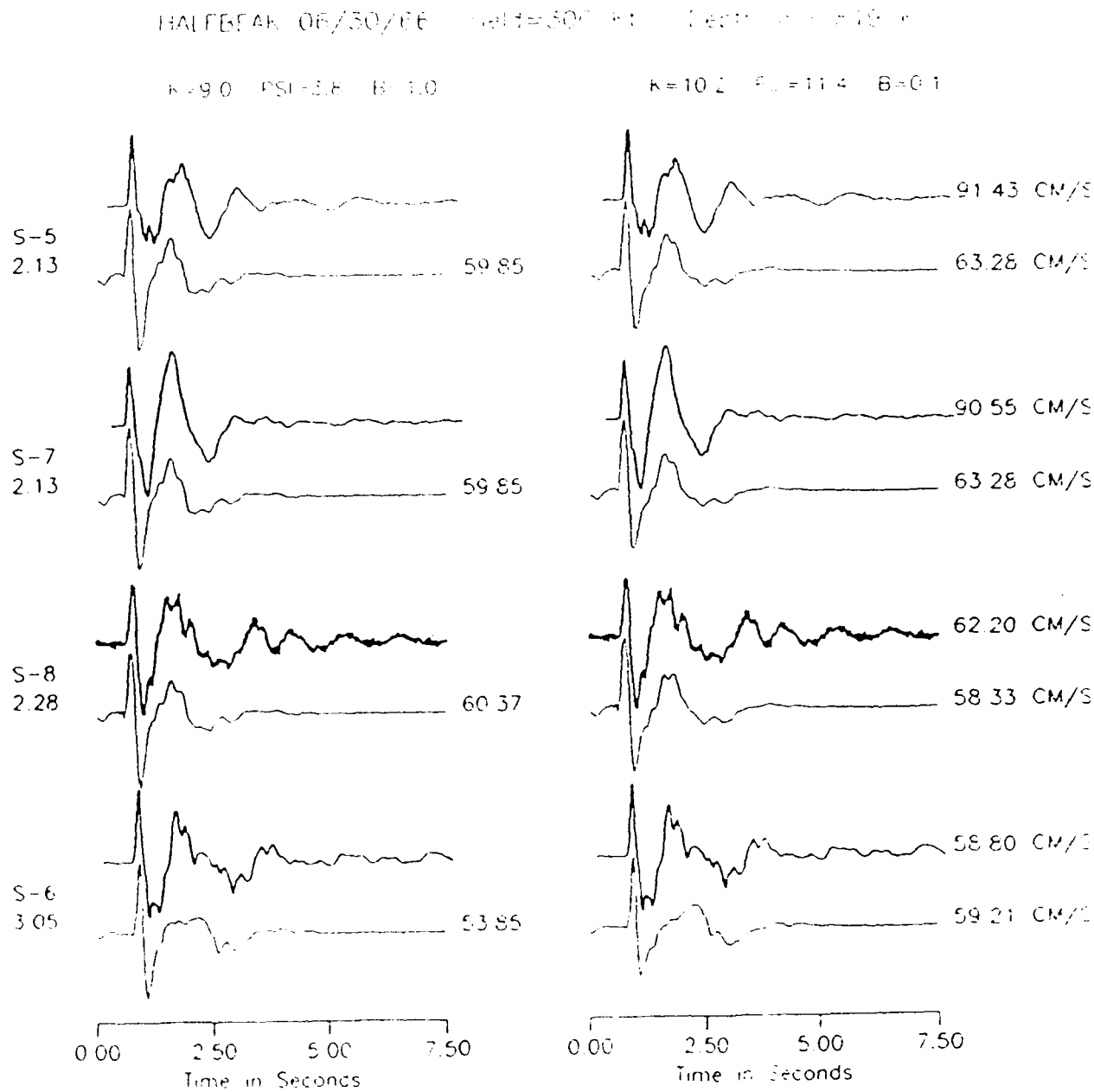

Figure 26 (d). Near-in observations (top bold traces) and predictions (bottom traces) for event HALFBEAK using Amchitka scaling. The station names and distances are printed on the left; amplitudes are printed on the right, and values of K, Ψ_- (PSI), and B are printed above each column.

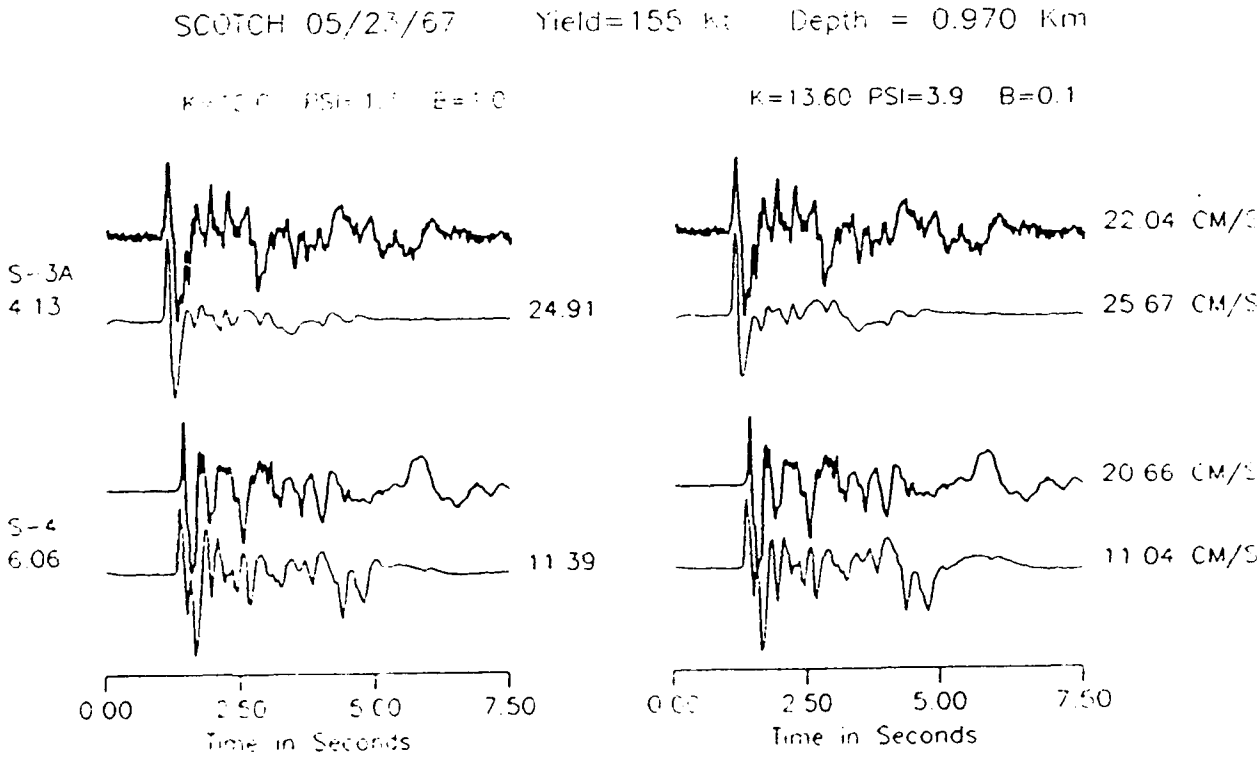

Figure 26 (e). Near-in observations (top bold traces) and predictions (bottom traces) for event SCOTCH using Amchitka scaling. The station names and distances are printed on the left; amplitudes are printed on the right, and values

appear to explain the anomalies (Der *et al.*, 1980). For example, the attenuation at the RULISON site is nearly the same as at GASBUGGY, and attenuation at FAULTLESS is the same as it is at NTS. Thus, anomalies in m_b remain unexplained. On the other hand, M_S values prove effective in estimating these yields as discussed by Yacoub (1983).

A) RULISON and GASBUGGY, a Test of Scaling: The two non-NTS nuclear blasts, RULISON and GASBUGGY, provide a particularly useful test case for determining the transportability of different methods of estimating yields (see Table 3). These two nuclear events were detonated 304 km apart in nearby sedimentary basins in New Mexico and Colorado. Although the announced yield of RULISON was 40 kt and that of GASBUGGY was 29 kt, GASBUGGY has a larger m_b. The most thorough analysis of this discrepancy was presented by Murphy and Archambeau (1986). Although the amplitude differences between the two events are of the order that might be expected from a difference in t_a^* of 0.4 sec between the two events, their analysis of the *P*-wave displacement spectra of the two events indicated that the effective t_a^* for the two events are essentially the same, in agreement with Der's (1980) results. Murphy and Archambeau present evidence that the RULISON-GASBUGGY anomaly is principally caused by tectonic release associated with RULISON. They suggest that this release of tectonic energy was oriented in such a fashion as to destructively interfere with, and reduce the amplitudes of, the teleseismic short-period *P*-waves for RULISON. The magnitude of their proposed release is such that the amplitude of the tectonic *P*-waves is roughly one half of the amplitude of the explosion *P*-waves.

TABLE 3. Explosion Source Parameters

Event	Location	Date	Yield (kt)	Depth (m)
GASBUGGY	36.68° N. 107.21° W.	10/12/1967	29	1292
RULISON	39.41° N. 107.95° W.	10/09/1969	40	2573

Although the tectonic release hypothesis cannot be ruled out, the amount of tectonic release required to produce this much interference is difficult to support from the results presented in Burdick *et al.* (1991a). Another interpretation is that this reduction in RULISON's amplitude is caused by a decrease in the *B* factor as suggested by the above scaling relations for Amchitka.

Using the Amchitka scaling relations, the predicted values for GASBUGGY (h=1.29 km, Y=29 kt) are B=0.64, K=31, and $\Psi_\infty = 4.5 \times 10^9 cm^3$ or M_0=2.6 x 10^{22} dyne-cm. For RULISON (h=2.57 km, Y=40 kt), the predicted values are B=0.27, K=37, and $\Psi_\infty = 5.9 \times 10^9 cm^3$ or M_0=3.7 x 10^{22} dyne-cm (Figure 27). Synthetic seismograms calculated using these source functions parameters and the crustal structures given by Murphy and Archambeau predict that the m_b for GASBUGGY is 0.23 units higher than that for RULISON. This difference is primarily caused by the small B value for RULISON.

Although the Amchitka scaling laws do a good job at predicting the m_b values of GASBUGGY and RULISON an examination of the recorded RDP's of GASBUGGY (Figure 28) shows that the prediction is not perfect. Only one of the RDP's shows a significant overshoot. The mean overshoot is 15%, corresponding to a B of 0.32. A K value approximately equal to 27 with a $\Psi_\infty = 6.4 \times 10^9 cm^3$, were needed to model the rise time (see the bottom trace). These observations of the direct RDP are rather unique in that gas-wells were available for subsurface observations (Perret, 1982). They were all taken at a slant range of about 0.5 km, well outside the nonlinear zone. The average RDP at the bottom of Figure 28 shows a higher Ψ_∞ and a lower overshoot than predicted by any scaling laws.

The moments obtained from modeling the surface waves (Burdick *et al.*, 1991a) are 2.0 x 10^{22} and 2.1 x 10^{22} dyne-cm, which are somewhat low compared to both the observed RDP and predicted RDP. These discrepancies are probably within modeling errors, but the evidence for undershoot in this experiment is strong.

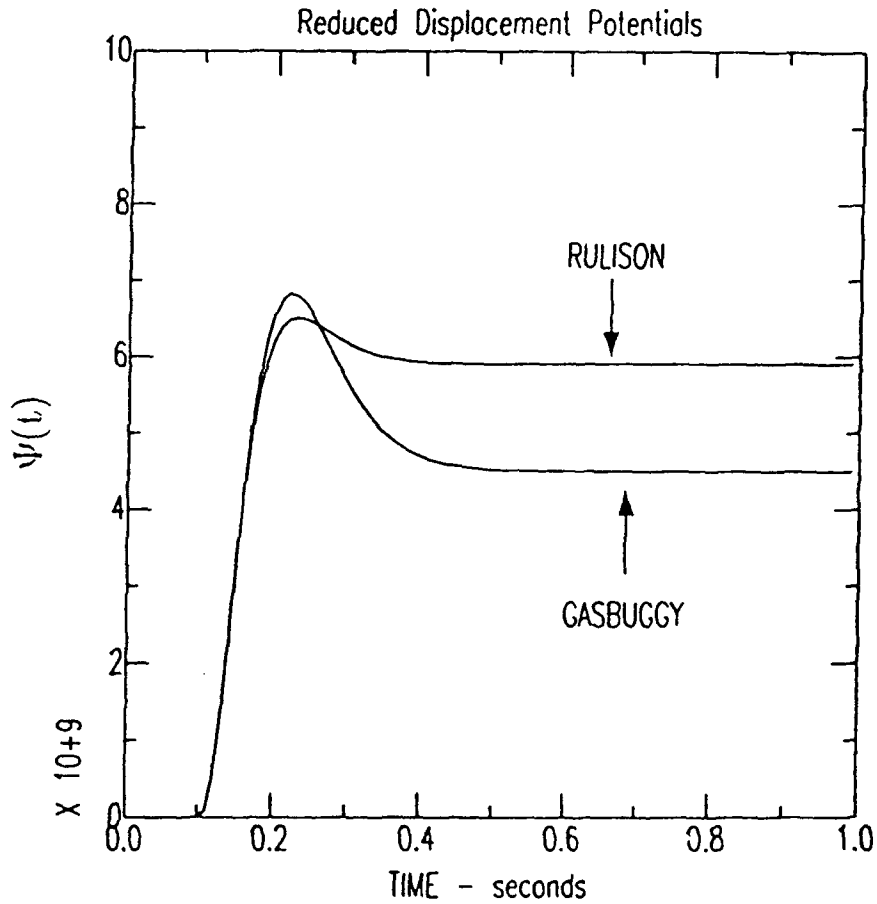

Figure 27. Reduced displacement potentials for PNE's GASBUGGY (B=0.64, K=31, Ψ_{∞}=4.5x10^9) and RULISON (B=0.27, K=37, Ψ_{∞}=5.9x10^9).

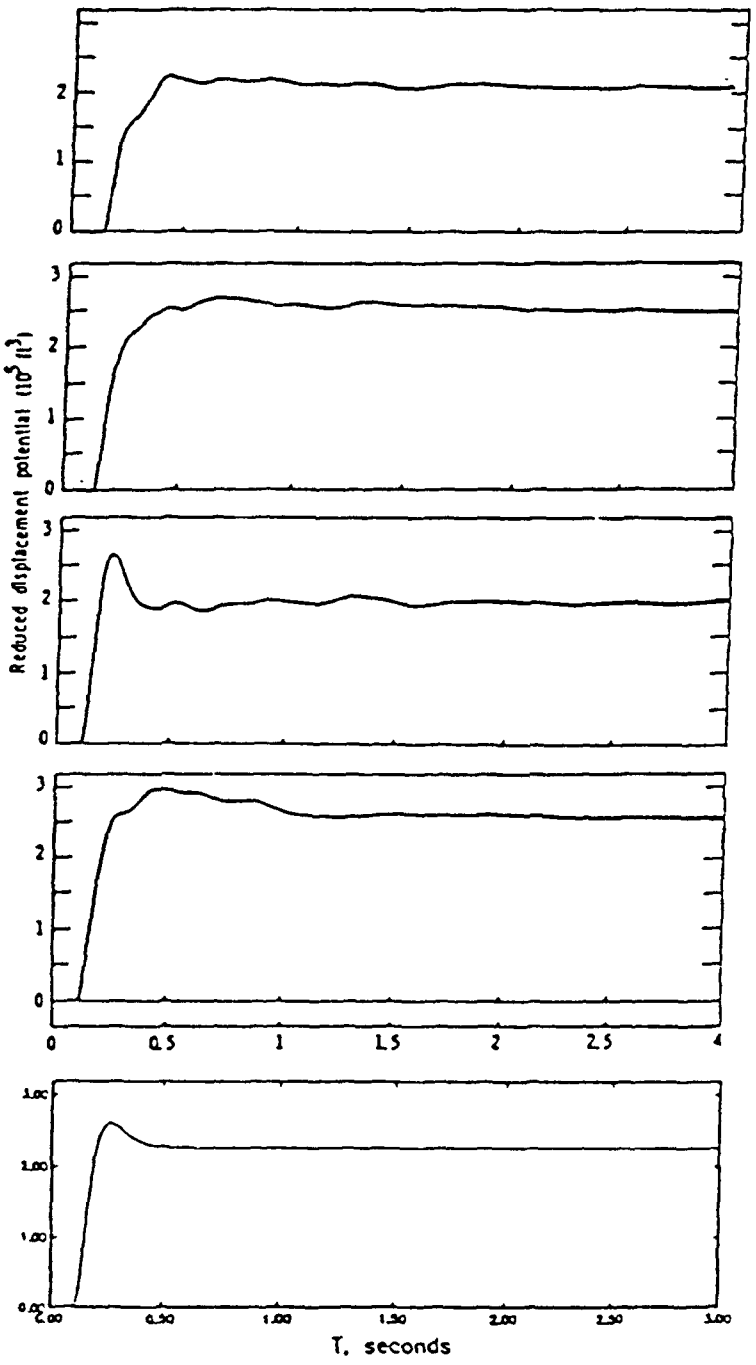

Figure 28. Upper four traces display the observed RDP's obtained from the GASBUGGY explosion, after Perret (1982). Bottom trace displays a scaled RDP.

B) FAULTLESS and ALMENDRO, Further Test of Scaling: Since the *P*-waveforms from Pahute Mesa events have been studied at great length by Burdick and his associates it is natural to compare data from the FAULTLESS event with a Pahute Mesa event (ALMENDRO) having comparable yield (see Figure 29). Both blasts were detonated in similar environments. ALMENDRO (m_b=6.41) was located roughly 150 km to the north. The pairs of seismograms are from the same teleseismic WWSSN stations. It appears that the FAULTLESS seismograms are anomalously long period for such a small event. This suggests a higher t_a^* but several detailed attenuation experiments indicate comparable values of t_a^* at these two sites. *NTS P*-waveforms for the large events such as BOXCAR are similar to FAULTLESS and intercorrelation of FAULTLESS using BOXCAR as a master event produce the same yields (Lay *et al.*, 1983). In short, the *P*-waveforms from FAULTLESS fall nicely into the Pahute Mesa population, but are too strong. Allowing the B to increase by roughly a factor of two for FAULTLESS can explain this δm_b anomaly as discussed in Burdick *et al.* (1991a). Since the M_S's for these events are roughly the same, we consider this a reasonable explanation.

Discussion: In previous sections we have reviewed the data and scaling law applications for various U.S. shots. In this section we discuss the yield equations put forward by other researchers for sites outside US and how we think these should be altered based on this study. Because of strong evidence for overshoot variations from site to site we believe that magnitudes based upon long-period excitation are the most reliable. Thus, we begin with yield estimation based on M_S. From Sykes and Wiggins (1986) we obtain the Novaya Zemlya scaling relation

$$M_S = 0.971 \log_{10} Y + 2.16$$

This equation, in fact, matches the Amchitka data better than does the Amchitka scaling relation presented earlier,

$$M_S = \log_{10} Y + 2.0$$

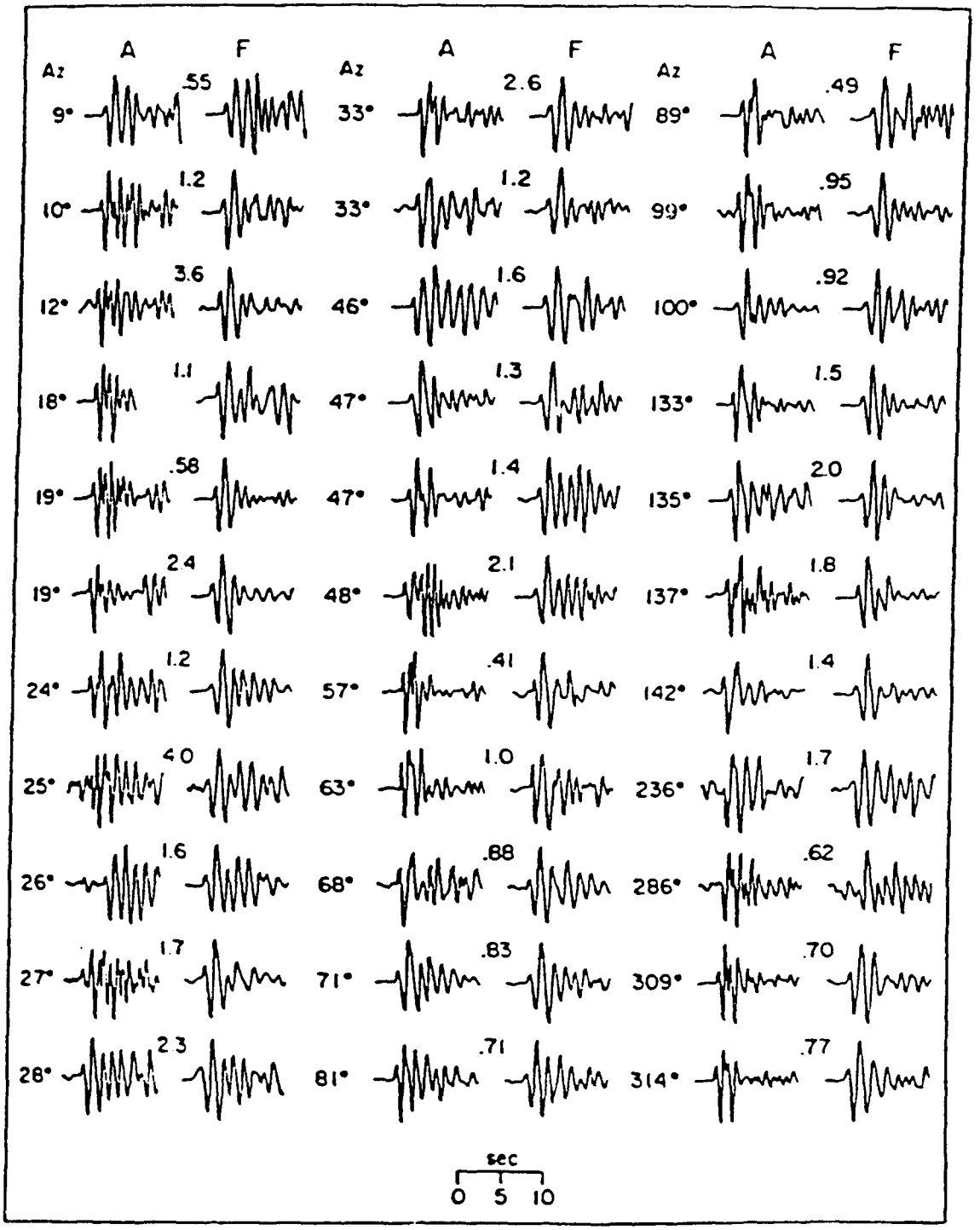

Figure 29. A comparison of seismograms of observed WWSSN *P*-waveforms for the two explosions ALMENDRO (A) and FAULTLESS (F) as a function of azimuth (same station). The numbers indicate the ratios of peak amplitudes (FAULTLESS/ALMENDRO).

when the most accurate yield values are inserted. This does not greatly change the modeling exercise discussed earlier except to make the dependence of B upon depth even stronger. The formula by Sykes and Cifuentes (1984) for Eastern Kazakh is nearly the same as above, namely,

$$M_S = 0.95 \log_{10} Y + 2.16$$

The results for NTS show an obvious off-set from Amchitka and other sites as discussed earlier. If we compare the 10 largest events fired at Shagan River versus the 10 largest events fired at NTS after the 1976 150 kt threshold (as suggested by Figure 16 of Stevens, 1986), we obtain

$$\overline{M_S}(\text{NTS}) - \overline{M_S}(\text{Shagan River}) = 0.63$$

with an average M_0 of 7.58 x 10^{22} dyne-cm at Shagan River *vs.* an average M_0 of 1.74 x 10^{23} dyne-cm at NTS. Our formula predicts a $\overline{M_S}$ for NTS which is 0.39 units higher than that for Amchitka. This suggests that the Ψ_- scaling laws for Amchitka are applicable to Soviet tests (as assumed by Sykes and his colleagues). Thus, NTS appears to have a unique scaling law characterized by undershoot compared to any other site. If we suppose that most of the Novaya Zemlya tunnel events are fired at similar depths, we conclude that the smallest events are over-buried while the larger events are under-buried. Thus, at Novaya Zemlya we would expect small B's for small events and large B's for large events, or m_b increasing with increasing yield more rapidly than at Amchitka (see Figure 30). For example, suppose we compare the larger events at Amchitka (where the data is the most complete) with comparable events at Novaya Zemlya. For the largest Novaya Zemlya event (October 27, 1973), the Sykes formula predicts a yield of 2840 kt for the observed M_S of 5.5. The Ψ_- obtained for this event by Cohee and Lay (1988) is 3.8 x 10^{11} cm^3 (assuming the SL8 attenuation model proposed by Anderson and Hart, 1978). This estimate was made using a t^*_β of 4.8, which is probably high. The trade-off between Ψ_- and t^*_β was shown earlier in Figure 24. Reducing t^*_α to 0.5 and t^*_β to 2.0 suggests a Ψ_- near 2 x 10^{11} cm^3, a value midway between that of MILROW and CANNIKIN. The m_b for the Novaya Zemlya event is 6.9 or that of CANNIKIN.

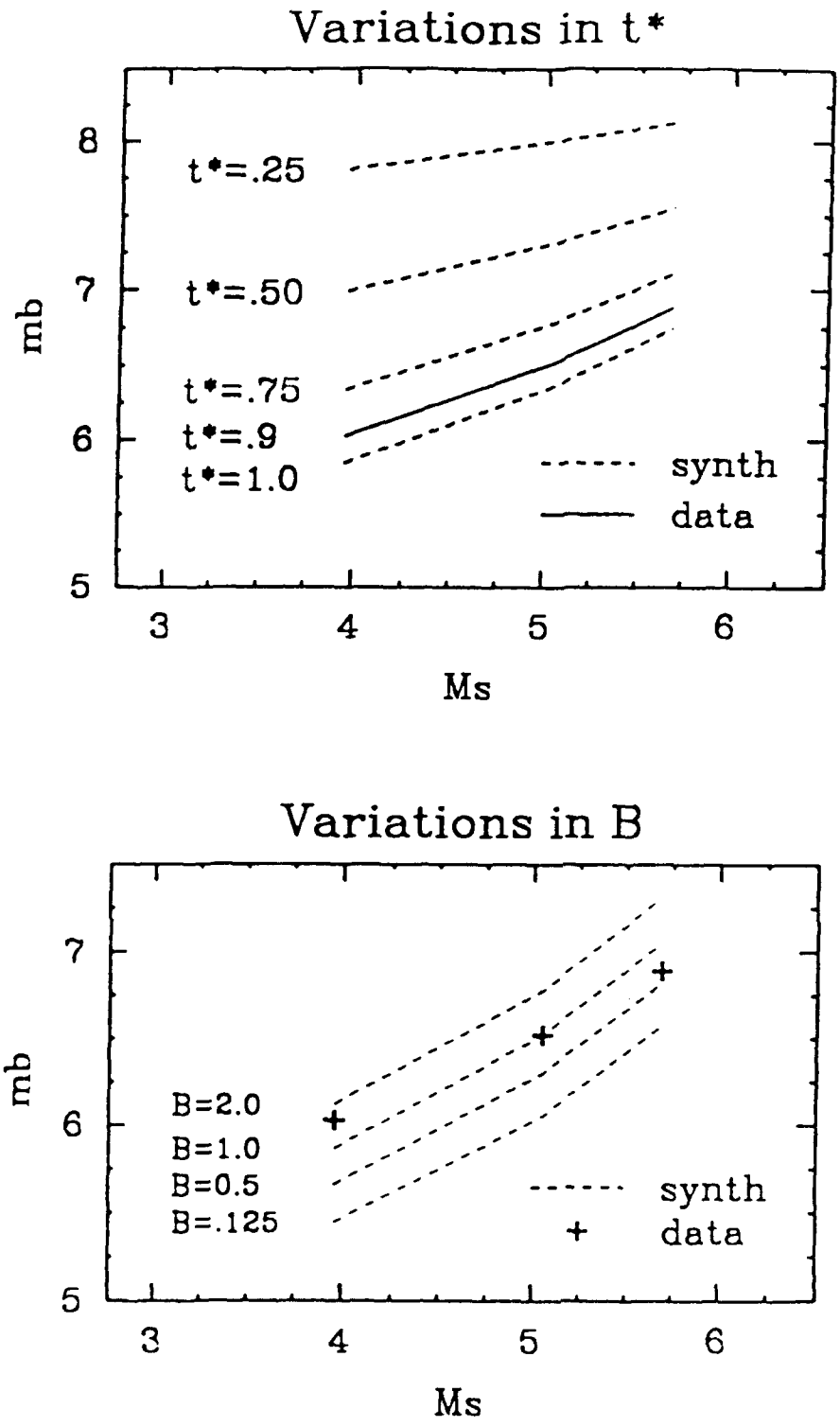

Figure 30. (Top panel) Effect of varying t_*^* on events LONGSHOT, MILROW, and CANNIKIN while holding source function and moment constant. The solid line represents actual m_b vs. M_S values. (Bottom panel) Effect of varying B for same events while holding t_*^* and moment constant. The crosses represent actual m_b *vs.* M_S values.

However, allowing B to grow for this large Novaya Zemlya event easily reduces its Ψ_- to a value near that of MILROW. In short, it is very difficult to use the m_b's to directly estimate yields while dealing with these trade-offs of t^* and B.

The m_b measurement thus is shown to have several problems in estimating the yield of bombs in geological regimes which do not have numerous test shots available. These include unknown factors of corner frequency, overshoot, tectonic release, and t^*. Using a regional M_S measurement, when possible, should serve to minimize the problems caused by these factors. Such factors as explosion coupling will still remain a problem.

In most instances, however, Soviet m_b's will still have to be used. Perhaps the simplest use of the Soviet m_b's is to directly relate them to Soviet M_S vs. yield relations. By taking

$$m_b = 1.05 M_S + 1.63$$

and substituting

$$M_S = 0.97 \log_{10} Y + 2.16$$

we obtain

$$m_b = 1.021 \log_{10} Y + 3.9.$$

Thus for events that have high F-factors we can still estimate the yields from m_b. This equation estimates the m_b of a 150 kt event at Shagan River to be 6.1 as observed during the recent PVE. However, instead of adjusting the U.S. curve by applying the δm_b bias correction, we adopt the scaling relation from that of Amchitka and explain the difference in m_b by overshoot and attenuation.

Q STUDIES PART I - EFFECT OF Q ON THE REGIONAL Pn and Sn COMPOSITION RECORDED IN U.S. AND U.S.S.R

Introduction: With the installation of the broad-band, high dynamic range IRIS instruments, it has become possible to compare the regional waveforms of earthquakes and explosions at magnitudes 3 to 6. The dynamic range feature of these systems allows the comparison of the relatively waek body waves (Pnl) with the stronger surface waves. The broad-band feature allows the examination of the frequency content of particular phases (Pn and Sn) to address the Q-issue. Computational methodologies have advanced in recent time which together with the development of recent fast computational facilities has made it feasible to investigate the response of a laterally varying crustal medium within a reasonable time frame. Among other methods, the generalized ray theory is a most widely used method for analysis of the composition of seismic phases that the source process and the propagation effect together make up at a receiving station. While this method is applied to a flat-layered crustal structure in most studies, the method has recently been extended to include range-dependent structure (Helmberger, personal communication). It is a computationally fast technique, but requires many generalized rays to be tracked between the source and the receiver for a regional waveguide. As the crustal medium becomes complicated, the method can quickly become quite cumbersome with the process of just tracking the rays. The anelasticity of the waveguide is applied to resulting response of many generalized rays in terms of t^* which is an average estimate of seismic attenuation. In actuality, seismic waves attenuate in different amounts depending on the material property and should be treated as an intrinsic behavior of the medium. Thus, Q (quality factor) should be defined for each crustal layer for both compressional and shear waves.

At high frequencies the effects of scattering in the crust become so intense that only statistical properties of waveforms are meaningful. The receiver related crustal structure can be complex and may cause additional complexity beyond that already caused by the triplications of seismic waves due to the gradual velocity increase of the crust-mantle transition zone. The presence of a

gradient structure near the receiver changes the timing of surface reflected phases and their reflection coefficients. Consequently, the waveforms become complex and generalized ray theory can be used to identify the significant arrivals within the composition of short-period signals (Saikia and Burdick, 1991). The most suitable computational method to apply for investigating the effect of a crustal waveguide of this nature is the method of frequency-wavenumber integration/reflectivity. It allows evaluation of full medium response where the intrinsic aspects of the attenuation of the medium can be specified and effects on the Pn and Sn composition can be investigated.

In a recent study, Saikia and Burdick (1991) showed that short-period P_{nl} waves (period as short as 2 s) are stable and can be modeled. They studied many observations from Nevada Test Site (NTS) explosions recorded at regional distances of 200 to 420 km and modeled the P_{nl} waveforms using a deterministic crustal waveguide. The sources of these waveforms were shallow. Also, the sources were predominantly isotropic, and the portion of P_{nl} waves which was included in the P_n and P_g waves had a duration of about 30 s and was dominated by compressional waves. To understand the observed data, they used the frequency-wavenumber algorithm to compute the explosion generated P_{nl} waves for several canonical crustal models and selected a crustal model based on the agreement between the data and the synthetic seismograms. The method was then utilized to understand the composition of the P_g wave group which was constituted of phases like PmP, pPmP, 2PmP, PmS, pPmS, PmPSmP, PmSPmP etc for realistic models. P_g is a wave group whose frequency content is widely used to discriminate events. In this study, we have taken a similar strategy to investigate the broadband composition of P_{nl} and S_{nl} seismograms recorded in the North American continent at regional distance from double-couple sources and of the P and S waveforms that are recorded within the Soviet Union. We shall mainly focus on identifying the rays important to model the regional waves within the S wave window and investigate how the intrinsic Q model affects the waveform composition.

Data: For the U.S. study, we used a set of three-component broadband seismograms recorded at Harvard (HRV) station at a distance of 640 km from the Saguenay earthquake of November 25, 1988 (Figure 31a). These seismograms were recorded on a Streckeisen seismometer. We selected these seismograms because many features recorded on the seismograms were successfully modeled by Zhao and Helmberger (1991). Beginning with their crustal model, we have directed our study towards the modeling the high-frequency details observed in the P_{nl} waves and the composition of waves identified as S_n and sS_n by Zhao and Helmberger (1991) using a multiple source model. A similar study was directed towards the modeling of the broadband seismograms recorded within the Soviet Union. We selected a set of three-component seismograms recorded at GARM from an earthquake which originated at a distance of 200 km at an azimuth of 290° on May 4, 1989 (38.73°N and 78.5°W, Figure 31b). Unlike for North American earthquakes, the waveforms of very few Soviet Union earthquakes have been modeled. Thus, it is necessary to develop a starting crustal model even to obtain a first-order agreement between data and synthetic.

Modeling of HRV Seismograms from the Saguenay Earthquake: Figure 32 shows the broadband displacements recorded at Harvard station. To investigate the influence of crustal structure on the various significant phases of the P_{nl} window, we have started with the crustal model shown in Figure 33 by dotted lines. This model extends from the surface to a half space at a depth of 55 km. The major velocity discontinuity is at a depth of 35 km where the P velocity jumps from 6.71 km/s to 8.1 km/s and the S velocity jumps from 3.82 km/s to 4.7 km/s. Zhao and Helmberger (1991) used a reflectivity code (Mallick and Frazer, 1988) to compute the medium response and used an elastic crustal structure to model the data. They used a Q_β (shear-wave quality factor) of 6200 and stated that a lower value of Q_β is not required to match the recorded wave form, although the conventional wisdom is that for eastern North America Q_β is of the order of 300 (Hwang and Mitchell, 1987). Based on this published information, we started to look for certain phases within the P_{nl} regime for which the agreement between the data and synthetic can be improved and in the process to learn more about the regional waveguide.

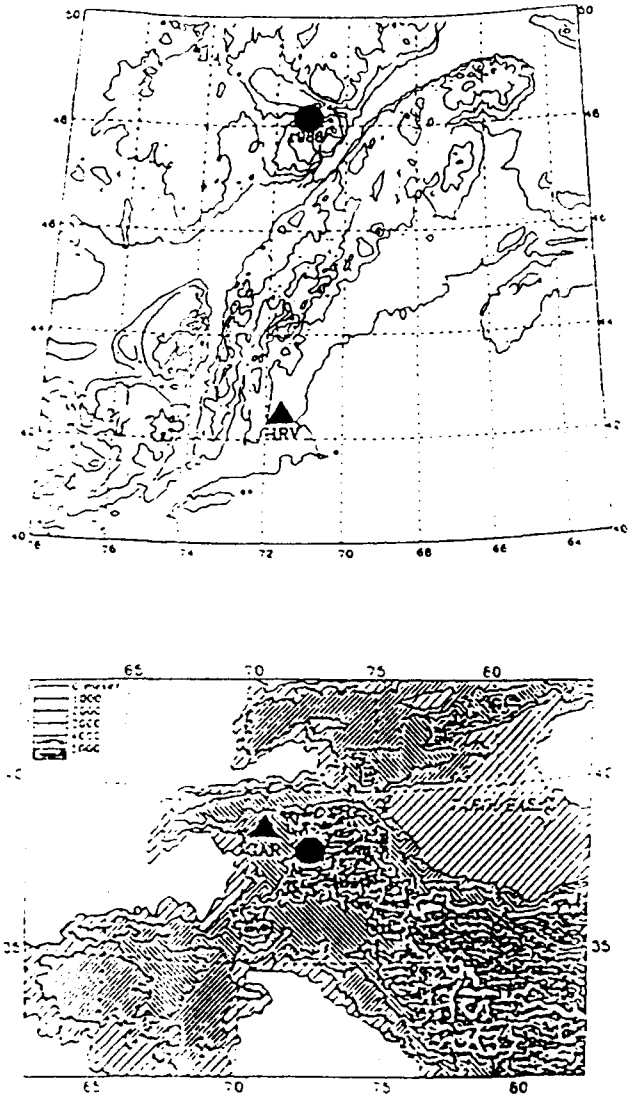

Figure 31. Geographical location of (a) HRV (Harvard0 station (solid triangle) and November 25, 1988 Saguenay earthquake (solid star) and (b) GAR (Garm) station (solid triangle) and May 4, 1989 USSR earthquake (solid star).

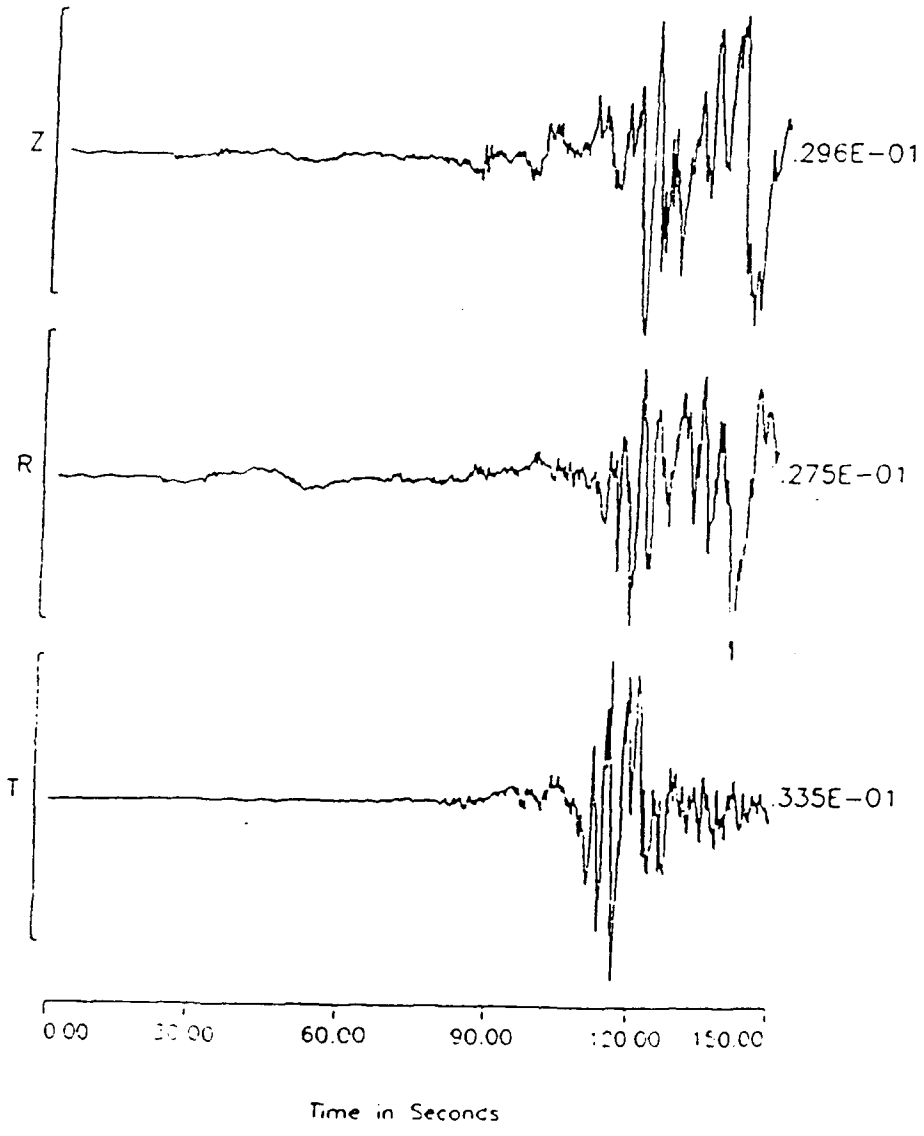

Figure 32. Broadband three-component displacement seismograms as recorded by Harvard station from the 1988, November 25 Saguenay earthquake. The original seismograms were integrated.

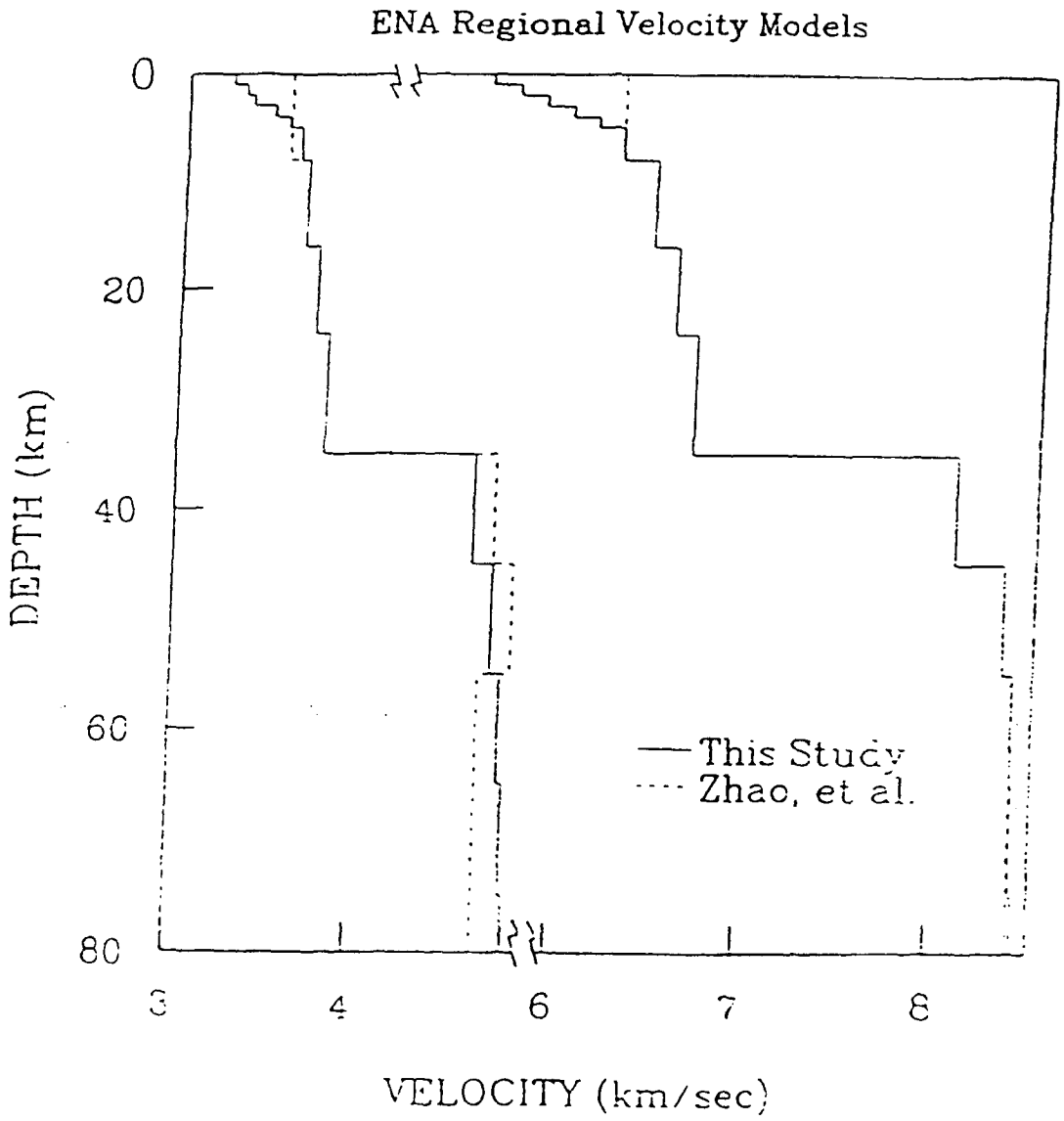

Figure 33. Regional crustal model developed by modeling the broad-band seismograms recorded at Harvard station from the November 25, 1988 Saguenay earthquake. The final model is shown by the solid lines. The model shown by the dotted lines is the initial crustal model developed by Zhao and Helmberger, 1990.

The phases marked as S_n and sS_n show the greatest misfit between the data and the synthetics computed by Zhao and Helmberger (1991) (see their Figure 16). The synthetic seismograms are definitely of lower frequency. So our initial attempt was to understand what part of the crustal waveguide would be most critical in development of these waveforms. In the present calculation, we used the frequency-wavenumber integration method and set the nyquist frequency at 10 hz. We computed theoretical seismograms for eight fundamental faults and used a focal mechanism with a dip 65°, a rake of 78° and a strike of 323° to predict the vertical, radial and tangential component seismograms. These synthetics were used to compute both the point and multiple source seismograms and the corresponding vertical component seismograms are shown in Figure 34. The source model contained three sub-sources, with seismic moments of $1.55x10^{24}$, $1.45x10^{24}$ and $1.95x10^{24}$ dyne-cm respectivelyi (after Zhao and Helmberger, 1991). The second source was delayed by 0.65 s and the third source by 1.45 s from the first source to account for the propagation of the rupture front. The first source was represented with a source time function defined by a trapezoid of 0.4s rise time, 0.05s of follow-on time and 0.25s of healing time. Similarly, the second and third sources were convolved with trapezoids of (0.2s, 0.15s, 0.15s) and (0.1s, 0.3s, 0.2s), respectively. We also show the synthetic seismograms generated by Zhao and Helmberger (1991) in Figure 35 using a nyquist frequency of 4 hz so that a direct comparison can be made with those shown in Figure 34. The frequency content in the Pnl waves of these seismograms is not as rich as those Pnl waves shown in Figure 34 where the high frequencies are the result of derived source complexity.

In Figure 36, we compare the vertical and radial component showing just the Pnl portion of the seismograms computed using the parameters of multiple sources. The high-frequency signals are adequately predicted with respect to those observed on the recorded data. The seismograms computed using the response up to 4 Hz were essentially identical to these seismograms.

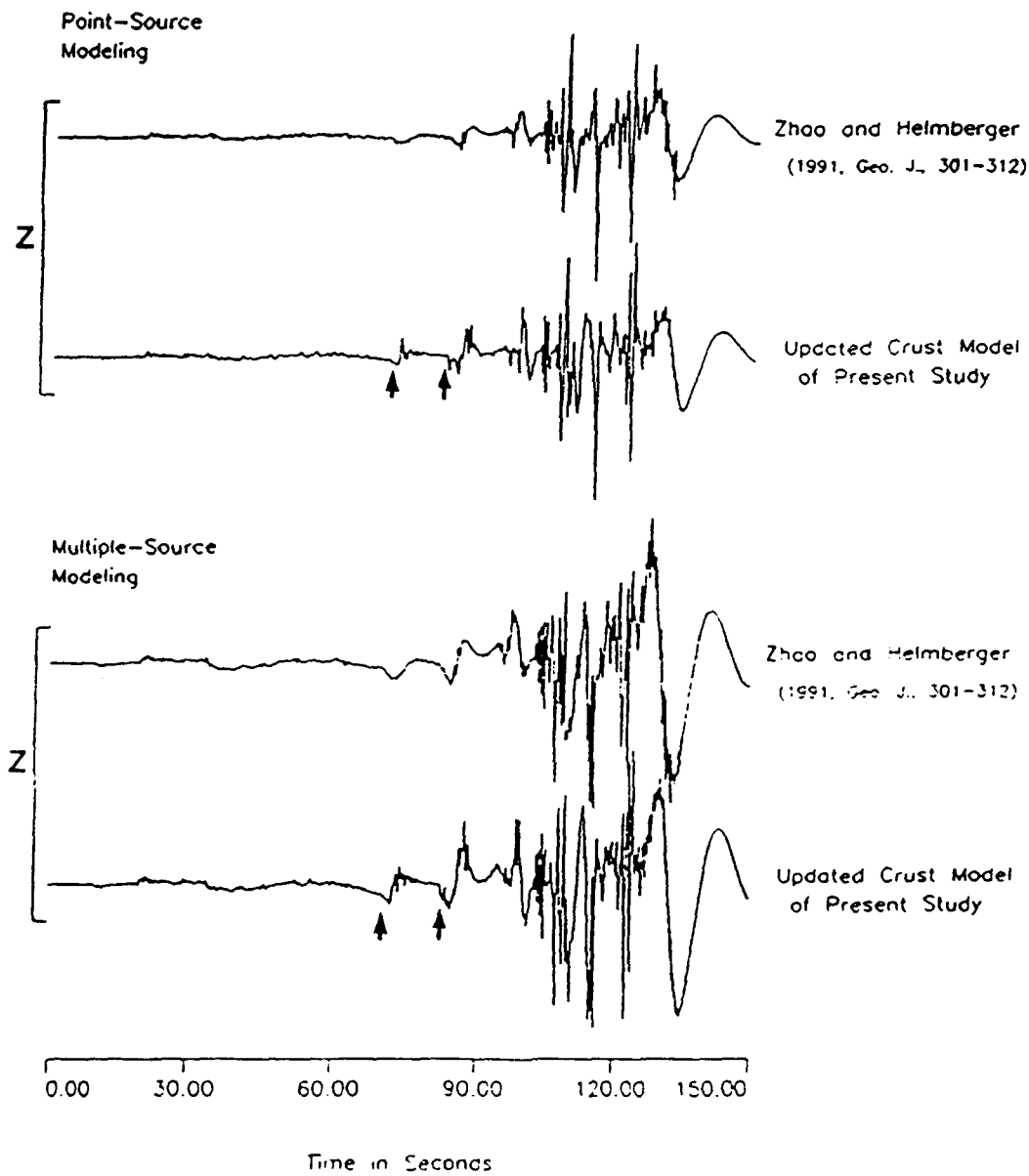

Figure 34. Comparison Between two sets of displacement seismograms synthesized using point and multiple sources. (a) Point-source displacements - the upper seismogram is computed using the model response of Zhao and Helmberger (1991) and the bottom seismogram is computed using the model response of the present crustal model, and (b) multiple-source displacements for the two crustal models.

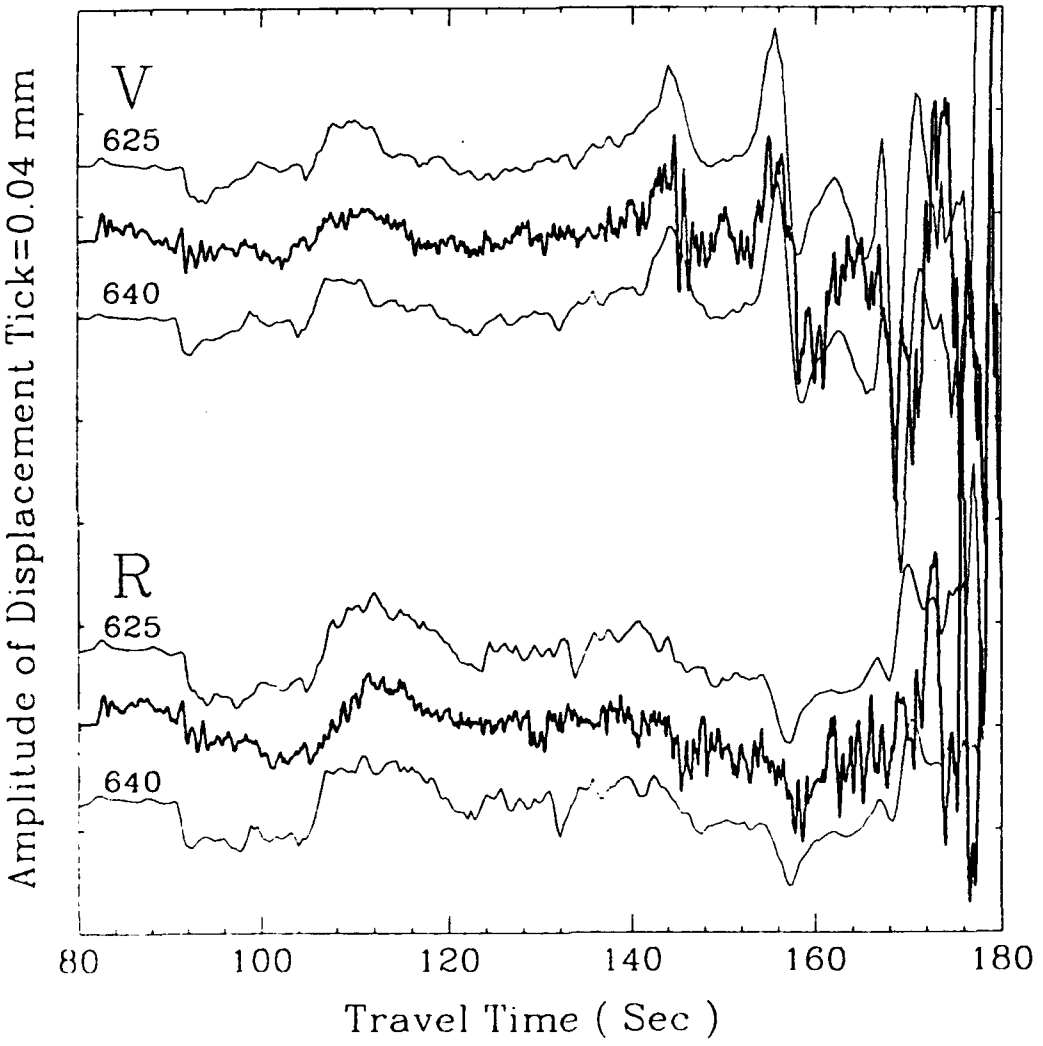

Figure 35. Comparison between data and synthetic displacements with a nyquist of 4 Hz. The seismograms for 625 km was computed using a different velocity crustal model (Figure taken from Zhao and Helmberger, 1991).

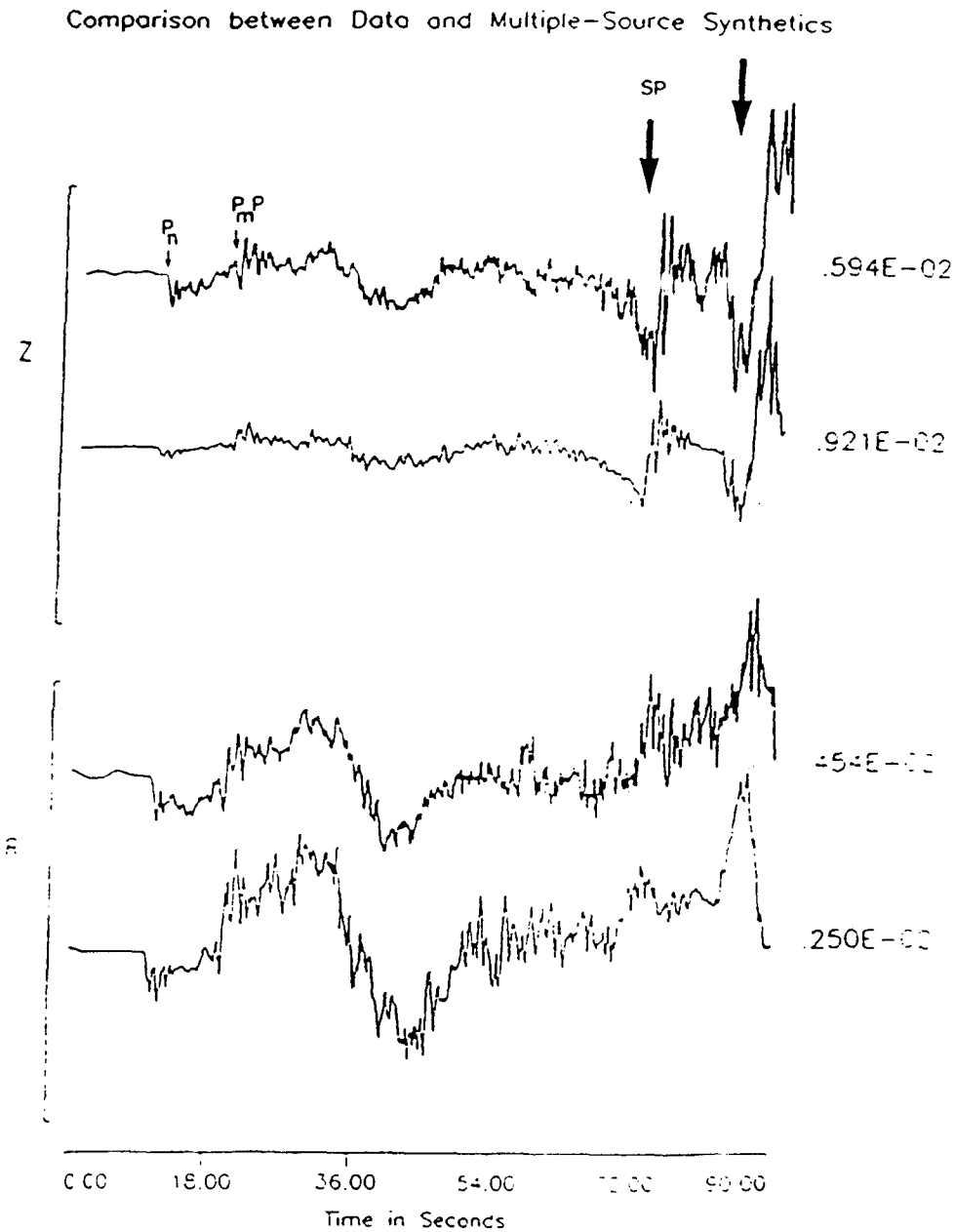

Figure 36. Comparison between data and synthetic displacements with a model response up to a nyquist of 10 Hz. Note the developement of high frequencies and agreement between phases marked by the arrows.

Ray Analysis of Pnl Seismograms: In this section, we discuss our investigation of the constituent phases of the recorded P_{nl} seismogram at Harvard station. The basic idea is to investigate the interaction of individual ray groups in creating the total seismogram. We computed generalized ray seismograms using the source process of the Saguenay earthquake for several groups of generalized rays. In Figure 37, we display vertical-component seismograms of these ray groups. The top six seismograms are normalized to their maximum amplitude. All the PmP and SmS rays were allowed to reflect from each interface beneath the crust-mantle boundary including the reflection from the Moho discontinuity. The total response of these PmP and SmS rays is plotted in the first seismogram. The geometric arrivals are indicated by PmP and SmS respectively. The S_n arrival is small and is preceded by a refracted phase SP. This refracted phase had developed due to a critical incidence of an S wave on an interface permitting the converted P phase to travel along the interface. The seismogram in the second row is for the sPmP, a ray which has departed from the source as a S wave and then converted to P mode at the free surface. The amplitude of this ray is small. The next seismogram is for sSmS. Both the geometric and head waves are strong for this ray group and contribute significantly to the total seismogram. The next two seismograms are for the SmSSmS and sSmSSmS ray groups. Both the ray groups have significant contributions. The sixth seismogram is for a ray group identified as SmSiSmS. The rays included in this group leave the source downward and reflect from each interface. The reflections are turned back into the lower crust again at the Moho discontinuity before they are reflected back to the receiver. The contributions from these rays do offer a significant contribution to the evolution of the S_n wave group. The seismogram "Total" is the result of direct sum of the upper six seismograms. Having obtained a good agreement between the data and the synthetics, we plotted the multiple-source frequency wavenumber seismogram computed using the frequency-wavenumber method beneath the total response for a direct comparison. This comparison produced good agreement among the dominant features within the so called "S_n waves".

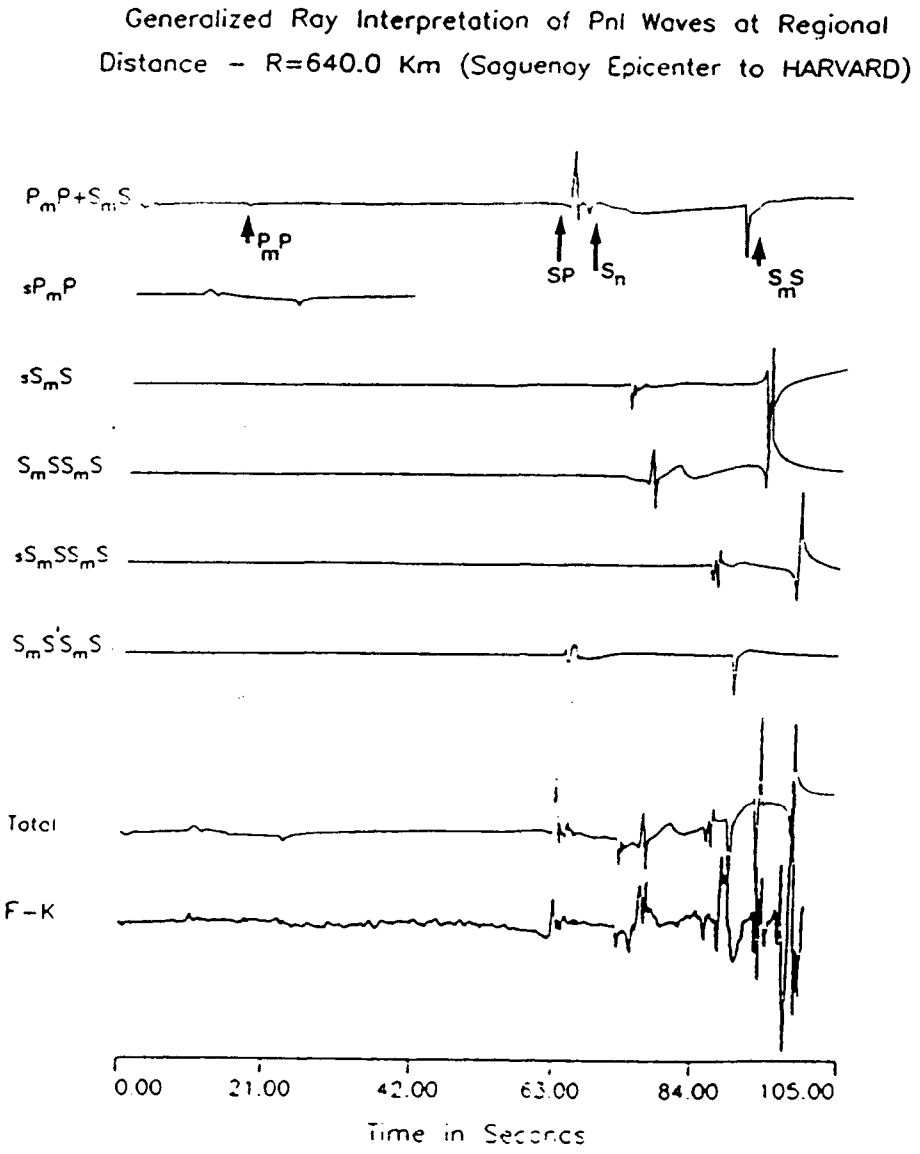

Figure 37. Understanding the wavform recorded at Harvard station using the ray decomposition technique. The top six seismograms are for the individual ray groups. The seismogram labelled "Total" is the total response of all the responses of upper six seismograms and the comparison with the F-K seismograms shown below suggests a good agreement between the two seismograms.

Thus, we have extended our previous study (Saikia and Burdick, 1991) on the deciphering of the ray composition of Pg waves from explosion sources to earthquake sources. As in the above study, we found that the waveforms within the Sn group can be studied in time domain in terms of a basic few rays, namely the SmS, sSmS, SmSSmS, sSmSSmS and SmS^{i}SmS rays. Since these phases leave the source as S waves, they are not excited by the explosion source. Therefore, the only phases that may arrive within the S_n widow from a pure isotropic source are the P waves that are converted to S waves.

Effect of Intrinsic Q on Pn and Sn: It is expected that anelasticity will influence the frequency content of the Pn and Sn waves. In this study, we wish to investigate the effects on regional Pn and Sn composition related to intrinsic Q, especially the changes relative to the seismograms of an elastic medium. Our objective is to determine the group of waves that is most sensitive to the variation in Q. We assume that Q varies significantly within the upper crustal medium. An initial anelastic calculation was performed using a Q_β of 250 in the upper 35 km of the crust. Q_α was assumed to be twice of Q_β. Below 35 km, the entire medium was treated as elastic. In an another Q model, Q_β was lowered subtantially from 250 to 50 within the upper 5 km of the crust. Figure 38 shows a comparison of the recorded broadband vertical seismograms at Harvard station (top seismogram) with three synthetic seismograms resulting from the elastic and two anelastic propagation media. The second seismogram is mutiple-source seismogram computed using the elastic model. While the frequency content of the signals marked by arrows compare well with the data, the surface waves are of much higher frequency. The third seismogram is synthesized using the anelastic model of Q_β equal to 250 throughout the 35 km thick crust. The fourth seismogram is synthesized with a Q_β of 50 as discussed. The bottom two seismograms are remarkably similar. The frequency content of the surface waves or other multiple bounces following the third arrow are in better agreement with the data although the fundamental-mode Rayleigh wave appears longer in period.

In Figure 38, we show only the first 75s of the seismograms plotted in the previous figure. Clearly the similarities between data and synthetics are striking, suggesting that the waveshape of the P_{nl} waves is least affected by the variation in Q model. Figure 39 shows a comparison of both Pn and Sn wave groups separately as a function of different Q models. The seismograms shown in the two boxes are the windowed Pn and Sn waves shown in the upper two seismograms. Included in the Pn panel are the classical/turning ray Pn and PmP wave, and in the Sn panel are the classical/turning ray Sn, surface refracted SP, sSn and SmSSn waves. As seen in the previous figure, the P waveforms are strikingly similar but the waveforms drawn in the Sn box, especially the sSn and SmSSn phases, show a large dependence on the Q model.

This study pertains to the Saguenay earthquake which is a deep event, depth 27 km. We would expect explosions to be shallow. But the Pn generated from such shallow sources spends only a slightly longer path in the low Q materials. Thus it can be assumed that the initial Pn waves from the two sources will be affected in an identical manner by anelasticity. However, the phases like sSmS and SmSSmS are more dramatically affected by the Q model. Therefore, any spectral ratios of Pn to SP+sSn; pPn to SP+Sn etc., may provide a reasonable measure of Q.

Modeling of GARM Seismograms from May 4, 1989 USSR Earthquake: In this study we have used a set of three-component seismograms recorded at the Garm station from an earthquake of May 4, 1989 (latitude: 39.436°N and longitude: 75.35°E, h=35 km, ISC). The station is located at a distance of 200 km from the source. Figure 40 shows the recorded displacements processed from the broadband velocity seismograms. A high-pass filter was applied to remove the long-period effects. The crustal structure encountered by the wavefield along its propagation path is complex which is reflected in the waveform. To begin to understand the waveforms, it was necessary to develop a crustal structure.

Our strategy for developing the crustal model was to begin with the tangential component seismogram because of the simplicity of the observed displacement. This component contains only three distinct individual arrivals as marked by the arrows. We used generalized ray theory to

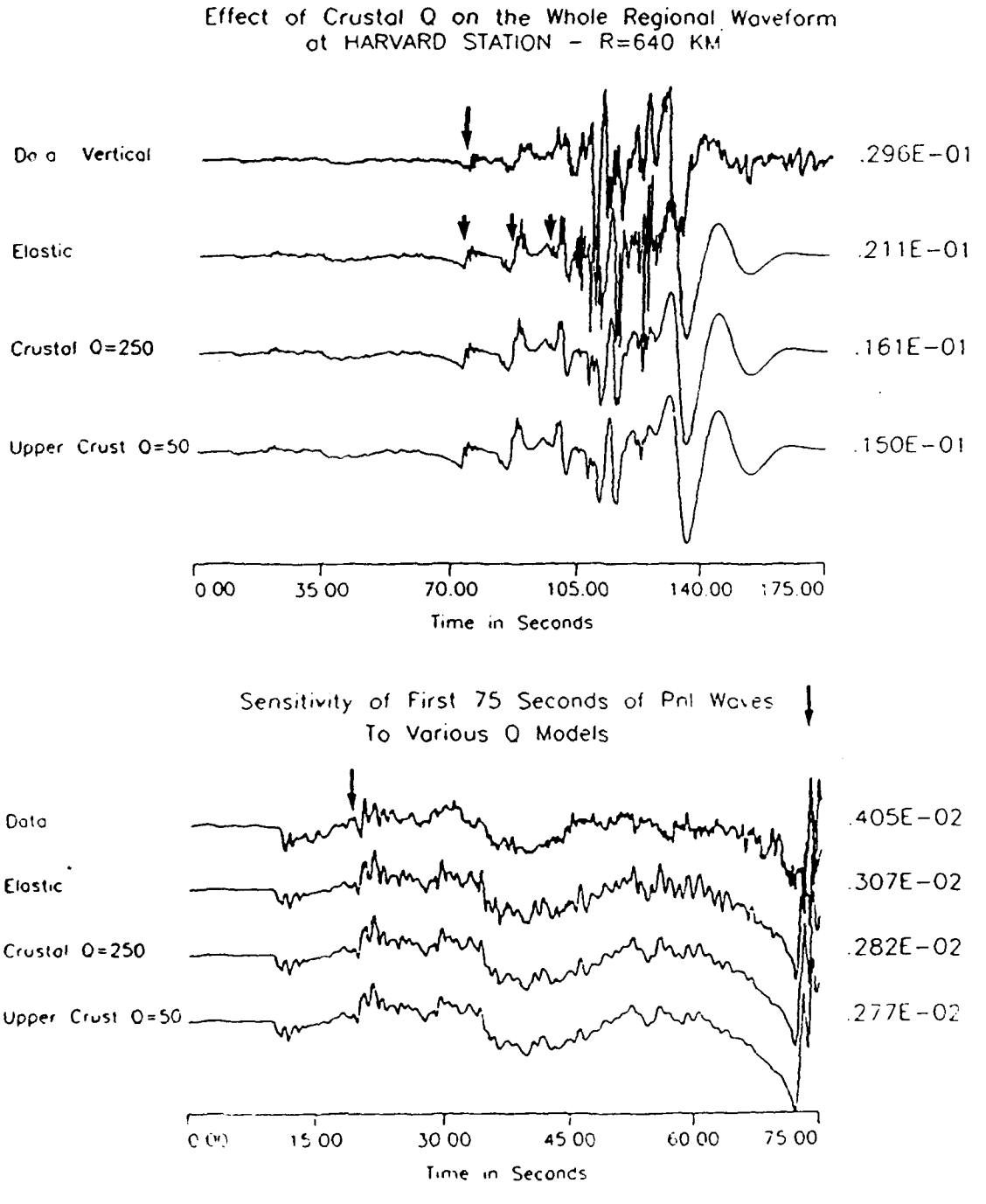

Figure 38. Comparison between broad-band vertical component data at Harvard station and corresponding synthetic seismograms computed for different Q-models including the elastic model. Also shown is the first 75 seconds of each seismogram for each Q model.

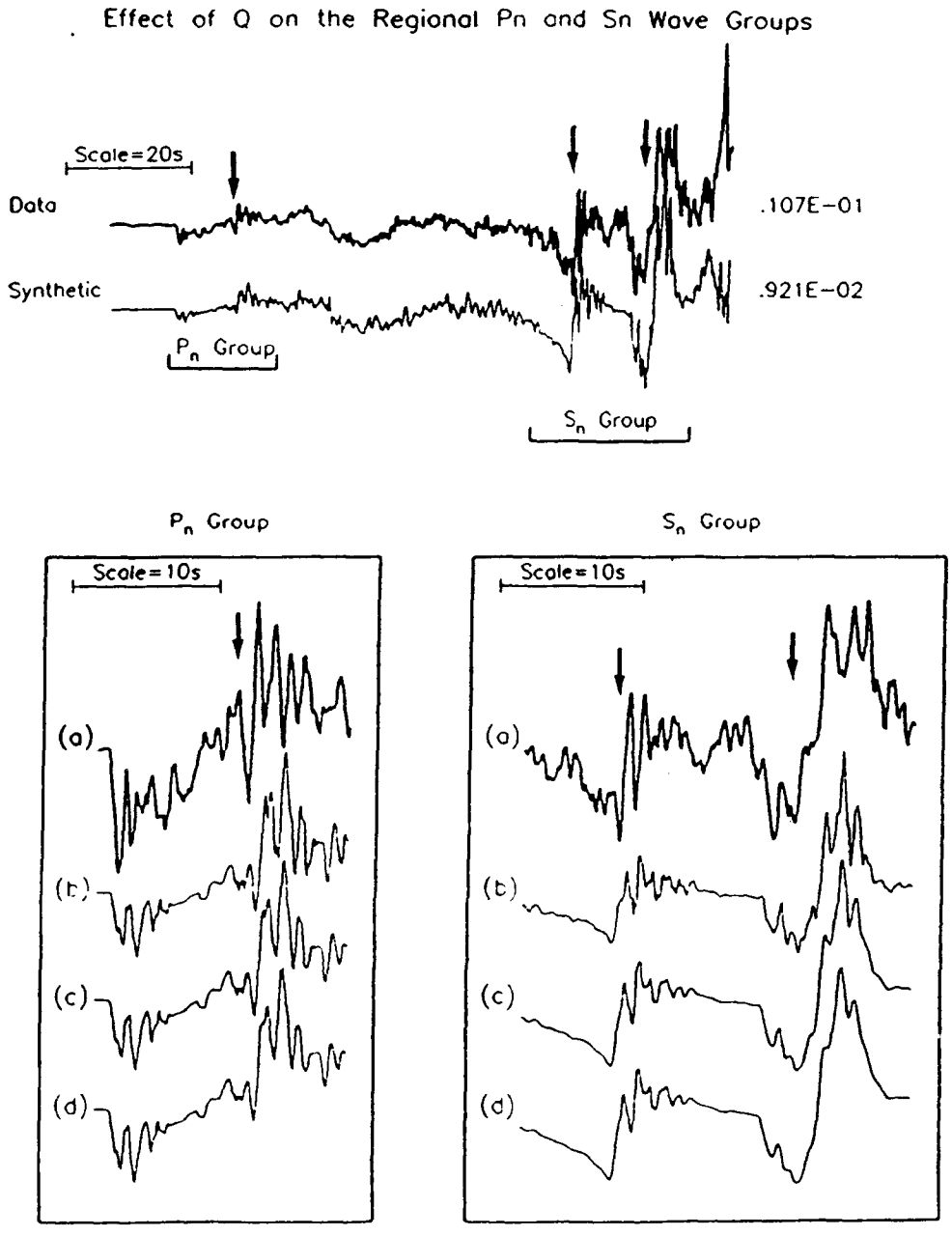

(a) Data. (b) Elastic. (c) Crustal Q=250. (d) Upper Crustal (5km) Q=50

Figure 39. Comparison between data broad-band vertical component Pn and Sn data and corresponding synthetic seismograms computed for different Q-models including the elastic model. The effect of Q on the Sn waves is more pronounced compared to the effect observed on the Sn waves.

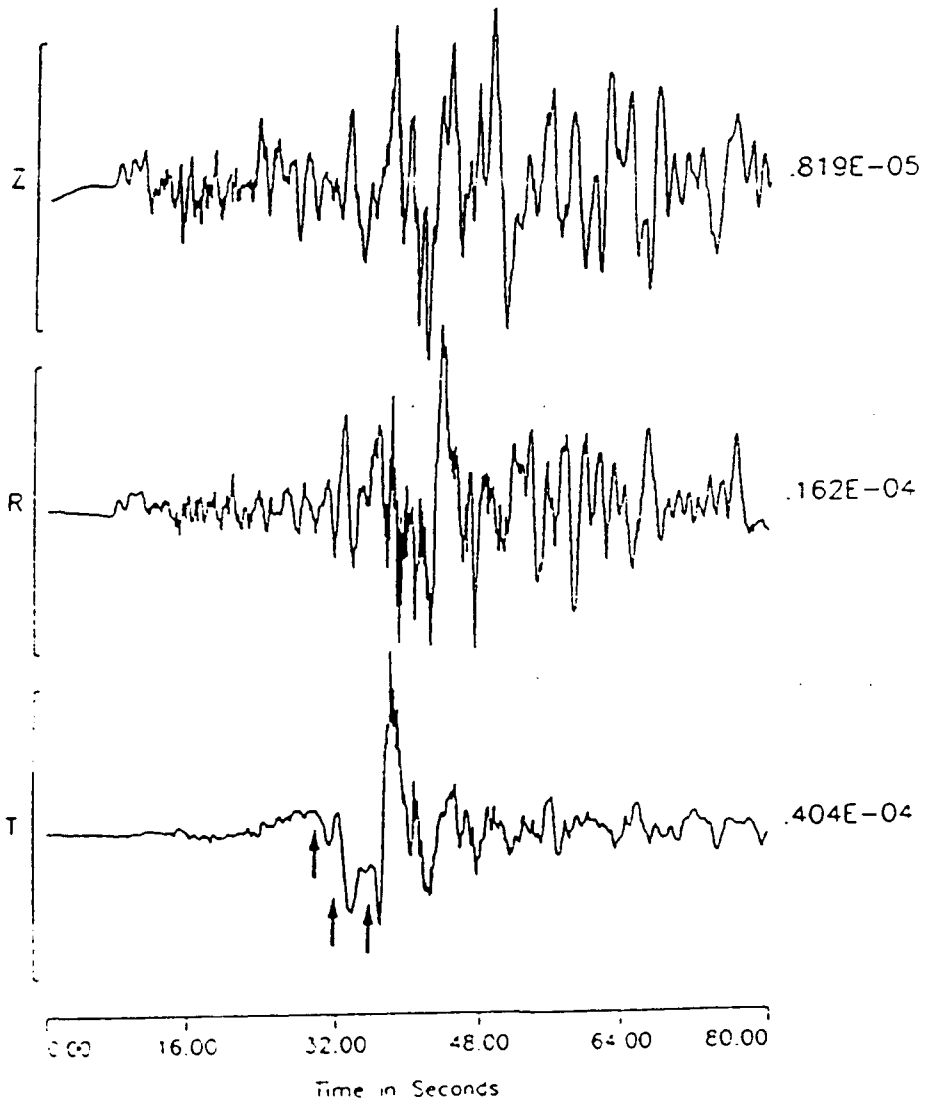

Figure 40. Broadband three-component displacement seismograms as recorded by Garm station from the USSR earthquake of May 4, 1989. The original seismograms were integrated.

synthesize this component for various crustal models and several source depths. The best prediction was obtained for a source depth of 25 km for the preliminary crustal model shown in Figure 41. We used the following focal mechanism: dip=75°, slip=-135° and a strike=32°. The structure contains two major discontinuities representing the Conrad and the Moho. We succeeded in modeling the tangential displacement using only three arrivals; the direct SH and two reflections from the discontinuities. The frequency-wavenumber seismograms were computed with these parameters and were compared with the recorded data. Figure 42 shows the comparison between the data and the synthetic seismograms for the vertical and tangential components. We are successful in producing a good agreement between the data and the synthetic for the tangential motion. We mark the individual arrivals in the synthetic and show their correspondence with the data by the thin arrows. The vertical component show agreement in the arrivals of Pn, PmP, ScS and SmS phases. The signal bracketed within the window of the vertical-component synthetic seismogram has a similar character in the frequency content to the signal bracketed within the data window. Figure 43 shows a generalized ray seismogram using the three rays. The vertical synthetic seismogram has a strong SmS which is smeared out in the data due to the interaction with the physically more complicated crust in the region. The vertical component of the recorded seismogram is also dominated by long-period P_{nl} signals shown by the solid window. These waves are also observed in the synthetic seismogram but arriving at Garm with a fast velocity. We also investigated the effect of a possible linear velocity gradient near the free surface to determine if such a velocity distribution would account for the mismatch between the data and the synthetics within bracketed the window shown in Figure 42. We discretized the top ten kilometers of the crust into ten layers of equal thickness and allowed a P-wave velocity increase from 4.5 km/sec to 5.5 km/sec from the surface. The S-wave velocity within each layer had a ratio of 1.73 to the P-wave velocity. This seemed to be a particularly reasonable explanation for the small complex phases between the major arrivals. However, the synthetic seismograms computed using this surface gradient did not improve the fit to a significant degree.

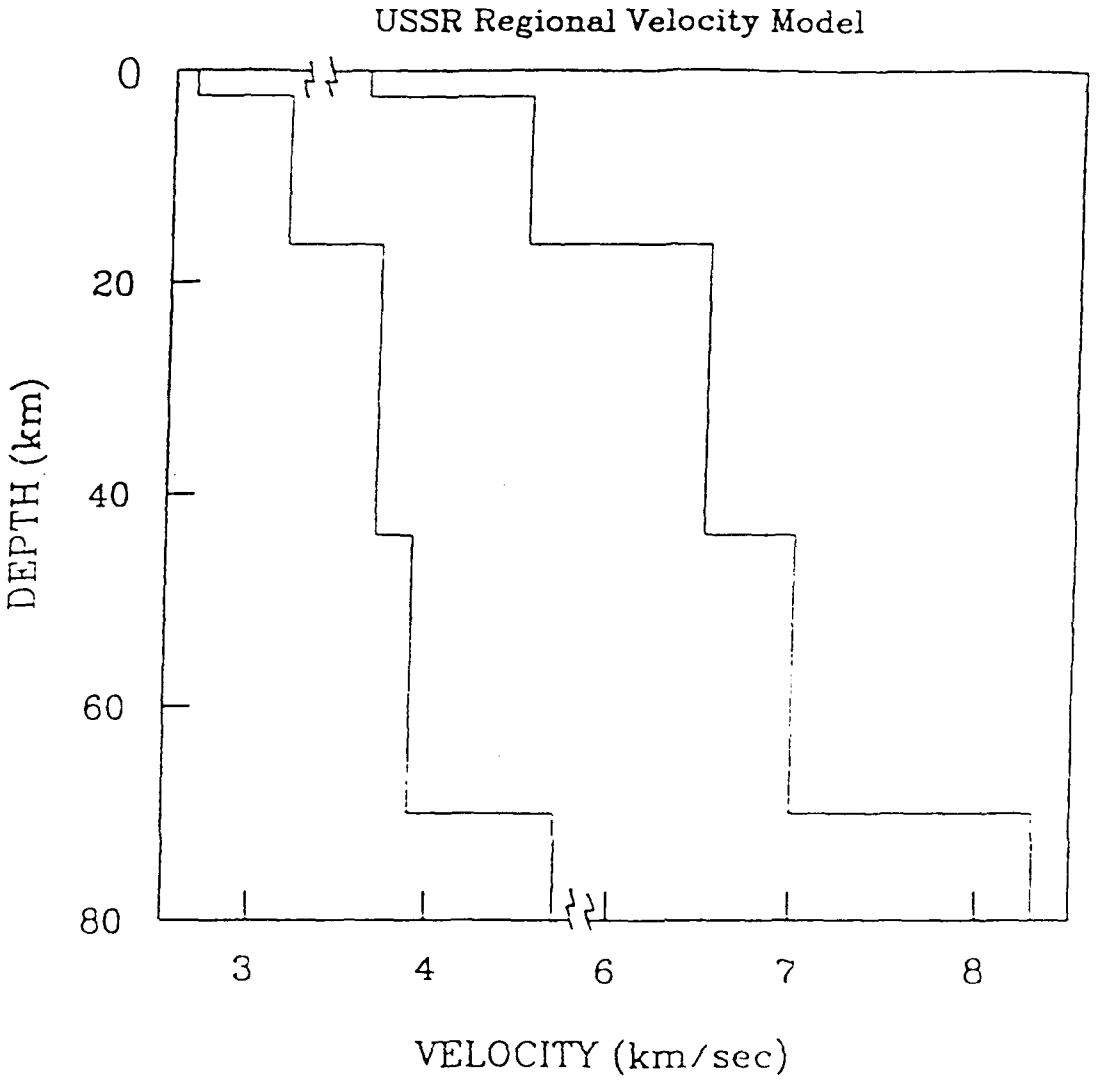

Figure 41. Regional velocity used for modeling GARM seismogram.

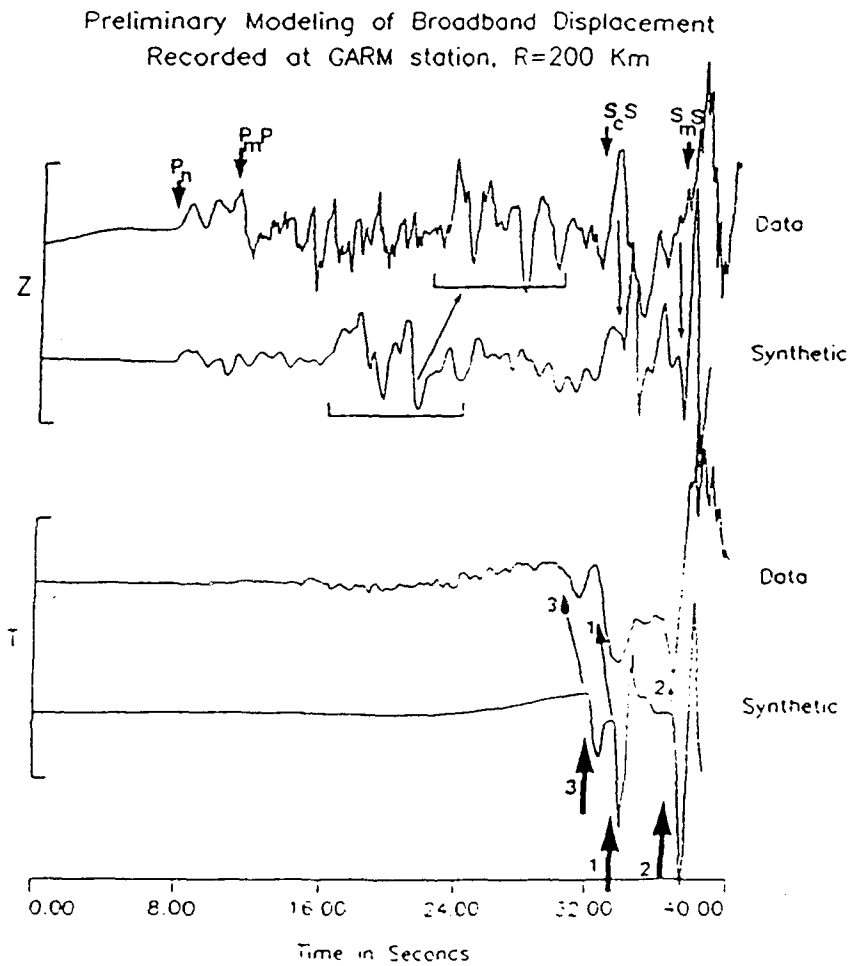

Figure 42. Comparison is shown between the data and the synthetic seismogram for the vertical and tangential components. The signal marked by arrow 1 is a phase reflected from the Conrad and by arrow 2 is form the Moho discontinuity. The phase marked by arrow 3 on the tangential component is the direct arrival. The signal within the window shows a possible correlation between the data and synthetics.

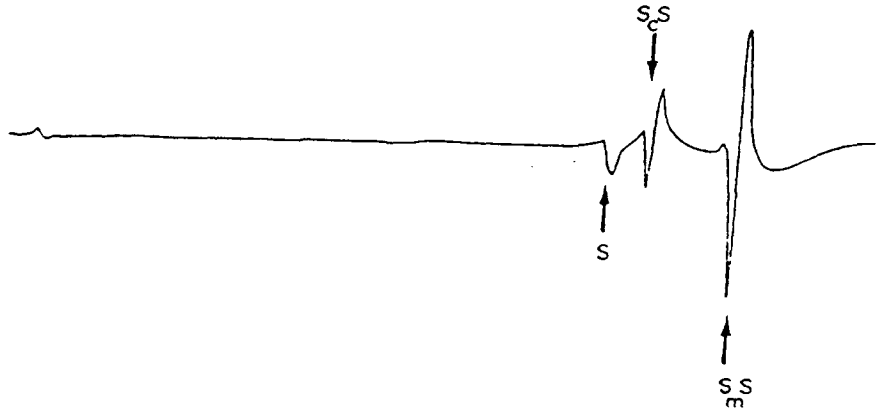

Figure 43. A vertical component seismogram computed using direct P and S, PcP ScS, and PmP and SmS phases. These arrivals can distinctly be observed on the recorded seismograms.

Effect of Intrinsic Q on S: The objective of this study is to determine a level of agreement in the frequency content between the recorded and the predicted SH waves. Similar to the study of Harvard seismogram, we tried two Q models and the agreement between the data and the synthetic is shown in Figure 44. The elastic model predicts a higher frequency content for both the direct and conrad reflected SH waves (marked by the arrows). It appears Q_β lying in between 100 and 250 would predict the frequency content of these two phases in better agreement with the data. The Q_β for the Harvard seismogram was close to 250. Thus, Q is smaller along this path in Garm. In Figure 45, we show four vertical component seismograms recorded at the Garm station from four separate earthquakes of magnitude ranging from 4.7 to 5.0. Two of the seismograms are recorded at an azimuth of about 355°. These seismograms have signals with much higher frequency than those shown in the other two seismograms recorded at an azimuth of about 313°. Thus, Q around Garm station is perhaps more complicated. We expect to establish this in our next phase of waveform modeling.

Comparison of Regional Pnl Waves from the US and USSR Crustal Models: In this section, we continue to investigate the regional waveforms that are likely to be predicted by the crustal models developed for North America and Soviet Union. Since the record at Harvard station was so successfully modelled and since it was at a range of 640 km, we examined the response of the USSR crust model at this range. In fact, seismograms at such distances are just becoming available from the Soviet Union. Figure 46 shows the comparison between the synthetic seismograms computed for the samples of the USSR and US crustal models for both the vertical and radial components assuming the same focal mechanism at the same azimuth. The seismograms were computed at the respective depths of the earthquakes and the two depths are similar. We also used the same source function. The GARM crustal model predicts a stronger PmP relative to the P_n. The S_n/SP and sS_n arrivals predicted in the seismograms by the US crustal model (marked by the arrows) seem to exhibit a correspondence to the long-period signals predicted in the response of the USSR crustal model. The difference in the amplitude ratios is caused by the differences

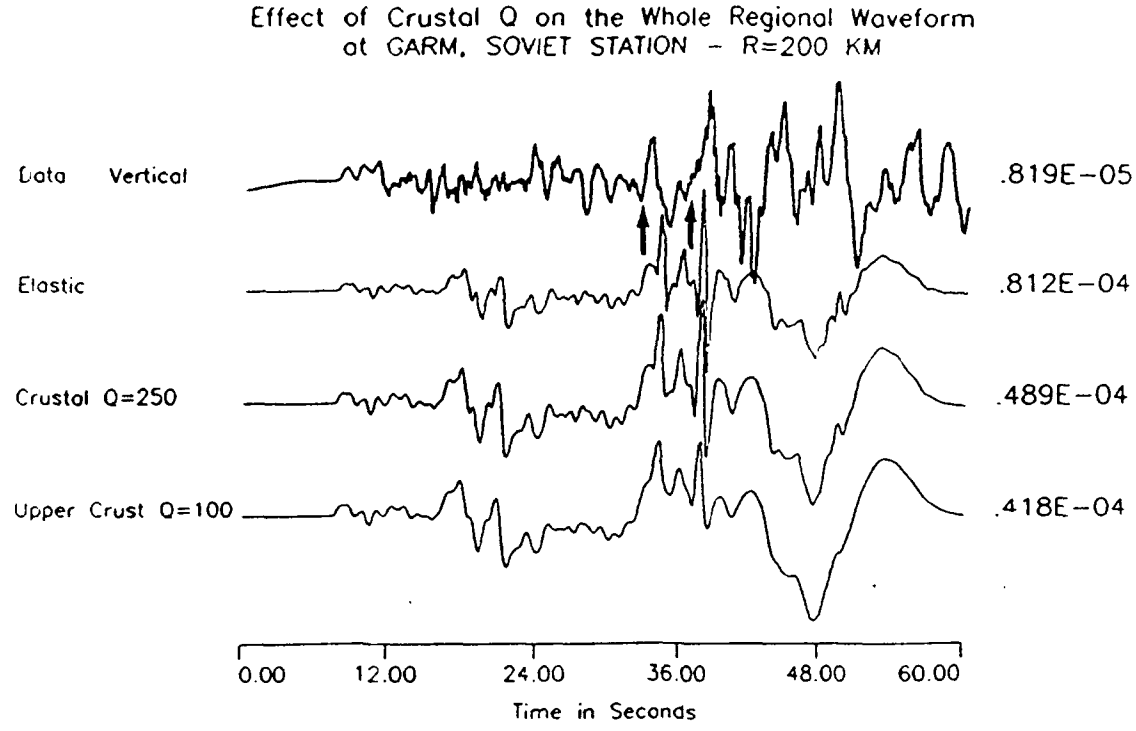

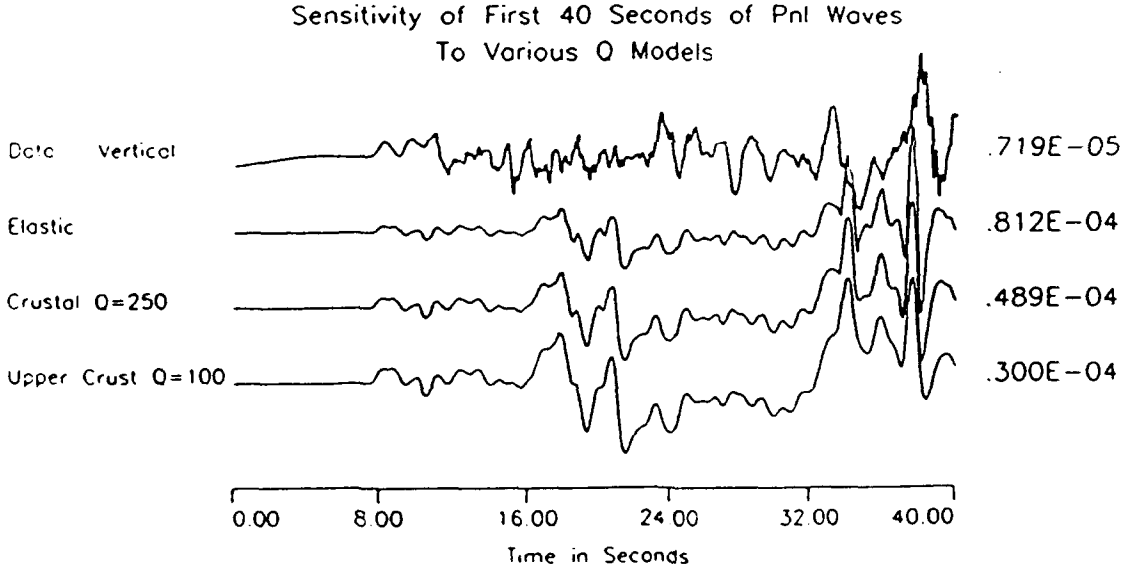

Figure 44. Comparison between broad-band vertical component data at GARM station and corresponding synthetic seismograms computed for different Q-models including the elastic model. Also shown is the first 75 seconds of each seismogram for each Q model.

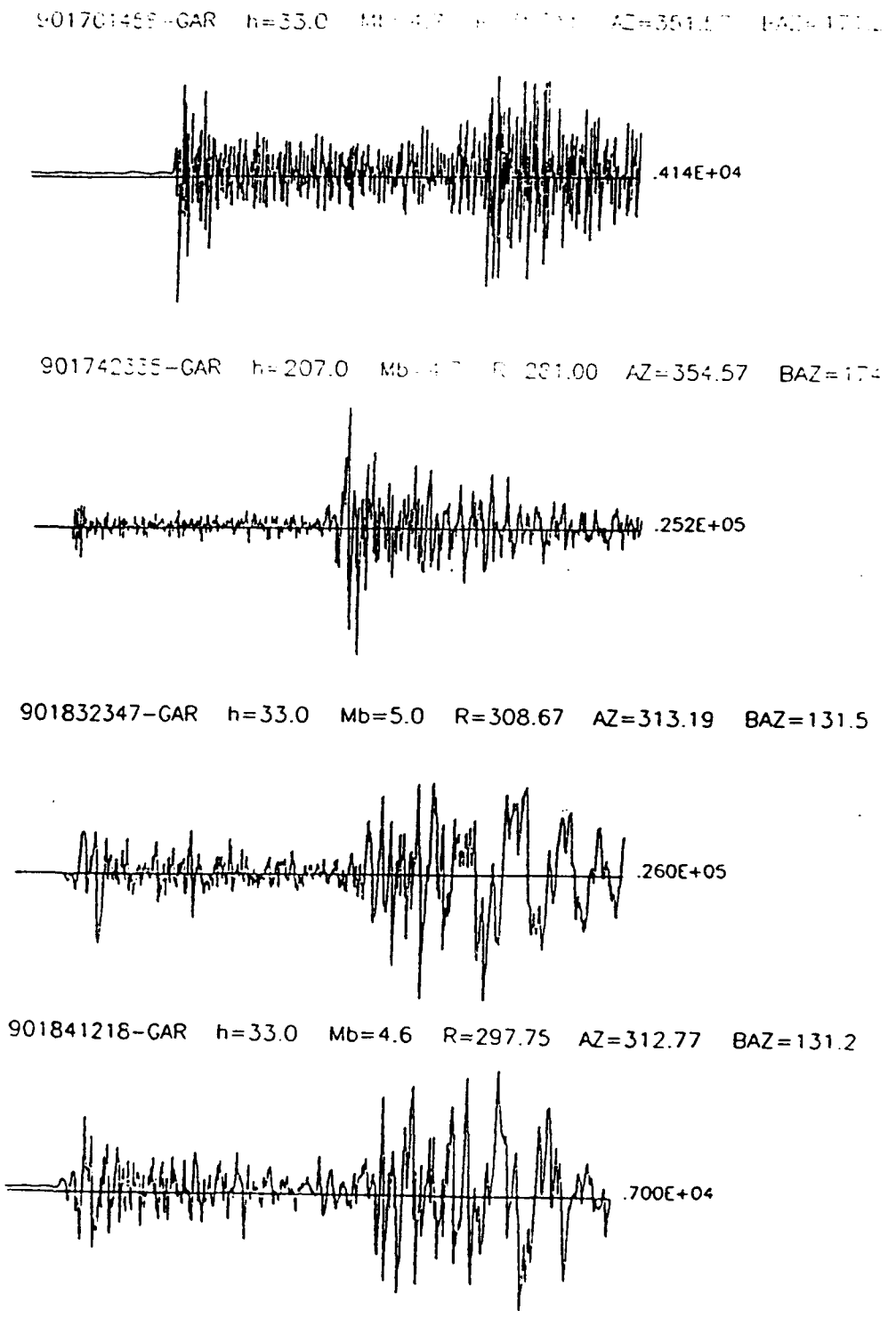

Figure 45. Broad-band seismograms recorded at GARM station from several azimuths where the variation of frequency content observed on these seismograms is a clear effect of crustal Q along the propagation paths.

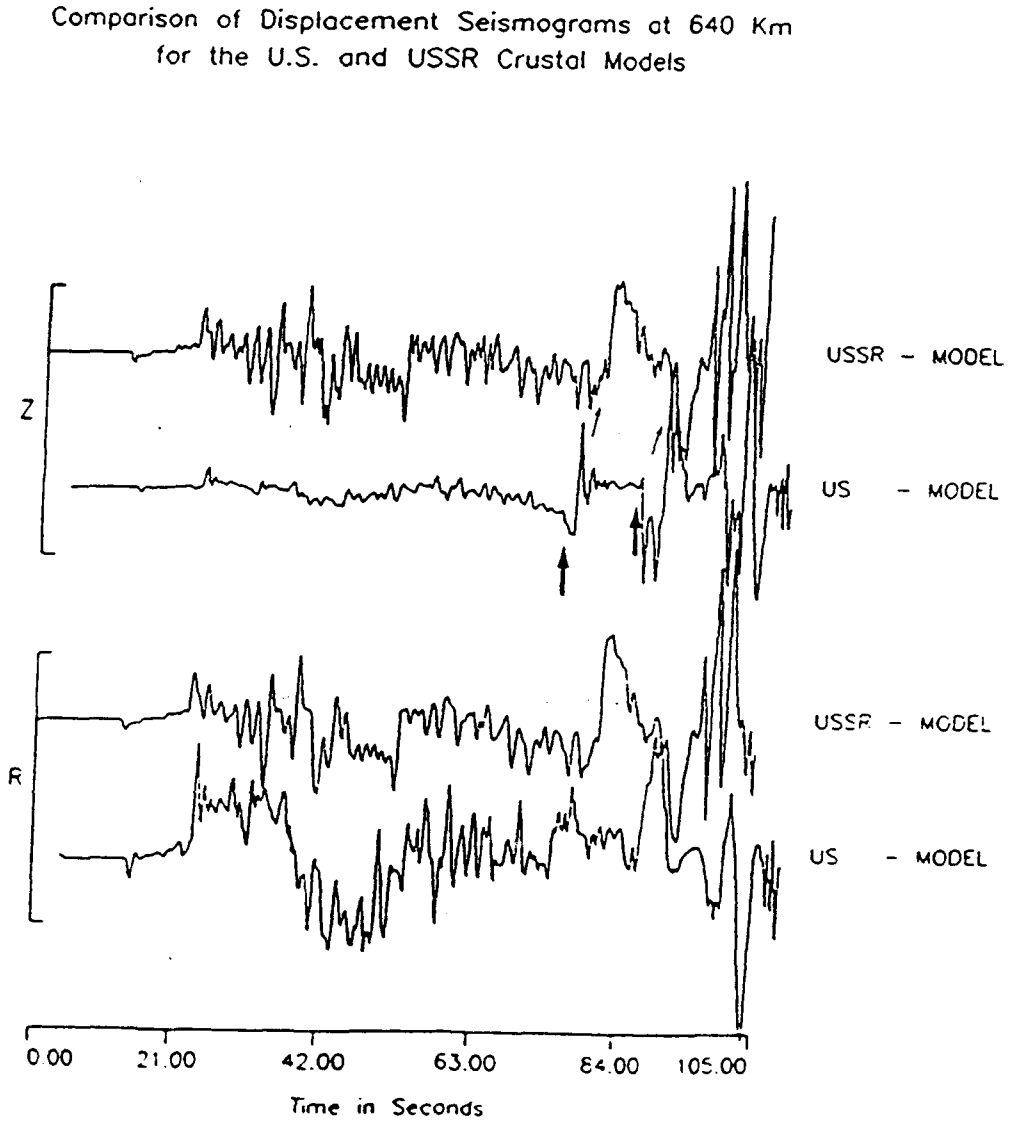

Figure 46. Comparison between the synthetic seismograms computed at 640 km for the USSR crustal model and the US crustal model. Both vertical and radial components are shown.

in the near-surface velocities of the two crustal models. For the North American crustal model, the crustal velocities have a gradient near the surface. The rays arrive at the receiver more steeply compared to the rays for the USSR crustal model, thus partitioning the energy in a significantly different ratio to the vertical and radial component.

We further investigated the composition of the P_{nl} and S_{nl} waves predicted by the USSR crustal model at 640 km in terms of generalized rays. We found that the S-wave reflections from the Moho and Conrad discontinuities are strong as shown in the top two seismograms of Figure 47. The Conrad reflection, ScS, arrives immediately following the Moho reflection SmS. The phase shown by an arrow on the SmS seismogram is arriving at the arrival time of S_n phase, but its waveshape is more complicated than is expected from a classical S_n phase. Among the other phases that contribute most significantly to the total P_{nl} seismogram within the S window are the sSmS, SmSSmS and ScSScS phases. The bottom two seismograms plotted in Figure 40 allow us to compare the agreement between the generalized ray (Total) and frequency wavenumber (F-K) seismograms. The agreement is poor following the PmP arrival. A strong long-period signal does propagate to the receiver in the frequency wavenumber seismogram. This must be a total effect of many generalized rays. This effect was also observed on the recorded seismogram at Garm station even at a distance of 200 km from the source.

Conclusions: Based on these investigations, it seems feasible to develop time-domain discriminants at different nuclear test sites which rely on the stable features that are observed in the recorded waveforms. The most stable phases are observed in the explosion generated P_{nl} waveforms for periods as short as 2 s (Burdick *et al.*, 1991c; Saikia and Burdick, 1991). In this study, we have extended our analysis approach to regional broadband seismograms from earthquake sources. The short-period P_{nl} waves have a functional dependence on the crustal waveguide. They can be deterministically modeled using average flat-layered crustal structures and using some selected generalized rays. By modeling the broadband displacement at Harvard station, we found that the structure across the crust-mantle transition zone and within the mantle can profoundly affect the

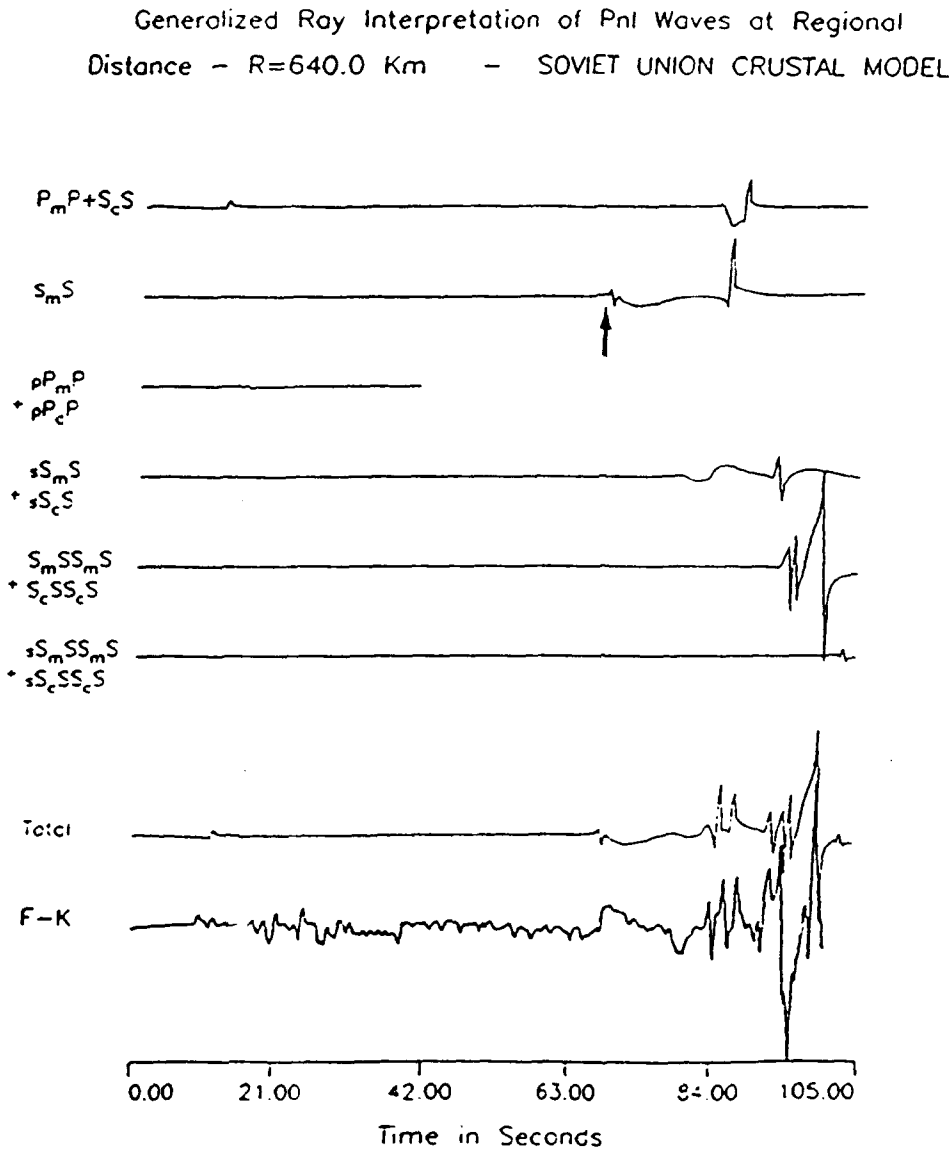

Figure 47. Understanding the waveform computed at 640 km from the USSR crustal model using the ray decomposition technique. The top six seismograms are for the individual ray groups.

frequency content of the phases like S_n and sS_n. The source multiplicity of an earthquake can also create added complexity in the frequency content of these phases. We found that the P_{nl} seismograms near the S-wave arrival can adequately be modeled using the ray responses of the following phases: SmS, sSmS, SmSSmS, sSmSSmS and SmS^{i}SmS.

For the Soviet Union, the most important requirement for understanding recorded seismograms is the crustal model. The structure within the Soviet Union is heterogeneous and the development of reliable crustal models is on-going (Gurrola and Minster, 1991). In this study, we have developed a crustal structure by modeling the recorded seismograms at Garm station from an earthquake at a distance of 200 km (Az=292°) which consisted of Conrad and Moho discontinuities. In addition, a slight gradient is allowed for the upper-mantle structure. The ray analysis indicated that the most important generalized rays for the composition of the $_{Snl}$ waves are the following phases: SmS, ScS, sSmS, sScS, SmSSmS and sSmSSmS.

We found that the phases with longitudinal propagation mode is less affected by varying attenuation structure. The phases like sSmS, SmSSmS which travel mostly with shear-mode of propagation are, however, significantly affected. Therefore, the spectra of the shear-wave phases will be deleted in high-frequency and the spectra ratio of PmP and PmPPmP phases to sSmS, SmSSmS phases may provide a better event discriminantion. For the problems related to the estimation of yield of a nuclear explosion, the dependence of the waveform amplitude on the Q models can be crucial. It can, however, be seen in Figure 38 that the intial Pnl waveform (say, first 20s after the Pn onset) is less sensitive compared to the Snl waveforms to the chosen variation in Q models. Thus, it may appear that the analysis based on the early part of the regional Pnl may be a better source for estimating yield of nuclear explosions. The explosions are expected to be shallow. If they are buried within the low Q material, it is likely that the effect may be severe. Further investigations are needed to find these effects.

Q STUDIES PART II - PRELIMINARY RESULTS FROM BROADBAND MODELING OF LONG RANGE REGIONAL SEISMOGRAMS

Introduction: Recent studies in the United States suggest that a great deal of information about structure and attenuation be obtained from braodband modeling of regional phases as demonstrated in the previous section (Saikia and Burdick, 1992). In this pilot effort, we have performed some basic calculations to test the usefulness of present earth models in predicting the observations. Figure 48 displays a map of Asia and digital stations recording two events from the Hindu-Kush region. Since many events of different focal mechanisms occur in this region at various depths, it becomes an ideal source region. Two events have been studied in detail as reported by Zhao and Helmberger (1991, see Figure 49). Broadband seismograms at several upper mantle distances are modeled in these studies using an earth model appropriate for the Tibet region, see Figure 50. The three stations, namely KIV, OBN and ARU, lie towards the northwest of this source region and the earth structure to these stations appears to be the most homogenous. In Figure 51 through 52, we show broadband recordings of two events of July 24, 1989 (3h 27m 48.77s) and February 5, 1990 (5h 16m 45.0s) at these sites. Both the events have simple seismograms with similar looking S at ARU. The P-waves are the most dissimilar, having different polarities and different strengths for pP and sP depth phases. Both events produced motions that rotate well into (P-SV) and (SH). The same is true for the other stations although the noise level at OBN is particularly strong. The P-waves are nearly nodal for the 1990 events at these stations.

From the previous studies of shield regions in North America, we would expect the paths to ARU, OBN and KIV to be similar to the paths decribed by SNA model for S waves (Grand and Helmberger, 1985) and by S25 model for P (LeFevre and Helmberger, 1989), see Figure 50. However, we have a problem in the source region where the crustal thickness is much greater than in SNA, roughly 60 km vs. 35 km. Thus, the broadband synthetics predicted by these models (SNA & S25) show an obvious problem in that sP and sS occur too early, see Figures 51 and 52. Note that observed sS is especially late on the 1990 KIV record. Since this event is at a depth of 102

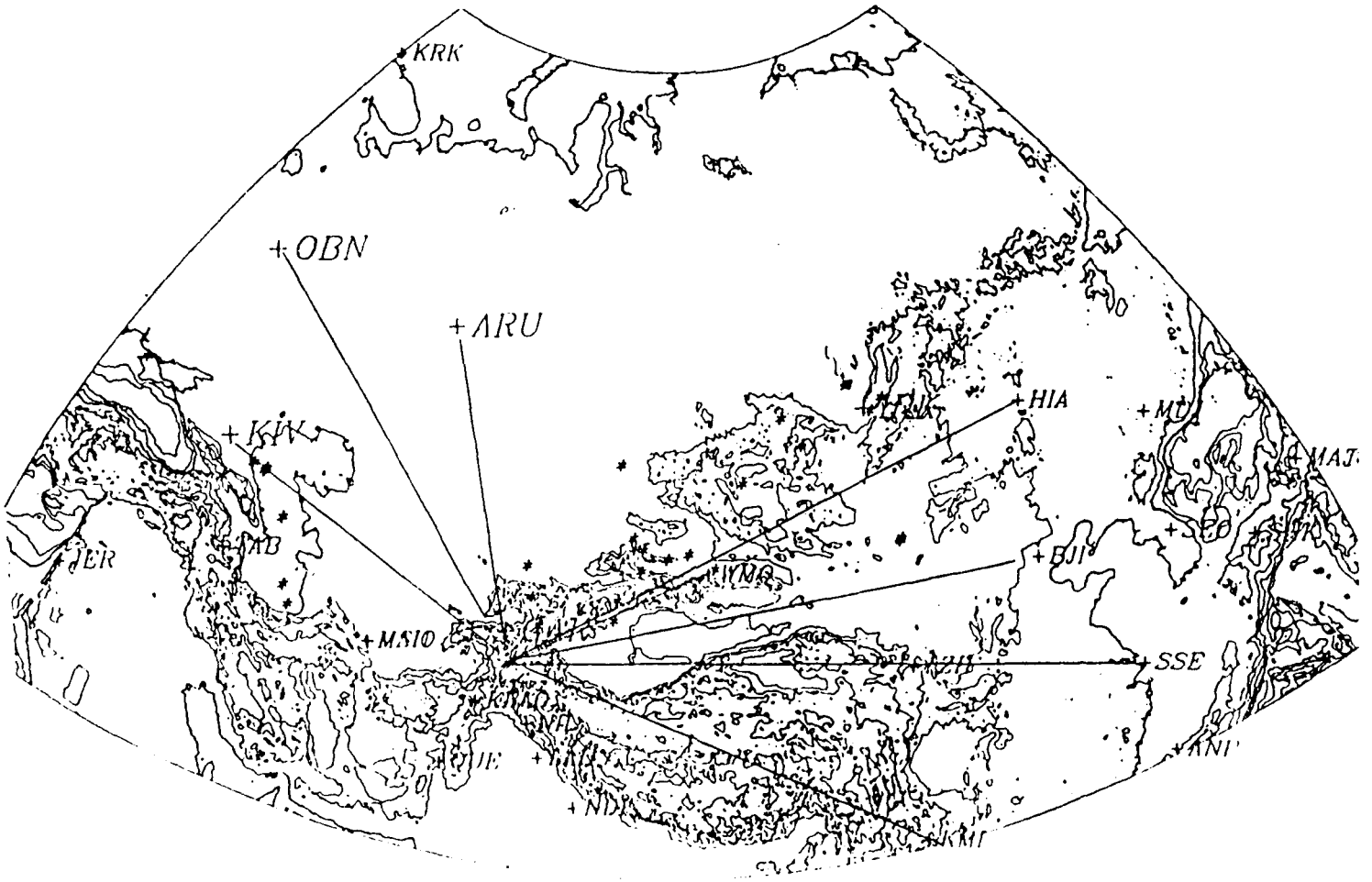

Figure 48. Map displaying a number of upper-mantle paths to various stations from events in the Hindu-Kush region. There are many events at depths between 50 to 150 km which provides relatively simply isolated sources.

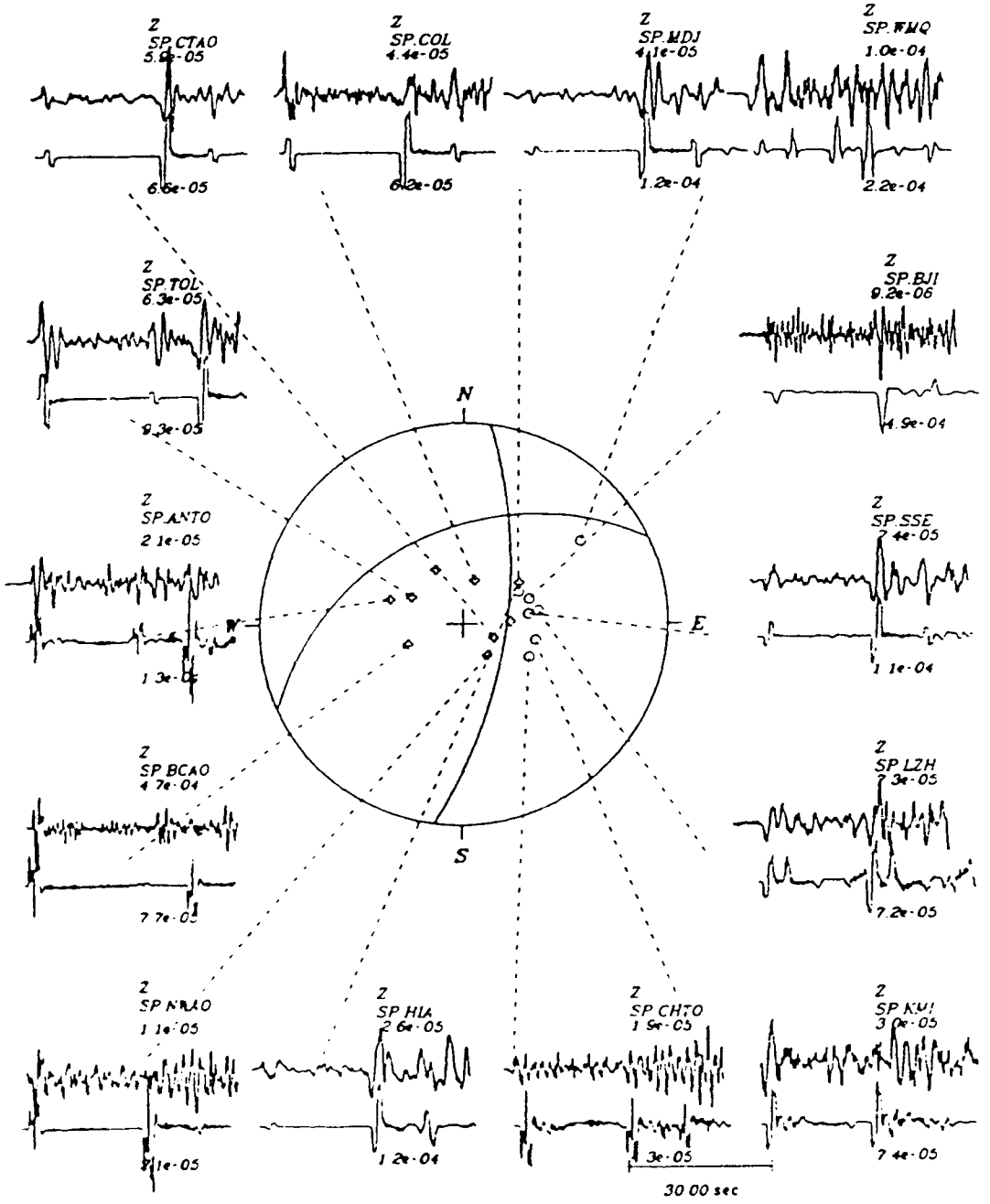

Figure 49a. Teleseismic modeling of broadband P-waves assuming a simple surface interaction, namely pP and sP, which fixes the source depth and allows relocation (Zhao et al., 1991). (Event 7/24/89)

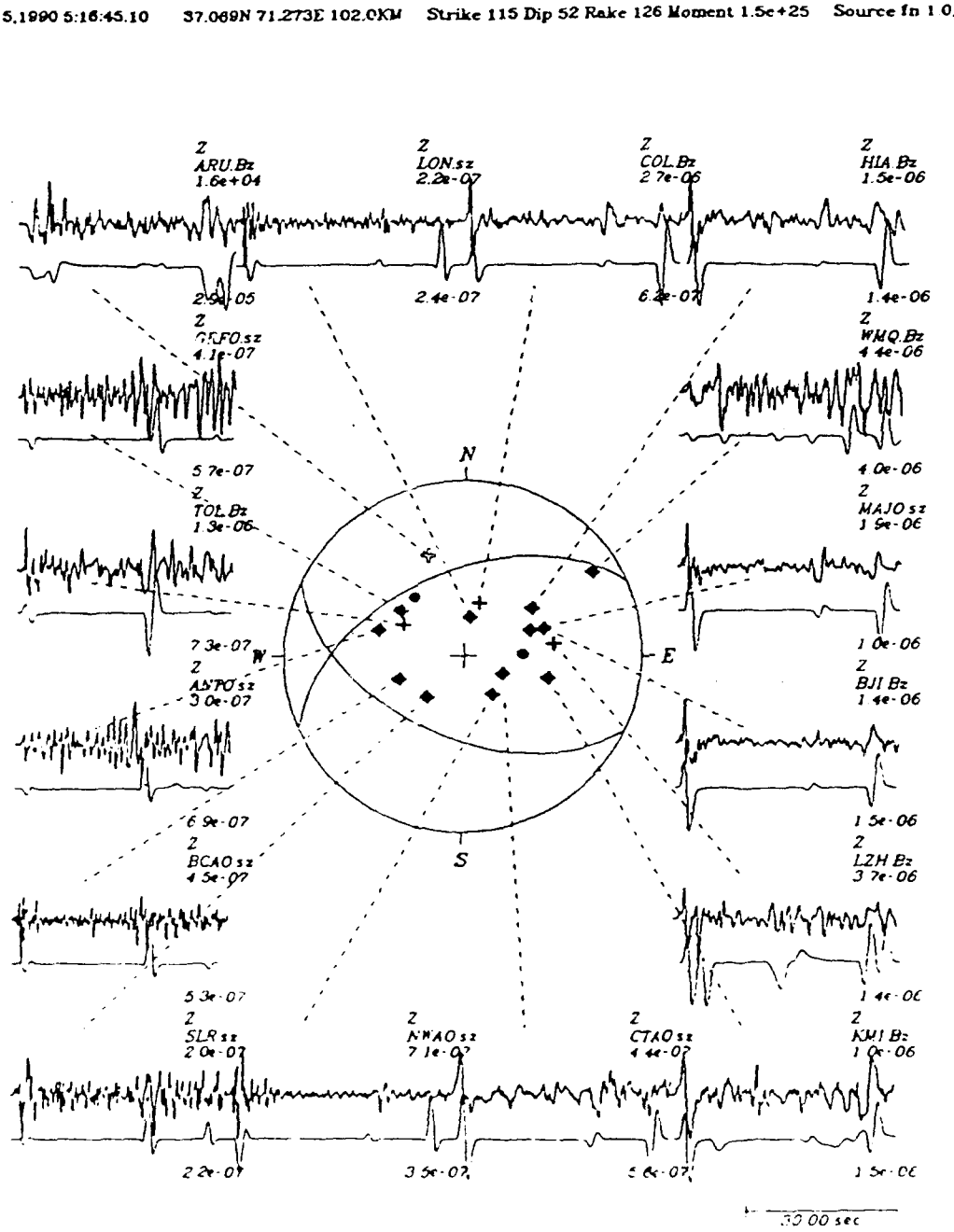

Figure 49b. Teleseismic modeling of broadband P-waves assuming a simple surface interaction, namely pP and sP, which fixes the source depth and allows relocation (Zhao et al., 1991). (Event 5/5/90)

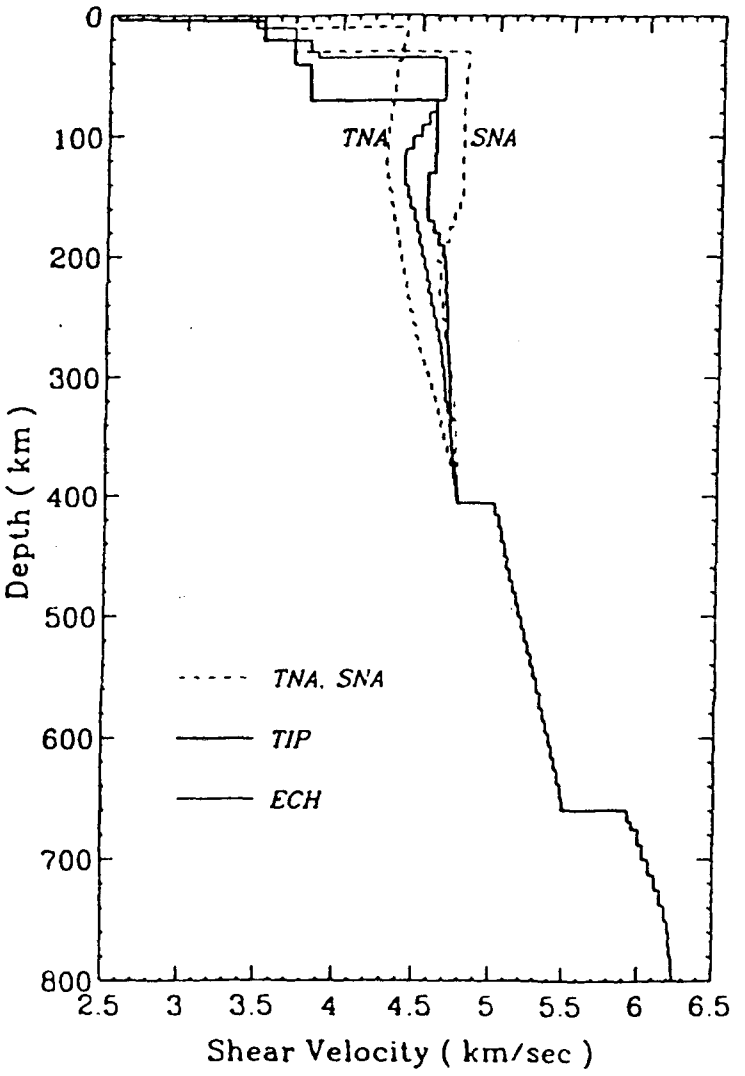

Figure 50. Upper-mantle models, TNA (Tectonic North America), SNA (Shield North America), TIP (Tibet), and ECH (Eastern China), after Zhao et al., 1991.

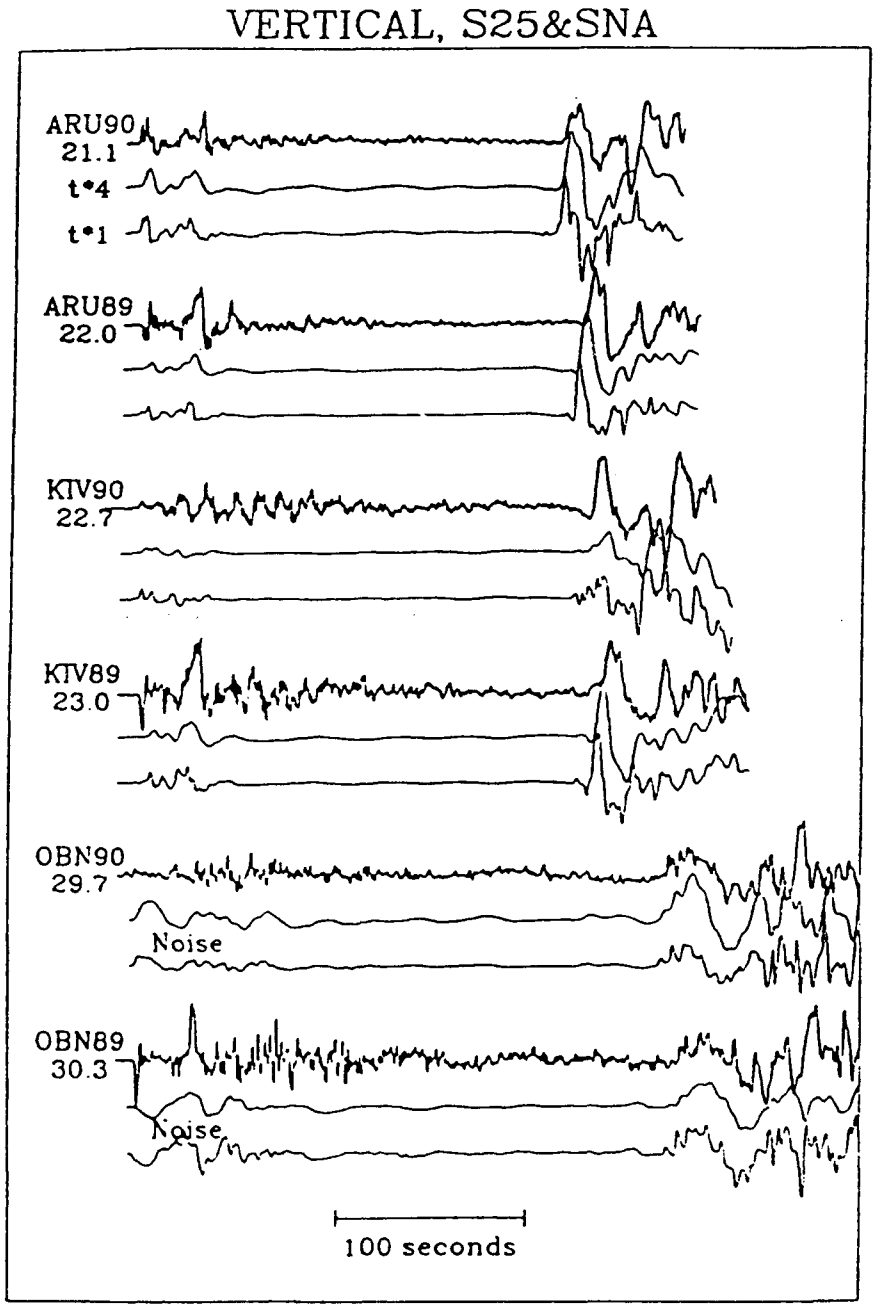

Figure 51. Vertical Component: broadband comparison of synthetics and observations where the synthetics were generated with reflectivity, restricted to periods greater than 1 sec.

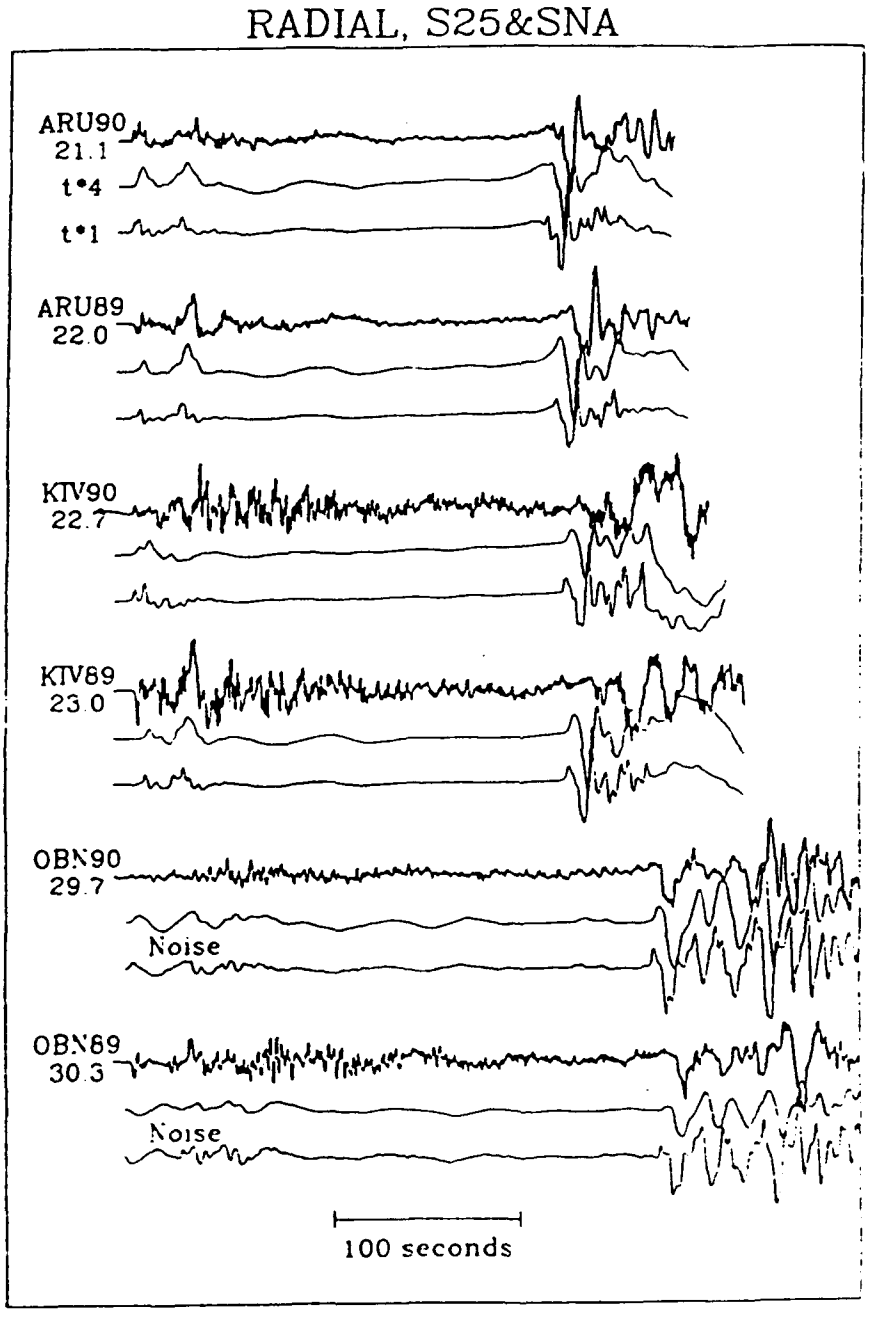

Figure 52. Radial Component: broadband comparison of synthetics and observations where the synthetics were generated with reflectivity, restricted to periods greater than 1 sec.

kms, we would expect this problem to occur. Another computational difficulty, at present, is the inability to include attenuation directly into our synthetics. The intrinsic Q structure for a given crustal medium can be handled in the frequency-wavenumber code. This code has been calibrated as discussed in the previous section and will be used in future studies to monitor the effect of Q on broadband signals. Alternatively, we can simulate the appropriate behavior by convolving these results with a t^* operator. For a world-wide average value, a t^* of 1 for P waves and a t^* of 4 for S waves are normally used. The later procedure is adopted in this present investigation.

A comparison of these synthetics with observations indicate some agreements and some disagreements. For example, the synthetic S waves show good agreement with the recorded data at most stations. The P wave synthetics show some inconsistencies with the data, especially at ARU 89 where the polarity is even wrong. But this much disagreement is, in overall, expected given that the source, structure and t^* are not known well at this stage of modeling.

An enlarged portion of the SV-wave for the best looking station, ARU, is given in Figure 53 along with various t^* operators. A t^* between 2 and 3 appears to fit the waveshape the best although some adjustments in the triplications are needed to improve the level of fits.

It is generally useful to decompose the synthetics into rays so that individual pulses can be isolated and modeled, and the agreement between the data and the synthetic is improved. Figures 54 and 55 display the synthetics containing the simple surface reflections, pP, sP, and pS, sS. These three arrivals do quite well at matching the reflectivity synthetics at the nearest distances but less well as the distance increases. This is caused by the neglect of the S-P interactions in the crust or the so-called S coupled PL waves. A detailed comparison of the S-waves at OBN as generated by the reflectivity code indicates that a small P-wave precursor occurs, see vertical and radial. This is caused by the SV-to-P conversion at the crustal receiver structure. This feature has not been included in the rays at this stage. The precursor in the ray synthetics are caused by diffracted P-waves along the crustal-mantle interface.

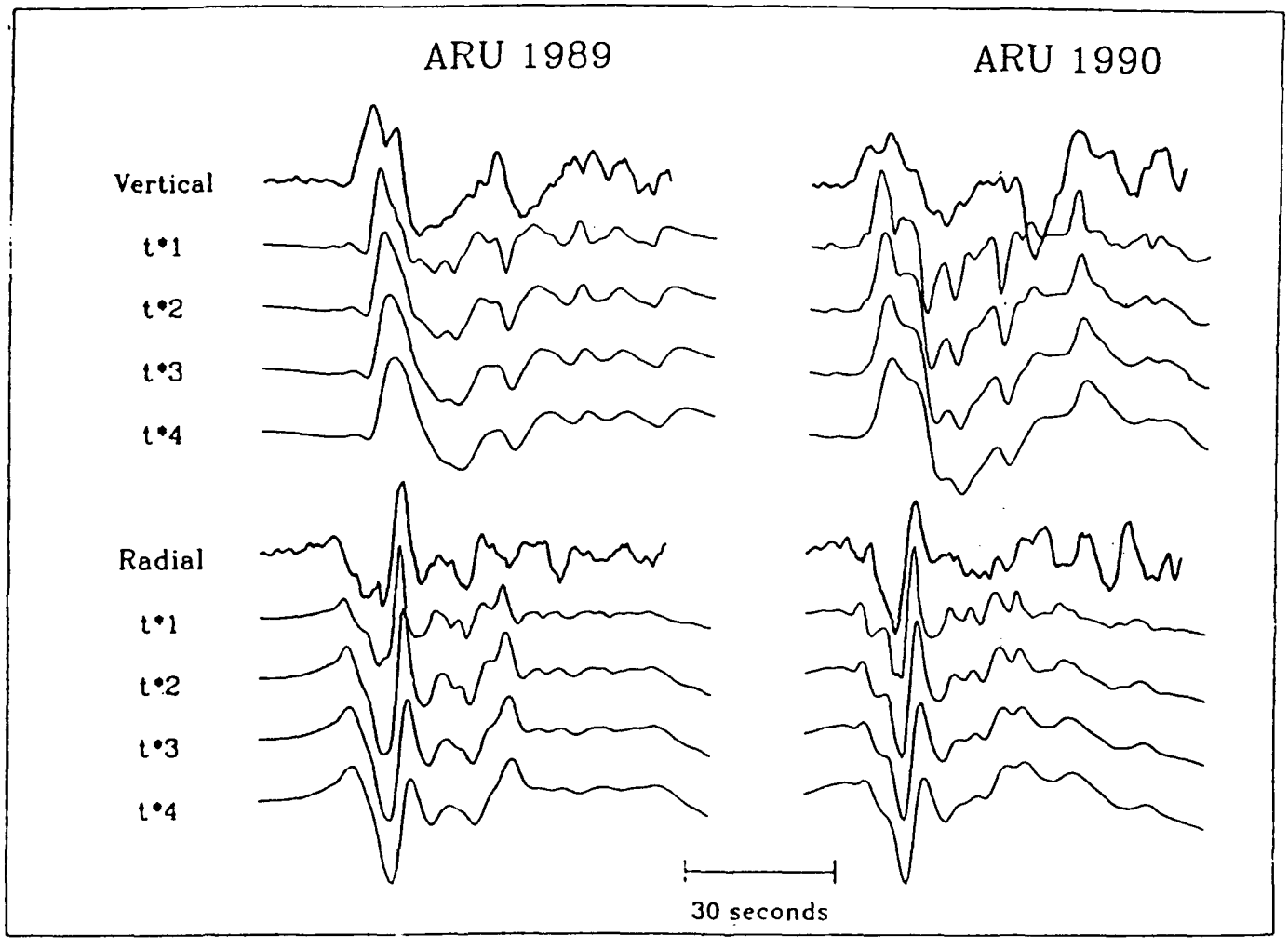

Figure 53. Comparisons of observations with reflectivity synthetics at ARU indicating the promise of detailed fits with some adjustments in upper-mantle triplications.

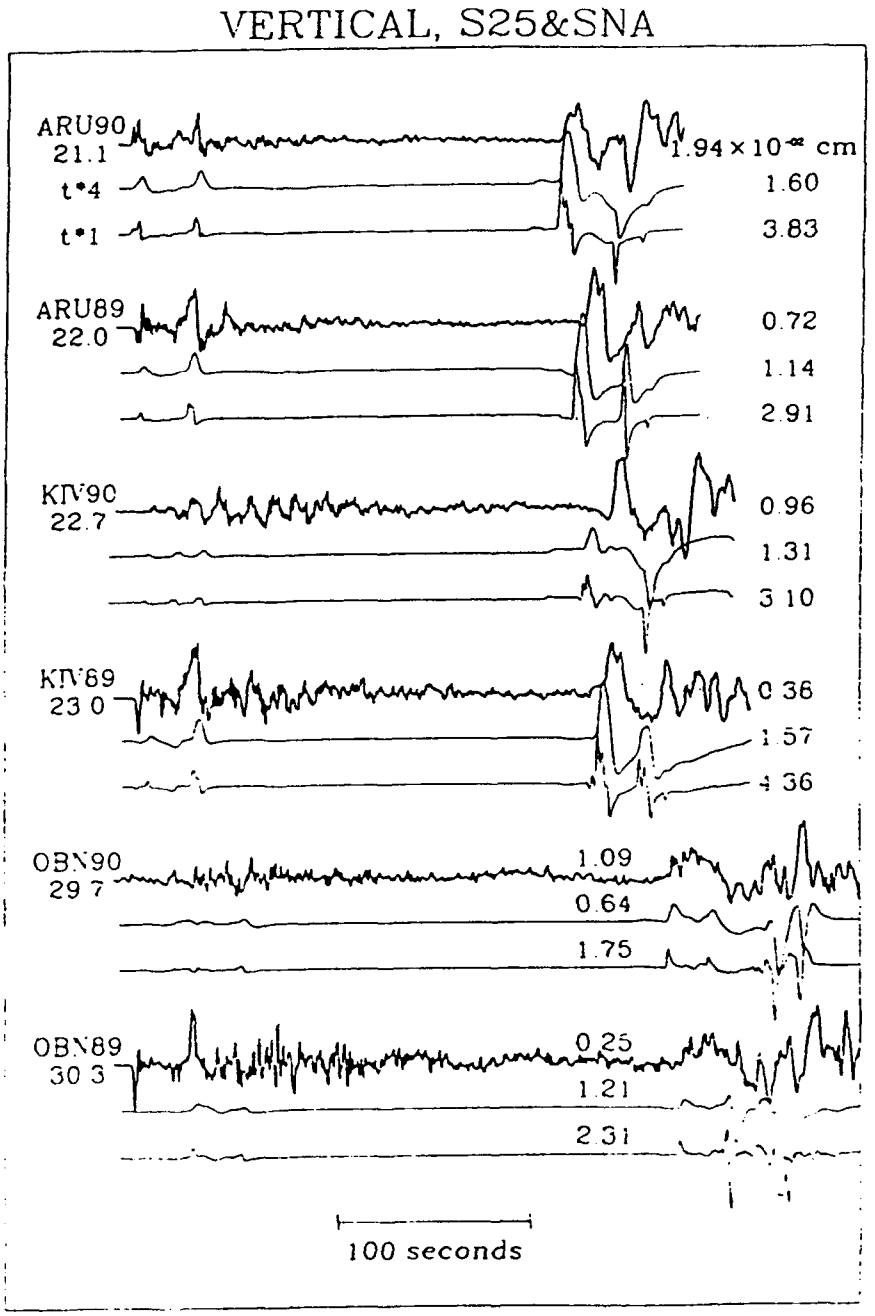

Figure 54. Vertical Component comparison of synthetics with observations when the phases P, pP, sP and S, pS, sS have been generated by ray theory assuming a $t^* = 1$ and 4.

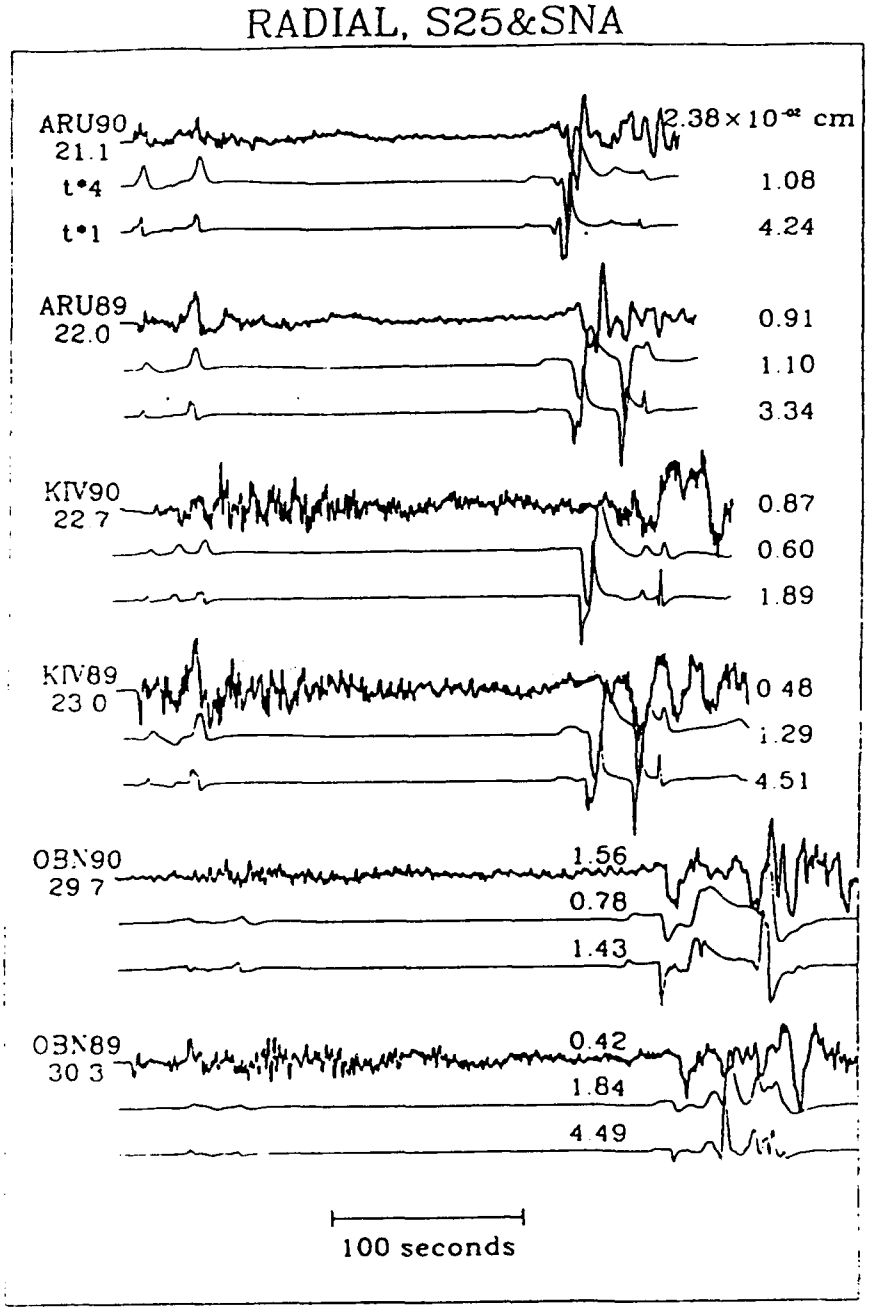

Figure 55. Radial Component comparison of synthetics with observations when the phases P, pP, sP and S, pS, sS have been generated by ray theory assuming a $t^* = 1$ and 4.

Included in the ray synthetics is the absolute amplitudes. In many cases the synthetics assuming t^*=1 and 4 bracket the data, at least for the event with the best mechanism, namely the 90 event. The timing of the surface reflected phases in these synthetics is different than is the reflectivity run because we used deeper sources to compensate for the thicker crust, that is h=102 and 117 kms respectively.

It is difficult to check the timing of P and S in these figures because of the mismatch in amplitudes. These features are more easily seen in synthetics where the radiation patterns have been supressed as in Figures 56 and 57. These figures contain only the down-going P and S where the sources are at their proper depths, 85 and 106 km respectively. Only the vertical componant is displayed which yields the clearest arrival onsets. We have included pure tectonic stlye synthetics for comparison. The P-waves are slightly early for the S25-SNA model but the SV waves are early by 10 secs or more, see ARU and KIV. On the other hand, from the GCA-TNA model the SV waves are late at KIV (2 secs) and ARU (8 secs). The travel times are in general agreement with the (SS-S) times reported on by Woodward and Masters (1991) and Grand and Helmberger (1985), see Figure 58. Results from the latter study indicate a sharp increase in velocity when crossing the high ridge of topography that extends from Hindu-Kush to Lake Baikal. Velocities north of this feature appear unusually fast, essentially SNA. This study as well as the earlier report by Rial et al. (1984) used the waveform and travel times of upper mantle (SS-S) data. The results from Woodward and Masters (1991) are teleseismic type (SS-S) measurements and can contain anomalies deeper than Upper-Mantle. Whatever the reason they see much more variability in velocity structures across Russia than previously concluded, along the Ural mountain extension from NZ to the Hindu-Kush. A deep anomaly running North and South beneath the Mid United States has also been seen by Grand (1991), perhaps this is a similar feature.

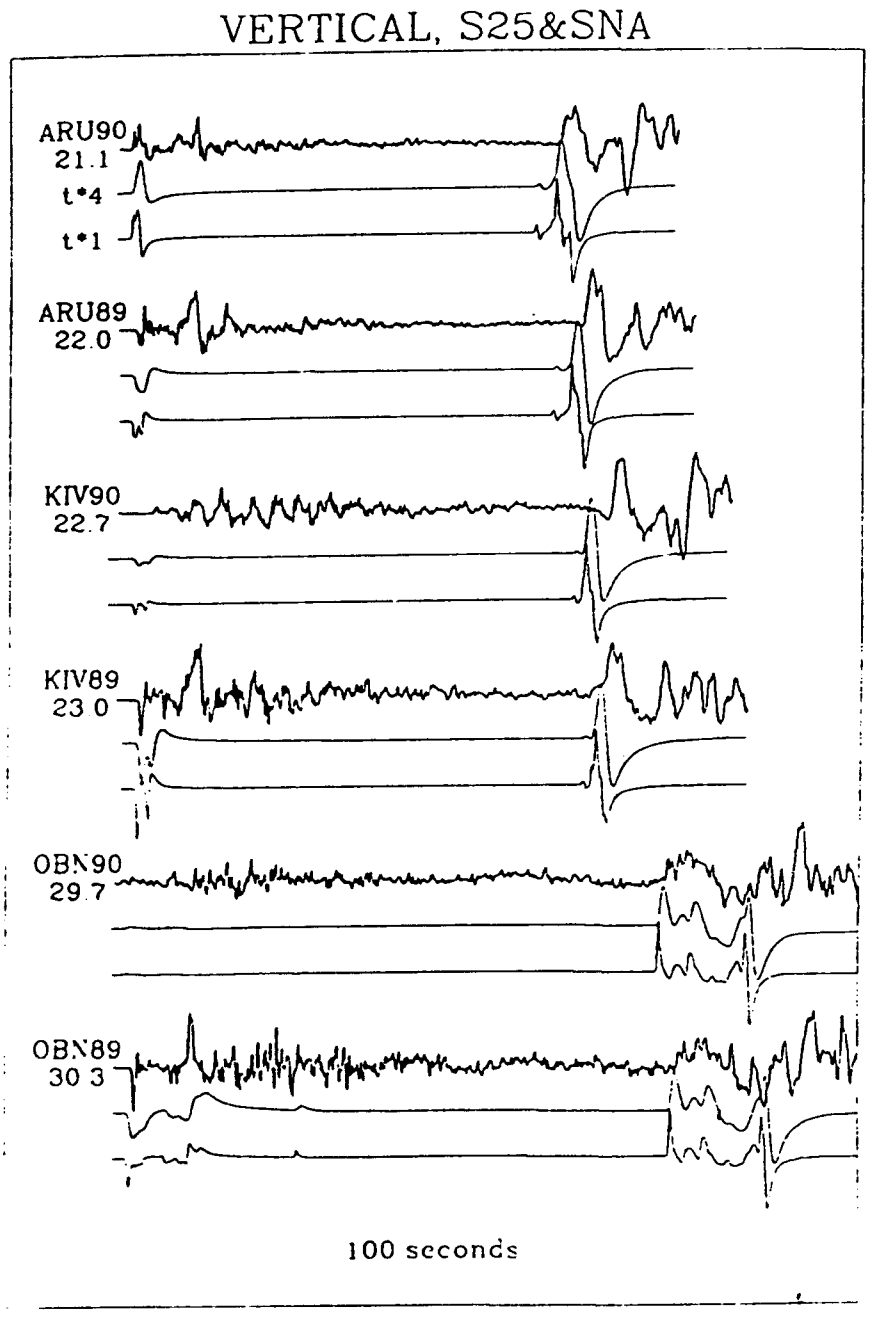

Figure 56. Comparison of synthetics and observations when only the direct P and S are displayed and the radiation pattern has been suppressed.

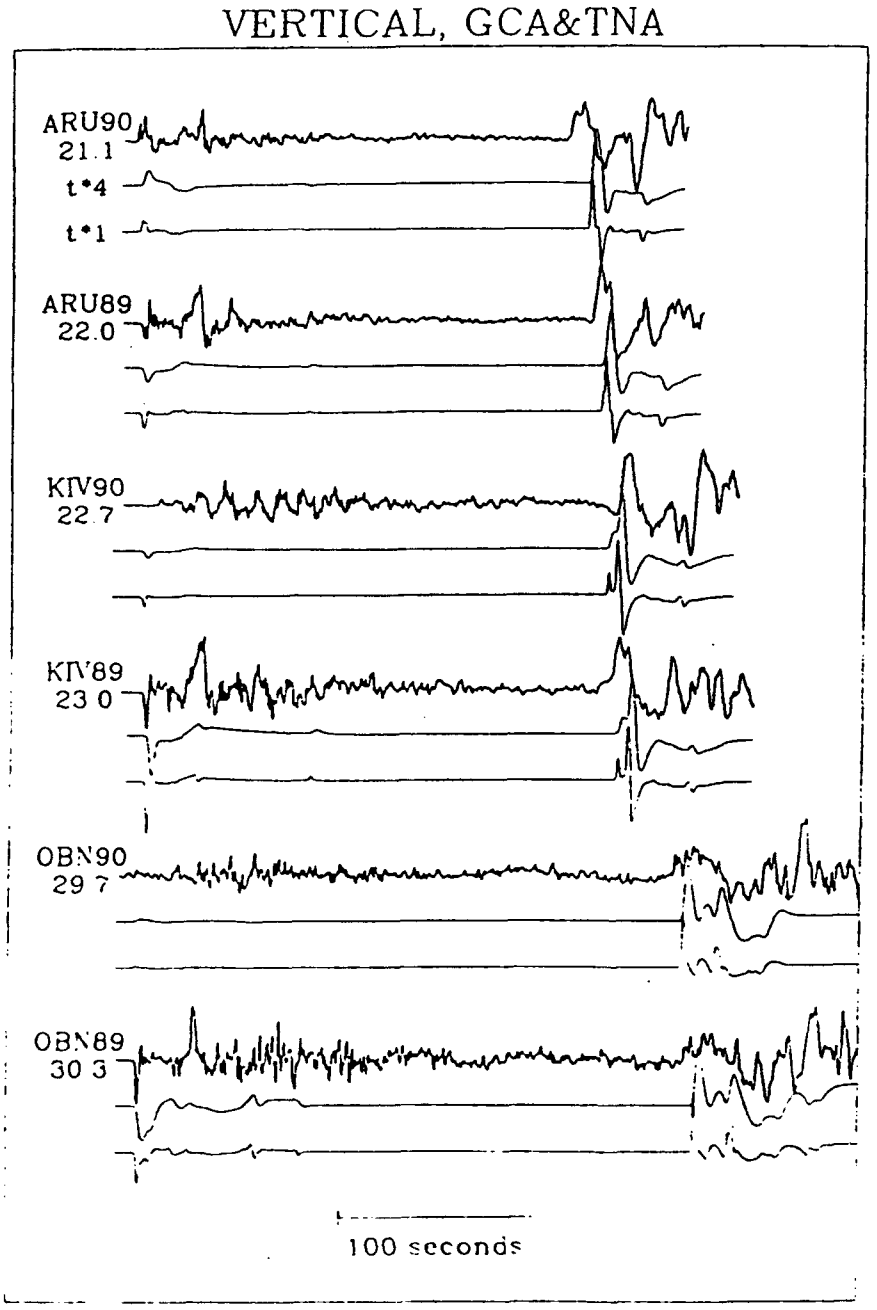

Figure 57. Comparisons of ray synthetics (GCA and TNA) with observations. The synthetic SV-waves are now too late by 2 secs at KIV and 8 secs at ARU.

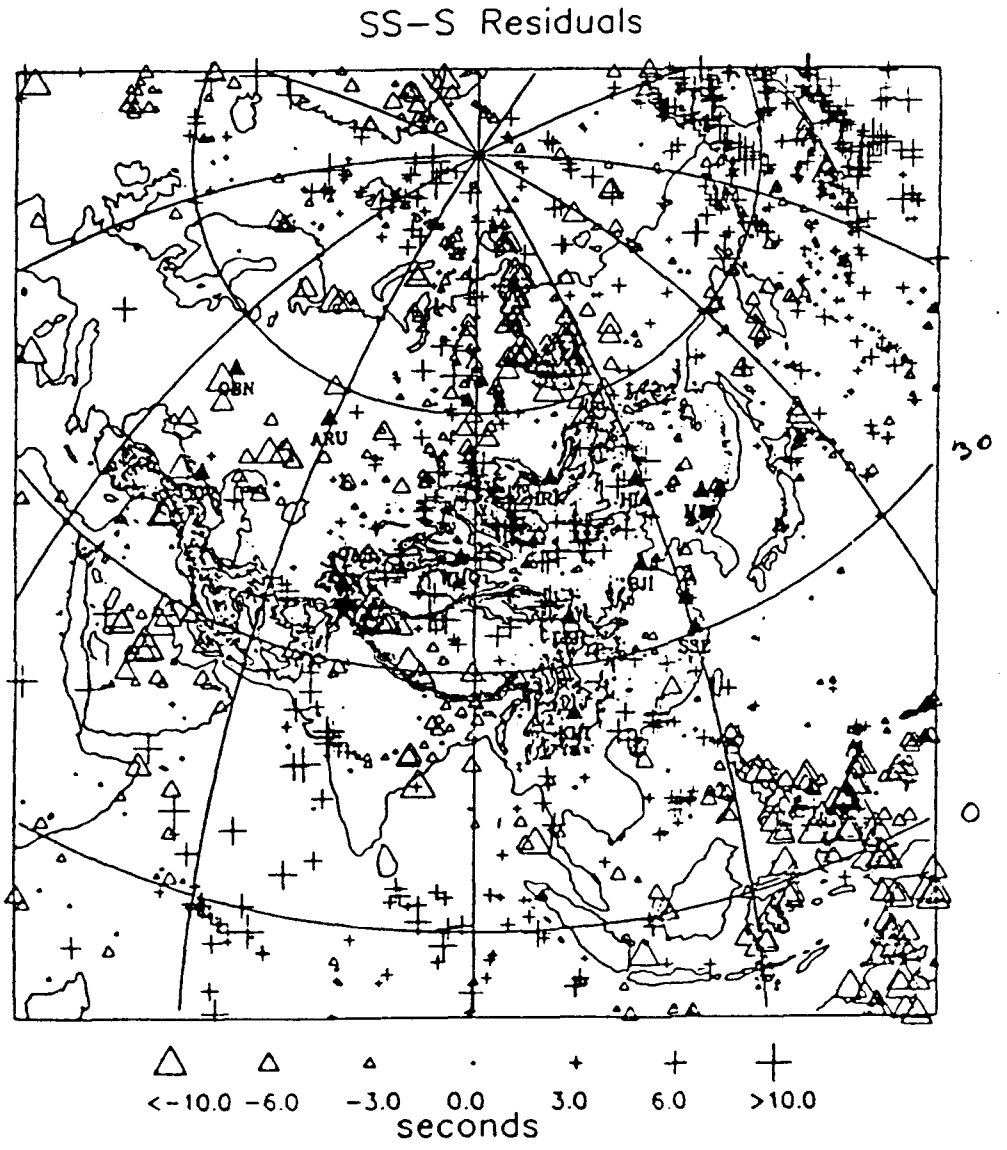

Figure 58. SS-S residuals in Eurasia. Negative residuals are indicative of faster than average velocity material, while positive residuals indicate slower velocity material, after Woodward and Masters (1991)

The most interesting events occur along the tectonic regions indicated by the topography display and are probably in slower structure than most of the Soviet stations. Thus, to model the many broadband records available would require approximateing these structures by at least 2 D models.

A common method of generating synthetics for 2D models is due to Chapman (1978), called the WKBJ method. Some short-period results for models formed by a linear connection between pure models is given in Figure 59, see Helmberger et al. (1985). Five profiles are displayed showing the upper-mantle triplications. The small first arrival at ranges near 18° is essentially a lid diffraction coming from a depth of about 185 kms in the pure S25 model. The large second arrival at 18° for this model is just the "400" triplication. Since the lid velocities are slower in the TIP model a third arrival coming from a depth near 250 km is apparent int he pure-TIP synthetics. The other three profiles correspond to placing the source at various positions along the 1000 km transition zone. Profile S25-TIP is appropriate for a midpoint and the other two are mostly SNA(-500) or TIP(+500). The synthetics for (S25-TIP fits the absolute travel times at ARU quite well. The code used in constructing these synthetics have been used primarily in modeling multibounce SH waves (Grand and Helmberger, 1985; Graves and Helmberger, 1988) and discussed in detail in previous WCC reports (WCCP-R-83-01).

A new technique of generating synthetics for 2D structures is presently going through the testing process but will allow broadband modeling since diffractions and tunneling will be treated. This method is essentially an extension of the Cagneard de-Hoop method to handle lateral variations. Figure 60 displays the basic geometry and rayset for a direct P or S. Following this approach requires finding a geometrical ray parameter (po) or snell's law angle (θ_o) that tracks rays from the source to the recevier after reflecting from each boundary. The shallowest generalized rays contribute both headwaves and post critical angle reflections. The timing of these various rays can also be used to generate synthetics directly as suggested by Burdick and Salvado (1986).

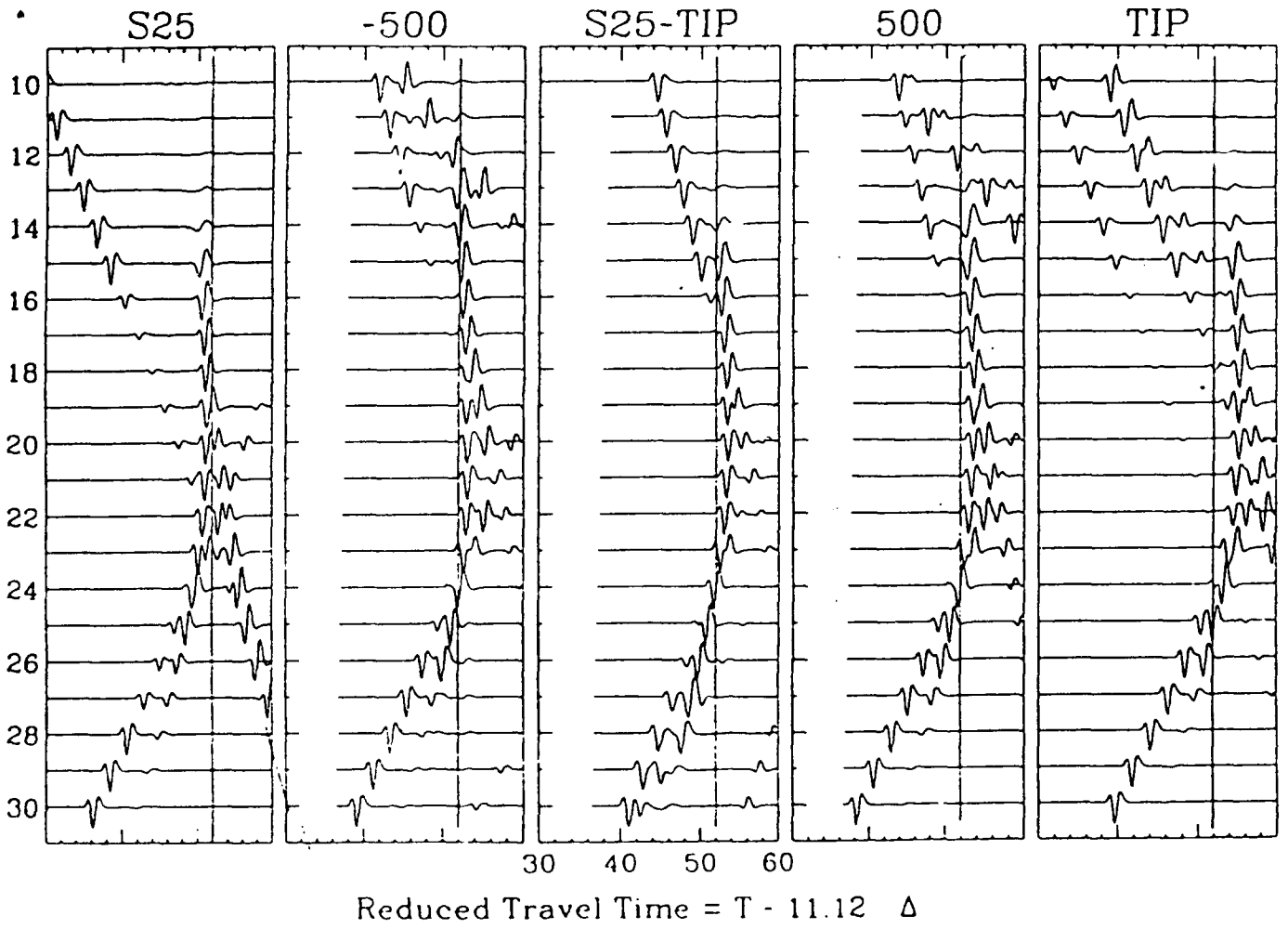

Figure 59. Profiles of WKBJ synthetics (P-waves) assuming 2D structure. Panels S25 and TIP are pure path results where the P-waves are about 3 secs faster for SNA relative to TIP. The synthetics for a model that starts with TIP and ends with S25 fits the timing at ARU quite well.

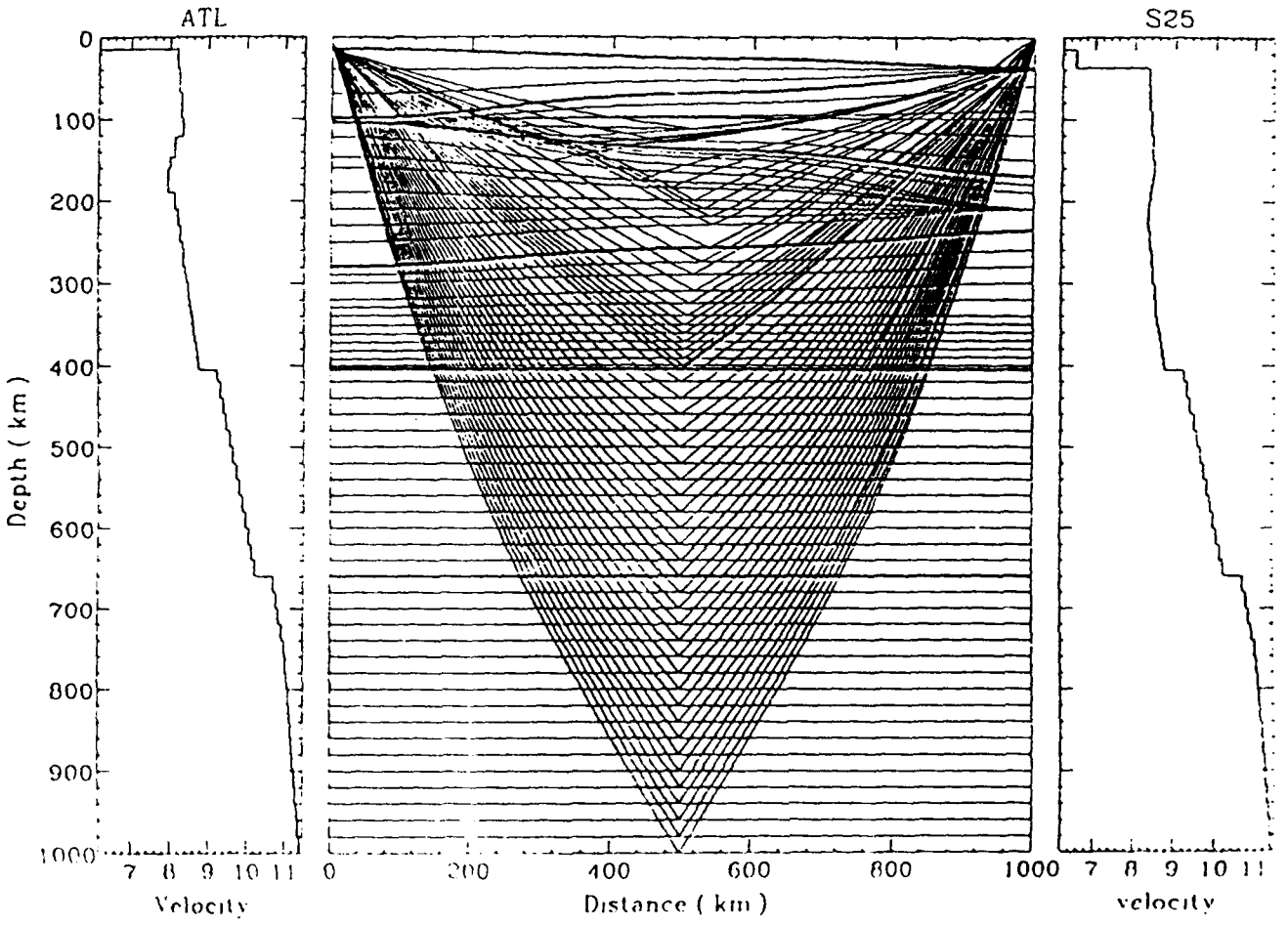

Figure 60. Display of ray paths connecting a source and receiver to reflectors used in generating synthetics for 2D models.

In conclusion, it appears that an excellent estimate of regionalized attenuation can be constructed from broadband data. However, to obtain high resolution will require refining the propagational corrections. This appears possible by applying the latest analytical techniques to the numerous data sets, namely explosions (Garnero et al., 1992) and earthquakes (Zhao et al., personal communication).

Conclusions and Recommendations: The release of internal data from the Soviet Union obviously presents some great opportunities for solving some of the most long-standing yield estimation problems. However, interpretation of the data is still complex, and we continue to face the challenges of modeling the source RDP, determining its dependence on depth and separating source from propagation effects. Here we have focused on the influence of Q. We recommend that integrated Q, velocity and source models be developed for the Soviet Union which yield consistent values for regional and teleseismic t^*. The Soviet PNE program has been much more extensive than the U.S., and intensive studies of this data should yield important new insights into source scaling. We also recommend an intensive effort to obtain near field explosion data from the Soviet Union since data of this type has proved so valuable in interpreting U.S. data.

REFERENCES

Anderson, D. L. and R. S. Hart, "Q of the Earth", J. Geophys. Res., 96, 5869-5882, 1978.

Barker, J.S., "Analysis of regional bodywave phases from earthquakes and explosions in eastern Asia", PL/DARPA Seismic Research Symposium, 64-70, PL-TR-91-2208, ADA241325, 1991.

Barker, J. S., S. H. Hartzell, L. J. Burdick, and D. V. Helmberger, "Analysis of local seismic waveforms from underground nuclear explosions: Forward modeling for effective surface functions at Pahute Mesa", J. Geophys. Res., 96, 10129-10143, 1991

Bennett, T. J., B. W. Barker, K. L. McLaughlin, and J. R. Murphy, "Regional discrimination of quarry blasts, earthquakes and underground nuclear explosions", ADA223148, Final Report, 1989.

Blandford, R. R., "Seismic discrimination problems at regional distances", in Identification of Seismic Sources, E. S. Husebye and S. Mykkelveit eds., D. Reidel Publishing Co., Dordrecht, The Netherlands, 695-740, 1981.

Brune, J. N., "Tectonic stress and spectra of seismic shear waves from earthquakes", J. Geophys. Res., 75, 4997-5009, 1970.

Burdick, L. J., "Estimation of the frequency dependence of Q from ScP and ScS", Geophys. J. R. Astr. Soc., 80, 35-55, 1985.

Burdick, L. J., E. J. Garnero, J. P. Mclaren, B. W. Woods, D. V. Helmberger and D. G. Harkrider, "Uncertainty in yield scaling at low yield". AFTAC Draft Report, 1991a.

Burdick, L. J. and D. V. Helmberger, "The upper mantle P velocity structure of the western United States", J. Geophys. Res., 83, 1699-1712, 1978.

Burdick, L. J., C. K. Saikia, E.J. Garnero, D. V. Helmberger, and L.S. Zhao, "Regional and upper mantle wave propagation in the Soviet Union", PL/DARPA Seismic Research Symposium, 100-107, PL-TR-91-2208, ADA241325, 1991b.

Burdick, L. J., C. K. Saikia and D. V. Helmberger, "Deterministic modeling of regional waveforms from the Nevada test site", ADA216641, Final Report, 1989.

Burdick L. J., C. K. Saikia and N. F. Smith, "Pn for the Nevada Test Site", in Geophysical Monograph 65: Explosion Source Phenomenology, Steven R. Taylor, Howard J. Patton, and Paul G. Richards, eds., American Geophysical Union, 2000 Florida Avenue, NW Washington DC 20009, 197-209, 1991c.

Burdick, L.J. and C. A. Salvado, Modeling body wave amplitude fluctuations using the three-dimensional slowness method, J. Geophys. Res., 91, 12,482-14,496, 1986

Burdick, L. J., T. C. Wallace and T. Lay, "Modeling the near field and teleseismic observations from the Amchitka test site", J. Geophys. Res., 89, 4373-4388, 1984.

Burger R. W., T. X. Lay and L. J. Burdick, "Examining the relative yield of the Novaya Zemlya tests by waveform intercorrelation", Geophys. J. R. Astr. Soc., 87, 775-800, 1986.

Chapman, C. H., "A new method for computing synthetic seismograms", Geophys. J. R. Astr. Soc., 57, 649-670, 1978.

Cohee, B. P., and T. Lay, "Modeling teleseismic SV waves from underground explosions with tectonic release: results for southern Novaya Zemlya", Bull. Seism. Soc. Am., 78, 1158-1178, 1988.

Der, Z. A., T. W. McElfresh and A. O'Donnell, "Results of the SDCS experiment", *SDAC-TR-80-4*, Teledyne-Geotech, Alexandria, Virginia, 1980.

Dowla, F. U., S. R. Taylor and R. W. Anderson, "Seismic detection with artificial neural networks: Preliminary results with regional spectral data", Bull. Seism. Soc. Am., (to be submitted), 1990.

Dreger, D. S. and D. V. Helmberger, "Broadband modeling of local earthquakes", Bull. Seism. Soc. Am., 80, 1162-1197, 1990.

Garnero, E. J. D. V. Helmberger, and L. J. Burdick, "Upper mantle triplications beneath Asia", (submitted to) Geophys. J. Int. 1992.

Given, J. W. and D. V. Helmberger, "Upper mantle structure of northwestern Eurasia", J. Geophys. Res., 85, 7183-7194, 1980.

Given, J. W., D. V. Helmberger, and L. S. Zhao, "A new aquisition of historical seismograms from the USSR emphasizing digital storage", EOS, Transactions, 72, 190, 1991.

Given, J. W. and G. R. Mellman, "Estimating explosion and tectonic release source parameters of underground nuclear explosions from Rayleigh and Love wave observations", Technical Report, DARPA, ARPA order No. 5308, 1986.

Grand, S. P., "Tomographic inversion for mantle shear velocity heterogeneity at intermediate periods, IRIS, Abstract, Spring meeting, 1991.

Grand, S. P. and X. Y. Ding, "Determination of Q as a function of depth and tectonic province', University of Texas Austin, Final Report, EL-TR-89-0157, 1989.

Grand, S. P. and D. V. Helmberger, "Upper mantle shear structure of North America", Geophys. J. R. Astr. Soc., 76, 399-438, 1984.

Grand, S. P. and D. V. Helmberger, "Upper mantle shear structure beneath Asia from multi-bounce S waves", Phys. Earth Planet. Inter., 41, 154-169, 1985.

Graves, R. W. and D. V. Helmberger, Upper mantle cross section from Tonga to Newfoundland, J. Geophys. Res., 93., 4701-4711, 1988.

Gurrola, H. and J. B. Minster, "Single-station estimates of crust and upper mantle velocity structure at broadband IRIS/IDA stations in the USSR", PL/DARPA Seismic Research Symposium, 225-236, PL-TR-91-2208, ADA241325, 1991.

Hartzell, S. H., L. J. Burdick, and T. X. Lay, "Effective source functions for Pahute Mesa nuclear tests", Final Tech. Report WCCP-R-83-3, Woodward-Clyde Pasadena, CA, 1983.

Helmberger, D. V., "Long period body-wave propagation from 4° to 13°", Bull. Seis. Soc. Am., 62, 325-341, 1972.

Helmberger, D. V., "Numerical seismograms of long-period body waves from seventeen to forty degrees", Bull. Seism. Soc. Am., 63, 633-646, 1973a.

Helmberger, D. V., "On the structure of the low velocity zone", Geophys. J. R. Astr. Soc., 34, 251-263, 1973b.

Helmberger, D. V., L. J. Burdick, and R. Stead, "Modeling near-field at NTS and Amchitka", in Geophysical Monograph 65: Explosion Source Phenomenology, Steven R. Taylor, Howard J. Patton, and Paul G. Richards, eds., American Geophysical Union, 2000 Florida Avenue, NW Washington DC 20009, 35-45, 1991a.

Helmberger D.V., D. Dreger, L.S. Zhao, S. Kedar, B. Woods, and D.G. Harkrider, "Source retrieval from regional seismograms", PL/DARPA Seismic Research Symposium, 249-260, PL-TR-91-2208, ADA241325, 1991b.

Helmberger D.V., G. Engen, and S. Grand, "Notes on wave propagation i a laterally varying structure", Geophys. J. 58, 82-91, 1985

Helmberger, D. H. and D. M. Hadley, "Seismic source functions and attenuation from local and teleseismic observations of the NTS events, JORUM and HANDLEY", Bull. Seism. Soc. Am., 71, 51-68, 1981.

Hwang, H-J., and B. J. Mitchell, "Shear velocities, Q_β, and the frequency dependent of the Q_β in stable and tectonically active regions from surface wave observation", Geophys. J. R. Astr. Soc., 90, 575-613, 1987.

Jones, L. E. and D. V. Helmberger, "Possible nature of the 520 Discontinuity", EOS, Transactions, 72, 200, 1991.

King, D. W. and G. Calcagnile, "P wave velocities in the upper mantle beneath Fennoscandia and western Russia", Geophys. J. R. Astron. Soc., 46, 407-432, 1976.

Langston, C. A. and D. V. Helmberger (1975). "A procedure for modeling shallow dislocation sources", Geophys. J. R. Astr. Soc., 42, 117-130, 1975.

Lay T. X., "Estimating explosion yield by analytical waveform comparison", Geophys. J. R. Astr. Soc., 82, 1-31, 1985.

Lay T. X., "The teleseismic manifestation of pP: Problems and paradoxes", in Geophysical Monograph 65: Explosion Source Phenomenology, Steven R. Taylor, Howard J. Patton, and Paul G. Richards, eds., American Geophysical Union, 2000 Florida Avenue, NW Washington DC 20009, 109-125, 1991.

Lay T. X., L. J. Burdick and D. V. Helmberger, "Estimating the yields of the Amchitka tests by waveform intercorrelation", Geophys. J. R. Astr. Soc., 78, 181-208, 1984a.

Lay, T. X., D. V. Helmberger and D. G. Harkrider, "Source models and yield scaling relations for underground nuclear explosions at Amchitka Island", Bull. Seism. Soc. Am., 74, 843-862, 1984b.

LeFevre, L. V. and Helmberger, D. V., "Upper mantle P velocity of the Canadian Shield", J. Geophys. Res., 94, 1749-1765, 1989.

Liebermann, R. C. and P. W. Basham, "Excitation of surface waves by the Aleutian underground explosion MILROW (October 2, 1969)", J. Geophys. Res., 76, 4030-4034, 1971.

Mallick, S., and L.N. Frazer, "Rapid computation of multioffset vertical seismic profile synthetic seismograms for layered media", Geophysics, 53, 479-491, 1988.

Marshall, P. D., D. L. Springer, and H. C. Rodean (1979). "Magnitude corrections for attenuation in the upper mantle", Geophys. J. R. Astr. Soc., 28, 431-458, 1979

Mueller, R. A. and J. R. Murphy, "Seismic characteristics of underground nuclear detonations: Part I, Seismic scaling law of underground detonations", Bull. Seism. Soc. Am., 61, 1675-1692, 1971

Murphy, J. R., "Seismic source functions and magnitude determinations for underground nuclear detonations", Bull. Seism. Soc. Am., 67, 135-158, 1977.

Murphy, J. R., "Free-field seismic observations from underground nuclear explosions",in Geophysical Monograph 65: Explosion Source Phenomenology, Steven R. Taylor, Howard J. Patton, and Paul G. Richards, eds., American Geophysical Union, 2000 Florida Avenue, NW Washington DC 20009, 25-34, 1991.

Murphy, J. R., "Network averaged teleseismic *P*-wave spectra for underground explosions Part 2: source characteristics of Pahute Mesa explosions", Bull. Seism. Soc. Am., 79, 156-171, 1989.

Murphy, J. R. and C. B. Archambeau, "Variability in explosion body wave magnitudes: an analysis of the RULISON/GASBUGGY anomaly", Bull. Seism. Soc. Am., 4, 1087-1113, 1986.

Murphy, J. R. and T. J. Bennett, "A discrimination analysis of short period regional seismic data recorded at Tonto Forest Observatory", Bull. Seism. Soc. Am., 72, 1351-1366, 1982.

Perret, W., "The physics of non-isotropic source effects", Close-in seismic source parameters DARPA/AFOSR symposium (GSD-8203), Las Vegas, Nevada, 1982.

Saikia, C. K. and L. J. Burdick, "Fine structure of Pnl waves from explosions", J. Geophys. Res., V 96, 14,383-14,401, 1991.

Saikia, C. K. and L. J. Burdick, "Effect of velocity and Q structure on the regional broadband composition of Pnl waves", J. Geophys. Res., (in press), 1992.

Savage, J. C., "Radiation from a realistic model of faulting", Bull. Seism. Soc. Am., 56, 577-593, 1966.

Somerville, P. G., J. P. Mclaren, L. V. LeFevre, R. W. Burger and D. V. Helmberger, "Comparison of source scaling relations of eastern and western North American earthquakes", Bull. Seism. Soc. Am., 77, 322-346, 1987.

Stevens, J. L., "Estimation of scalar moments from explosion generated surface waves", Bull. Seism. Soc. Am., 76, 123-151, 1986.

Sykes, L. R., and J. L. Cifuentes, "Yields of Soviet underground nuclear explosions from seismic surface waves: compliance with the Threshold Test Ban Treaty", Proceedings of the National Academy of Sciences, 81, March 1984, 1922-1925, 1984.

Sykes, L. R. and G. C. Wiggins, "Yields of Soviet underground nuclear explosions, Novaya Zemlya, 1964 - 1976 from seismic body and surface waves", Proceedings from the National Academy of Sciences, USA, (submitted), 1986.

Taylor, S. R., N. W. Sherman and M. D. Denny, "Spectral discrimination between NTS explosions and western United States earthquakes at regional distances", Bull. Sies. Soc. Am., 78, 1563-1579, 1988.

Toksöz, M. N. and H. H. Kehrer, "Tectonic strain-release characteristics of CANNIKIN", Bull. Seism. Soc. Am., 62, 1425-1438, 1972.

Vidale, J. E., and D. V. Helmberger, "Path effects in strong motion seismology", in Methods of Computational Physics, Bruce Bolt, Editor, Academic Press, New York, 267-319, 1987.

von Seggern, D. H., "Intersite magnitude-yield bias exemplified by the underground nuclear explosion MILROW, BOXCAR and HANDLY", Technical Report *SDAC-TR-77-4*, Teledyne Geotech, Alexandria, Virginia, 1972.

Willis, D. E., G. D. George, K. G. Poetzl, C. E. Saltzer, A. F. Shakal, R. D. Torfin, T. L. Woodzik, and C. Woolsin, "Seismological aspects of the CANNIKIN nuclear explosion", Bull. Seism. Soc. Am., 62, 1377-1395, 1972

Woodward R. L., and G. Masters, "Global upper mantle structure from long-period differential travel times", J. Geophys. Res., 96, 6351-6377, 1991.

Yacoub, N. K., "Instantaneous amplitudes: A new method to measure seismic magnitude", Bull. Seism. Soc. Am., 73(5), 1345-1355, 1983.

Yacoub N. K., "Seismic network effect on yield estimation from body wave magnitude for NTS explosions", AFTAC-TR-84-2, (1984)

Zhao, L. S., And D. V. Helmberger, "Broadband modeling along a regional shield path, Harvard recording of the Saguenay earthquake", Geophys. J. Int. 105, 301-312, 1991.

APPENDIX A

The following publications contain additional results related to this effort:

(i) "Analysis of local seismic waveforms from underground nuclear explosions: Forward modeling for effective surface functions at Pahute Mesa", Barker, J. S., S. H. Hartzell, L. J. Burdick, and D. V. Helmberger, J. Geophys. Res., 96, 10129-10143, 1991

(ii) "Pn for the Nevada Test Site", Burdick L. J., C. K. Saikia and N. F. Smith, Geophysical Monograph 65: Explosion Source Phenomenology, Steven R. Taylor, Howard J. Patton, and Paul G. Richards, eds., American Geophysical Union, 2000 Florida Avenue, NW Washington DC 20009, 197-209, 1991c.

(iii) "Upper mantle triplications beneath Asia", Garnero, E. J. D. V. Helmberger, and L. J. Burdick, (submitted to) Geophys. J. Int, 1992.

(iv) "Modeling near-field at NTS and Amchitka", Helmberger, D. V., L. J. Burdick, and R. Stead, Geophysical Monograph 65: Explosion Source Phenomenology, Steven R. Taylor, Howard J. Patton, and Paul G. Richards, eds., American Geophysical Union, 2000 Florida Avenue, NW Washington DC 20009, 35-45, 1991a.

(v) "Broadband Source models for US underground nuclear explosions", Helmberger, D. V., J. P. McLaren, E. J. Garnero, C. K. Saikia, and L. J. Burdick, (submitted to) Bull. Seism. Soc. Am., 1992.

(vi) "Fine structure of PNL waves from explosions", C. K. Saikia and L. J. Burdick, J. Geophys. Res., V 96, 14,383-14,401, 1991.

DISTRIBUTION LIST

Prof. Thomas Ahrens
Seismological Lab, 252-21
Division of Geological & Planetary Sciences
California Institute of Technology
Pasadena, CA 91125

Prof. Keiiti Aki
Center for Earth Sciences
University of Southern California
University Park
Los Angeles, CA 90089-0741

Prof. Shelton Alexander
Geosciences Department
403 Deike Building
The Pennsylvania State University
University Park, PA 16802

Dr. Ralph Alewine, III
DARPA/NMRO
3701 North Fairfax Drive
Arlington, VA 22203-1714

Prof. Charles B. Archambeau
CIRES
University of Colorado
Boulder, CO 80309

Dr. Thomas C. Bache, Jr.
Science Applications Int'l Corp.
10260 Campus Point Drive
San Diego, CA 92121 (2 copies)

Prof. Muawia Barazangi
Institute for the Study of the Continent
Cornell University
Ithaca, NY 14853

Dr. Jeff Barker
Department of Geological Sciences
State University of New York
at Binghamton
Vestal, NY 13901

Dr. Douglas R. Baumgardt
ENSCO, Inc
5400 Port Royal Road
Springfield, VA 22151-2388

Dr. Susan Beck
Department of Geosciences
Building #77
University of Arizona
Tuscon, AZ 85721

Dr. T.J. Bennett
S-CUBED
A Division of Maxwell Laboratories
11800 Sunrise Valley Drive, Suite 1212
Reston, VA 22091

Dr. Robert Blandford
AFTAC/TT, Center for Seismic Studies
1300 North 17th Street
Suite 1450
Arlington, VA 22209-2308

Dr. G.A. Bollinger
Department of Geological Sciences
Virginia Polytechnical Institute
21044 Derring Hall
Blacksburg, VA 24061

Dr. Stephen Bratt
Center for Seismic Studies
1300 North 17th Street
Suite 1450
Arlington, VA 22209-2308

Dr. Lawrence Burdick
Woodward-Clyde Consultants
566 El Dorado Street
Pasadena, CA 91109-3245

Dr. Robert Burridge
Schlumberger-Doll Research Center
Old Quarry Road
Ridgefield, CT 06877

Dr. Jerry Carter
Center for Seismic Studies
1300 North 17th Street
Suite 1450
Arlington, VA 22209-2308

Dr. Eric Chael
Division 9241
Sandia Laboratory
Albuquerque, NM 87185

Prof. Vernon F. Cormier
Department of Geology & Geophysics
U-45, Room 207
University of Connecticut
Storrs, CT 06268

Prof. Steven Day
Department of Geological Sciences
San Diego State University
San Diego, CA 92182

Marvin Denny
U.S. Department of Energy
Office of Arms Control
Washington, DC 20585

Dr. Zoltan Der
ENSCO, Inc.
5400 Port Royal Road
Springfield, VA 22151-2388

Prof. Adam Dziewonski
Hoffman Laboratory, Harvard University
Dept. of Earth Atmos. & Planetary Sciences
20 Oxford Street
Cambridge, MA 02138

Prof. John Ebel
Department of Geology & Geophysics
Boston College
Chestnut Hill, MA 02167

Eric Fielding
SNEE Hall
INSTOC
Cornell University
Ithaca, NY 14853

Dr. Mark D. Fisk
Mission Research Corporation
735 State Street
P.O. Drawer 719
Santa Barbara, CA 93102

Prof Stanley Flatte
Applied Sciences Building
University of California, Santa Cruz
Santa Cruz, CA 95064

Dr. John Foley
NER-Geo Sciences
1100 Crown Colony Drive
Quincy, MA 02169

Prof. Donald Forsyth
Department of Geological Sciences
Brown University
Providence, RI 02912

Dr. Art Frankel
U.S. Geological Survey
922 National Center
Reston, VA 22092

Dr. Cliff Frolich
Institute of Geophysics
8701 North Mopac
Austin, TX 78759

Dr. Holly Given
IGPP, A-025
Scripps Institute of Oceanography
University of California, San Diego
La Jolla, CA 92093

Dr. Jeffrey W. Given
SAIC
10260 Campus Point Drive
San Diego, CA 92121

Dr. Dale Glover
Defense Intelligence Agency
ATTN: ODT-1B
Washington, DC 20301

Dr. Indra Gupta
Teledyne Geotech
314 Montgomery Street
Alexanderia, VA 22314

Dan N. Hagedon
Pacific Northwest Laboratories
Battelle Boulevard
Richland, WA 99352

Dr. James Hannon
Lawrence Livermore National Laboratory
P.O. Box 808
L-205
Livermore, CA 94550

Dr. Roger Hansen
HQ AFTAC/TTR
Patrick AFB, FL 32925-6001

Prof. David G. Harkrider
Seismological Laboratory
Division of Geological & Planetary Sciences
California Institute of Technology
Pasadena, CA 91125

Prof. Danny Harvey
CIRES
University of Colorado
Boulder, CO 80309

Prof. Donald V. Helmberger
Seismological Laboratory
Division of Geological & Planetary Sciences
California Institute of Technology
Pasadena, CA 91125

Prof. Eugene Herrin
Institute for the Study of Earth and Man
Geophysical Laboratory
Southern Methodist University
Dallas, TX 75275

Prof. Robert B. Herrmann
Department of Earth & Atmospheric Sciences
St. Louis University
St. Louis, MO 63156

Prof. Lane R. Johnson
Seismographic Station
University of California
Berkeley, CA 94720

Prof. Thomas H. Jordan
Department of Earth, Atmospheric &
Planetary Sciences
Massachusetts Institute of Technology
Cambridge, MA 02139

Prof. Alan Kafka
Department of Geology & Geophysics
Boston College
Chestnut Hill, MA 02167

Robert C. Kemerait
ENSCO, Inc.
445 Pineda Court
Melbourne, FL 32940

Dr. Max Koontz
U.S. Dept. of Energy/DP 5
Forrestal Building
1000 Independence Avenue
Washington, DC 20585

Dr. Richard LaCoss
MIT Lincoln Laboratory, M-200B
P.O. Box 73
Lexington, MA 02173-0073

Dr. Fred K. Lamb
University of Illinois at Urbana-Champaign
Department of Physics
1110 West Green Street
Urbana, IL 61801

Prof. Charles A. Langston
Geosciences Department
403 Deike Building
The Pennsylvania State University
University Park, PA 16802

Jim Lawson, Chief Geophysicist
Oklahoma Geological Survey
Oklahoma Geophysical Observatory
P.O. Box 8
Leonard, OK 74043-0008

Prof. Thorne Lay
Institute of Tectonics
Earth Science Board
University of California, Santa Cruz
Santa Cruz, CA 95064

Dr. William Leith
U.S. Geological Survey
Mail Stop 928
Reston, VA 22092

Mr. James F. Lewkowicz
Phillips Laboratory/GPEH
Hanscom AFB, MA 01731-5000(2 copies)

Mr. Alfred Lieberman
ACDA/VI-OA State Department Building
Room 5726
320-21st Street, NW
Washington, DC 20451

Prof. L. Timothy Long
School of Geophysical Sciences
Georgia Institute of Technology
Atlanta, GA 30332

Dr. Randolph Martin, III
New England Research, Inc.
76 Olcott Drive
White River Junction, VT 05001

Dr. Robert Masse
Denver Federal Building
Box 25046, Mail Stop 967
Denver, CO 80225

Dr. Gary McCartor
Department of Physics
Southern Methodist University
Dallas, TX 75275

Prof. Thomas V. McEvilly
Seismographic Station
University of California
Berkeley, CA 94720

Dr. Art McGarr
U.S. Geological Survey
Mail Stop 977
U.S. Geological Survey
Menlo Park, CA 94025

Dr. Keith L. McLaughlin
S-CUBED
A Division of Maxwell Laboratory
P.O. Box 1620
La Jolla, CA 92038-1620

Stephen Miller & Dr. Alexander Florence
SRI International
333 Ravenswood Avenue
Box AF 116
Menlo Park, CA 94025-3493

Prof. Bernard Minster
IGPP, A-025
Scripps Institute of Oceanography
University of California, San Diego
La Jolla, CA 92093

Prof. Brian J. Mitchell
Department of Earth & Atmospheric Sciences
St. Louis University
St. Louis, MO 63156

Mr. Jack Murphy
S-CUBED
A Division of Maxwell Laboratory
11800 Sunrise Valley Drive, Suite 1212
Reston, VA 22091 (2 Copies)

Dr. Keith K. Nakanishi
Lawrence Livermore National Laboratory
L-025
P.O. Box 808
Livermore, CA 94550

Dr. Carl Newton
Los Alamos National Laboratory
P.O. Box 1663
Mail Stop C335, Group ESS-3
Los Alamos, NM 87545

Dr. Bao Nguyen
HQ AFTAC/TTR
Patrick AFB, FL 32925-6001

Prof. John A. Orcutt
IGPP, A-025
Scripps Institute of Oceanography
University of California, San Diego
La Jolla, CA 92093

Prof. Jeffrey Park
Kline Geology Laboratory
P.O. Box 6666
New Haven, CT 06511-8130

Dr. Howard Patton
Lawrence Livermore National Laboratory
L-025
P.O. Box 808
Livermore, CA 94550

Dr. Frank Pilotte
HQ AFTAC/TT
Patrick AFB, FL 32925-6001

Dr. Jay J. Pulli
Radix Systems, Inc.
2 Taft Court, Suite 203
Rockville, MD 20850

Dr. Robert Reinke
ATTN: FCTVTD
Field Command
Defense Nuclear Agency
Kirtland AFB, NM 87115

Prof. Paul G. Richards
Lamont-Doherty Geological Observatory
of Columbia University
Palisades, NY 10964

Mr. Wilmer Rivers
Teledyne Geotech
314 Montgomery Street
Alexandria, VA 22314

Dr. George Rothe
HQ AFTAC/TTR
Patrick AFB, FL 32925-6001

Dr. Alan S. Ryall, Jr.
DARPA/NMRO
3701 North Fairfax Drive
Arlington, VA 22209-1714

Dr. Richard Sailor
TASC, Inc.
55 Walkers Brook Drive
Reading, MA 01867

Prof. Charles G. Sammis
Center for Earth Sciences
University of Southern California
University Park
Los Angeles, CA 90089-0741

Prof. Christopher H. Scholz
Lamont-Doherty Geological Observatory
of Columbia University
Palisades, CA 10964

Dr. Susan Schwartz
Institute of Tectonics
1156 High Street
Santa Cruz, CA 95064

Secretary of the Air Force
(SAFRD)
Washington, DC 20330

Office of the Secretary of Defense
DDR&E
Washington, DC 20330

Thomas J. Sereno, Jr.
Science Application Int'l Corp.
10260 Campus Point Drive
San Diego, CA 92121

Dr. Michael Shore
Defense Nuclear Agency/SPSS
6801 Telegraph Road
Alexandria, VA 22310

Dr. Matthew Sibol
Virginia Tech
Seismological Observatory
4044 Derring Hall
Blacksburg, VA 24061-0420

Prof. David G. Simpson
IRIS, Inc.
1616 North Fort Myer Drive
Suite 1440
Arlington, VA 22209

Donald L. Springer
Lawrence Livermore National Laboratory
L-025
P.O. Box 808
Livermore, CA 94550

Dr. Jeffrey Stevens
S-CUBED
A Division of Maxwell Laboratory
P.O. Box 1620
La Jolla, CA 92038-1620

Lt. Col. Jim Stobie
ATTN: AFOSR/NL
Bolling AFB
Washington, DC 20332-6448

Prof Brian Stump
Institute for the Study of Earth & Man
Geophysical Laboratory
Southern Methodist University
Dallas, TX 75275

Prof. Jeremiah Sullivan
University of Illinois at Urbana-Champaign
Department of Physics
1110 West Green Street
Urbana, IL 61801

Prof. L. Sykes
Lamont-Doherty Geological Observatory
of Columbia University
Palisades, NY 10964

Dr. David Taylor
ENSCO, Inc.
445 Pineda Court
Melbourne, FL 32940

Dr. Steven R. Taylor
Los Alamos National Laboratory
P.O. Box 1663
Mail Stop C335
Los Alamos, NM 87545

Prof. Clifford Thurber
University of Wisconsin-Madison
Department of Geology & Geophysics
1215 West Dayton Street
Madison, WS 53706

Prof. M. Nafi Toksoz
Earth Resources Lab
Massachusetts Institute of Technology
42 Carleton Street
Cambridge, MA 02142

Dr. Larry Turnbull
CIA-OSWR/NED
Washington, DC 20505

Dr. Gregory van der Vink
IRIS, Inc.
1616 North Fort Myer Drive
Suite 1440
Arlington, VA 22209

Dr. Karl Veith
EG&G
5211 Auth Road
Suite 240
Suitland, MD 20746

Prof. Terry C. Wallace
Department of Geosciences
Building #77
University of Arizona
Tuscon, AZ 85721

Dr. Thomas Weaver
Los Alamos National Laboratory
P.O. Box 1663
Mail Stop C335
Los Alamos, NM 87545

Dr. William Wortman
Mission Research Corporation
8560 Cinderbed Road
Suite 700
Newington, VA 22122

Prof. Francis T. Wu
Department of Geological Sciences
State University of New York
at Binghamton
Vestal, NY 13901

AFTAC/CA
(STINFO)
Patrick AFB, FL 32925-6001

DARPA/PM
3701 North Fairfax Drive
Arlington, VA 22203-1714

DARPA/RMO/RETRIEVAL
3701 North Fairfax Drive
Arlington, VA 22203-1714

DARPA/RMO/SECURITY OFFICE
3701 North Fairfax Drive
Arlington, VA 22203-1714

HQ DNA
ATTN: Technical Library
Washington, DC 20305

Defense Intelligence Agency
Directorate for Scientific & Technical Intelligence
ATTN: DTIB
Washington, DC 20340-6158

Defense Technical Information Center
Cameron Station
Alexandria, VA 22314 (2 Copies)

TACTEC
Battelle Memorial Institute
505 King Avenue
Columbus, OH 43201 (Final Report)

Phillips Laboratory
ATTN: XPG
Hanscom AFB, MA 01731-5000

Phillips Laboratory
ATTN: GPE
Hanscom AFB, MA 01731-5000

Phillips Laboratory
ATTN: TSML
Hanscom AFB, MA 01731-5000

Phillips Laboratory
ATTN: SUL
Kirtland, NM 87117 (2 copies)

Dr. Michel Bouchon
I.R.I.G.M.-B.P. 68
38402 St. Martin D'Heres
Cedex, FRANCE

Dr. Michel Campillo
Observatoire de Grenoble
I.R.I.G.M.-B.P. 53
38041 Grenoble, FRANCE

Dr. Kin Yip Chun
Geophysics Division
Physics Department
University of Toronto
Ontario, CANADA

Prof. Hans-Peter Harjes
Institute for Geophysic
Ruhr University/Bochum
P.O. Box 102148
4630 Bochum 1, GERMANY

Prof. Eystein Husebye
NTNF/NORSAR
P.O. Box 51
N-2007 Kjeller, NORWAY

David Jepsen
Acting Head, Nuclear Monitoring Section
Bureau of Mineral Resources
Geology and Geophysics
G.P.O. Box 378, Canberra, AUSTRALIA

Ms. Eva Johannisson
Senior Research Officer
National Defense Research Inst.
P.O. Box 27322
S-102 54 Stockholm, SWEDEN

Dr. Peter Marshall
Procurement Executive
Ministry of Defense
Blacknest, Brimpton
Reading FG7-FRS, UNITED KINGDOM

Dr. Bernard Massinon, Dr. Pierre Mechler
Societe Radiomana
27 rue Claude Bernard
75005 Paris, FRANCE (2 Copies)

Dr. Svein Mykkeltveit
NTNT/NORSAR
P.O. Box 51
N-2007 Kjeller, NORWAY (3 Copies)

Prof. Keith Priestley
University of Cambridge
Bullard Labs, Dept. of Earth Sciences
Madingley Rise, Madingley Road
Cambridge CB3 OEZ, ENGLAND

Dr. Jorg Schlittenhardt
Federal Institute for Geosciences & Nat'l Res.
Postfach 510153
D-3000 Hannover 51, GERMANY

Dr. Johannes Schweitzer
Institute of Geophysics
Ruhr University/Bochum
P.O. Box 1102148
4360 Bochum 1, GERMANY